IRE Transactions

n Microwave Theory and Techniques

Volume MTT-5 **JULY, 1957** Number 3

In This Issue

For complete Table of Contents, see page 171.

PUBLISHED BY THE
fessional Group on Microwave Theory and Techniques

IRE PROFESSIONAL GROUP ON MICROWAVE THEORY AND TECHNIQUES

The Professional Group on Microwave Theory and Techniques is an association of IRE members with professional interest in the field of Microwave Theory and Techniques. All IRE members are eligible for membership and will receive all Group publications upon payment of the prescribed annual assessment of $3.00.

IRE TRANSACTIONS®
on Microwave Theory and Techniques

Published by the Institute of Radio Engineers, Inc., for the Professional Group on Microwave Theory and Techniques, at 1 East 79th Street, New York 21, New York. Responsibility for the contents rests upon the authors, and not upon the IRE, the Group, or its members. Price per copy: IRE PGMTT members, $1.15; IRE members, $1.70, nonmembers, $3.45. Annual subscription price: IRE members, $8.50; colleges and public libraries, $12.75; nonmembers, $17.00.

Address all manuscripts to K. Tomiyasu, PGMTT Editor, General Electric Microwave Laboratory, 601 California Ave., Palo Alto, Calif. Submission of three copies of manuscripts, including figures will expedite the review.

IRE Transactions on Microwave Theory and Techniques

Published by the Professional Group on Microwave Theory and Techniques

Volume MTT-5 JULY, 1957 Number 3

TABLE OF CONTENTS

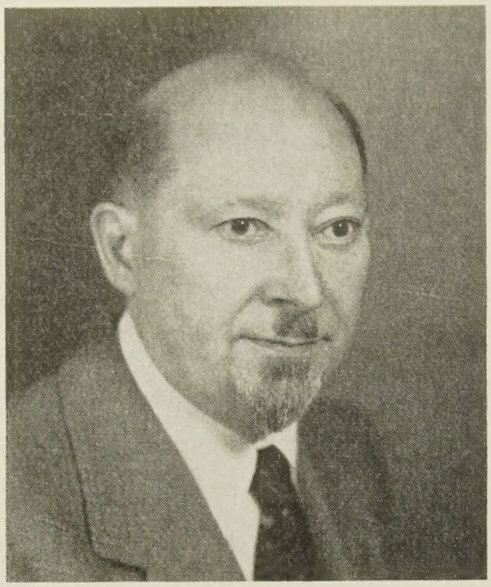

Sergei Alexander Schelkunoff

Sergei Alexander Schelkunoff was born in Russia in 1897. In the early years of his primary and secondary education he was interested in almost everything except mathematics which he would not have passed at all if it were not for the kindness of his teachers. At the age of 13, however, he came across Cauchy's *Algebraic Analysis*. In this book, Cauchy defined exponential and circular functions throughout the entire complex plane as solutions of appropriate functional equations, and thus obtained their essential properties. From then on Schelkunoff became an avid reader of the mathematical writings of the masters. He was profoundly impressed by Felix Klein's *Elementary Mathematics from the Higher Standpoint*. In Weber-Wellstein's mathematical trilogy, he was fascinated with the account of the realization of Lobachevskian and Riemannian geometries in Euclidean space, since one could hardly demonstrate more dramatically that these geometries stand or fall together with Euclidean geometry.

Most of his mathematical education was gained through such reading, for he had little formal training after he left high school. During his early college years he spent most of his time in defense plants. Then came military training as an officer, active military duty, and finally the chaos of revolution. It was not until late in September, 1921, when he landed in Seattle and went to Pullman, Wash. that this nomadic period in his life ended.

By the end of January, 1922, he had learned enough English to enter the State College of Washington, and in June, 1923, he received the BA and MA degrees in mathematics. Then he joined the Engineering Department of the Western Electric Company and became engaged in *experimental* studies of electromechanical systems.

In 1926 he was invited to return to the State College of Washington. He did and taught mathematics until June, 1929. In the meantime he received the Ph.D. degree in mathematics from Columbia University.

Dr. Schelkunoff rejoined the Bell Telephone Laboratories (an outgrowth of the Engineering Department of the Western Electric Company), and became a member of the newly organized Mathematical Research Department. It was at this time that he began his work on electromagnetic theory and its applications. He wrote numerous articles in this field, and is the author of *Electromagnetic Theory*, *Applied Mathematics for Scientists and Engineers*, and *Advanced Antenna Theory*. He is also the co-author, with Harald T. Friis, of *Antennas—Theory and Practice*.

He is a member of Phi Kappa Phi, the American Mathematical Society, and the Mathematical Association of America; he is also a Fellow of the American Association for the Advancement of Science, the Institute of Radio Engineers, and the American Institute of Electrical Engineers. In 1942 he was awarded the Morris Liebmann Memorial Prize by the IRE for his contributions to the theory of radio wave propagation. In 1949 he received the Stewart Ballentine Medal for outstanding research in communications and reconnaissance from the Franklin Institute. At present, he is Assistant Director of Mathematical Research at the Bell Telephone Laboratories.

Microwaves and Mathematics

Mathematics and mathematicians play an essential role in the development of science and engineering. This is particularly conspicuous in the case of electromagnetic theory and microwave engineering. In the preface to his famous treatise, Maxwell refers to Gauss as the man who " . . . brought his powerful intellect to bear on the theory of magnetism, and on the methods of observing it, and [who] not only added greatly to our knowledge of the theory of attractions, but reconstructed the whole of magnetic science as regards the instruments used, the methods of observation, and the calculation of the results. . . . " Maxwell also adds: "The great success which these eminent men [Gauss, Weber, Riemann, J. & C. Neumann, Lorentz, etc.] attained in the application of mathematics to electrical phenomena, gives, as is natural, additional weight to their theoretical speculations. . . . " But a note of dissatisfaction is sounded in "There is also a considerable mass of mathematical memoirs which are of great importance in electrical science, but . . . they are for the most part beyond the comprehension of any but professed mathematicians."

As a matter of fact, the influence of mathematics on the development of science transcends direct application of mathematical methods either in establishing precise relations between observable physical quantities or in solving specific problems. Even more important is the role of mathematics in the creation of "physical" concepts and suitable models to aid our understanding and mastery of natural phenomena. First comes a recognition of essential similarities in apparently different physical phenomena; that is, a discovery of the analogy between them. Then follow abstractions and generalizations. As mathematical concepts grow and age, they gather flesh about them and gradually become "physical" concepts. This happened to the energy concept and the impedance concept. And somewhere creative imagination enters the picture.

Examples are plentiful. We have Lord Kelvin who formulated his theory of electrical discharge of a Leyden jar by drawing a parallel between electrical and mechanical phenomena. We have Faraday who created a model of an electromagnetic field which is essentially geometric even though he endowed his "lines of force" and "tubes of force" with some mechanical properties. And it takes a mathematician to make bold use of analogies and pictures without being ashamed of it. How many mathematical equations do we find in *Maxwell's Theory and Hertzian Oscillations*, a book of over one hundred pages by Henri Poincaré? None.

Microwave theory and engineering are particularly indebted to mathematics in its various forms: to Faraday's basic mathematical model of an electromagnetic field, to Maxwell's imaginative concept of displacement current and to his translation of Faraday's geometric language into analytic, thus enabling Hertz to calculate the field around a dipole and Lord Rayleigh to predict that electromagnetic waves of sufficiently high frequency can travel inside cylindrical tubes. While some mathematical predictions might have been anticipated by experimental discoveries, there are instances in which this would have been extremely unlikely. To establish experimentally that the attenuation of a circular electric wave decreases with increasing frequency would have required a tremendous amount of effort and ingenuity and expense to keep the wave "clean." Would anyone have been willing to make the investment without some idea of the possible outcome?

Abstract model building in the microwave theory is not over. About a century ago, Lord Kelvin formulated his telegraphist's equations for cables, or electric transmission lines as we now call them. Then, in more recent times, the concept of "normal transmission mode" was evolved which enabled us to think of coupled transmission lines as a certain number of uncoupled transmission lines. More recently still, the concept of waveguide mode was further generalized so that we can think of each normal mode as the result of superposition of coupled modes belonging to a rather arbitrarily chosen set. In this way it was possible to obtain from Maxwell's equations generalized telegraphist's equations for quite general types of waveguides. By this generalization, the gap between Kelvin's theory of transmission lines, based on the concept of distributed circuit parameters, and Maxwell's field theory was closed.

The future? Mathematics should continue to exert great influence on microwave theory and engineering. There certainly will be continued problem solving. And, who knows, some ingenious mind may create a model which will throw a new light on diffraction phenomena, or present us with a particularly satisfying way of thinking about propagation in large waveguides.

SERGEI A. SCHELKUNOFF

Well Done, Ted

We are all indebted to Ted Saad for his three years of tireless work as editor of our magazine.

It does not take more than a brief glance through these pages to see what an exhausting time-consuming job it must be to both edit and coordinate the material for such a highly technical and valuable publication.

Older members will recall that before Ted Saad volunteered his services, Al Beck and Bill Mumford combined their talents to put out previous issues. Al served as Chairman of the Paper Procurement Committee and Bill served as Chairman of the Publication Committee. When they were forced to resign the positions in 1954 because of the pressure of other business, Ted agreed to take over both jobs.

Ted accepted the satisfaction that goes with real accomplishment as his sole reward. Our publishing budget is presently based on the assumption that we will be able to publish this rather expensive periodical without paying staff salaries.

If it were not for members like Ted and Kiyo Tomiyasu, who succeeds him with this issue, we would indeed be hard pressed. We would be left with the unhappy choice of curtailing publication or increasing dues to hire a professional staff.

Obviously, the first alternative is out. To reduce publication would be to impede the flow of the life blood of our organization. Holding at most one or two meetings a year, as we do, we need the TRANSACTIONS to keep in step with each other during the months in between.

As for the second alternative, I think we all agree that the dues are high enough.

Just how Ted was able to carry water on both shoulders for us for three years and still keep things humming at his research center, Sage Laboratories in Waltham, Mass., remains a mystery to me. And I'm sure Ted's wife, and their two daughters were not exactly crestfallen to learn that Ted had handed the reigns to Kiyo and was free to spend more time around the Saads' West Roxbury home.

An indication of how seriously Ted felt about the publishing work is his choice of Kiyo as his successor. Ted had decided to step down some time back but stayed on until he found a man who shared his enthusiasm for the important project.

So everything has turned out well. Ted, recently installed as our Vice- Chairman, has a bit more time for outside interests (that is, if he has any besides microwave theory and techniques).

We, in the group, can be thankful that the changeover took place so smoothly and that in Kiyo Tomiyasu, we have another double-duty man who can provide us with the same high quality we have grown accustomed to in our publications.

Ted, from all of us, our lasting thanks and best wishes. Kiyo, we only ask that you keep up the good work. You certainly have made a fine start.

Herbert F. Engelmann, *Chairman*, PGMTT

A Modified Equal-Element Band-Pass Filter*

R. BAWER† AND G. KEFALAS‡

Summary—A method is presented whereby considerable improvement in the frequency response of a five-stage, equal-element waveguide filter can be realized while preserving nearly all the structural simplicity of this realization. It is shown that by increasing the loaded Q of the center resonant element of a five-stage, equal-element filter, the pass band ripple can be appreciably reduced and the skirt selectivity improved. The modified design also provides a simple means of bandwidth adjustment.

Introduction

FABRICATION problems and cost of a waveguide band-pass filter are appreciably reduced when the structure is realized as a cascade combination of n identical sections.[1] Plots of the power transfer function show, however, that the pass band insertion loss ripple rapidly increases with n. This fact has generally limited the use of the equal-element realization to filters with less than five sections.

In the case of a five-stage filter, a considerable improvement can be achieved while still maintaining nearly all the desirable features of the equal-element realization. It will be shown that by simply increasing the loaded Q of the center resonant element, the 2-db pass band ripple inherent in the equal-element case can be appreciably reduced and the skirt selectivity improved. This may be seen intuitively by comparing the symmetrical low-pass equal-element prototype with that of an equal-ripple Tchebycheff response (see Table I).

TABLE I

Response	Prototype Ladder Elements				
	C_1	L_2	C_3	L_4	C_5
¼ db Tchebycheff	1.414	1.318	2.241	1.318	1.414
Equal-element	1.414	1.414	1.414	1.414	1.414

It is clear that, except for the value of C_3, the five identical elements are reasonably close to the corresponding Tchebycheff values. Thus, one might reasonably expect that upon increasing the center element capacity (directly proportional to the loaded Q of the band-pass realization), the resulting structure should have a reduced pass band ripple and a skirt selectivity approaching that of the Tchebycheff unit.

* Manuscript received by the PGMTT, September 17, 1956.
† Emerson Res. Labs., Washington, D. C. Formerly with Melpar, Inc., Falls Church, Va.
‡ Melpar, Inc., Falls Church, Va.
[1] G. L. Ragan, "Microwave Transmission Circuits," McGraw-Hill Book Co., Inc., New York, N. Y., pp. 681–682; 1948.

Theory

The general expression for the insertion loss of a symmetrical five-section, low-pass filter is given by

$$\text{I.L.} = 1 + w^2/4\left[w^4(L^2C_1^2C) - w^2(2LC_1^2 + 2LC_1C - L^2C) + (2C_1 + C - 2L)\right]^2 \quad (1)$$

where

w = frequency variable in radians per second
$L = L_2 = L_4$
$C_1 = C_5$, and
$C_3 = C$.

Since the only effect of multiplying the L's and C's by a constant is a change of the frequency scale, choose $L = C_1 = 1$. Substituting these values into (1), one can obtain the frequencies at which the insertion loss extrema occur:

$$w_1 = 0,$$

$$w_{2,3}^2 = \frac{1}{2}\left[\left(\frac{C+2}{C}\right) \pm \sqrt{\left(\frac{C+2}{C}\right)^2 - 4}\right], \text{ and}$$

$$w_{4,5}^2 = \frac{1}{10}\left[3\left(\frac{C+2}{C}\right) \pm \sqrt{9\left(\frac{C+2}{C}\right)^2 - 20}\right].$$

From the above equations it follows that the number of insertion loss extrema, hence pass band ripples, will depend upon the value of the center element C.

Case I.	$0 < C < 2$	5 extrema.
Case II.	$C = 2$	3 extrema (double root at $w = 1$).
Case III.	$2 < C < 4.07$	3 extrema.
Case IV.	$C = 4.07$	2 extrema.
Case V.	$C > 4.07$	1 extremum.

The theoretical response of a five-section, low-pass filter is plotted in Fig. 1 for various values of the center element C. To more clearly visualize the effect of this parameter, the curves are replotted in Fig. 2. Note the rapid reduction in the maximum pass band ripple, the broad minimum, and the uniform reduction in bandwidth as the capacity of the center element is increased.

The skirt selectivity of a modified equal-element filter has been compared to that of a Tchebycheff filter having a comparable pass band ripple. Apart from a slightly lower insertion loss for $w \gg 1$, the general behavior of the modified filter, for losses less than 20 db, follows the

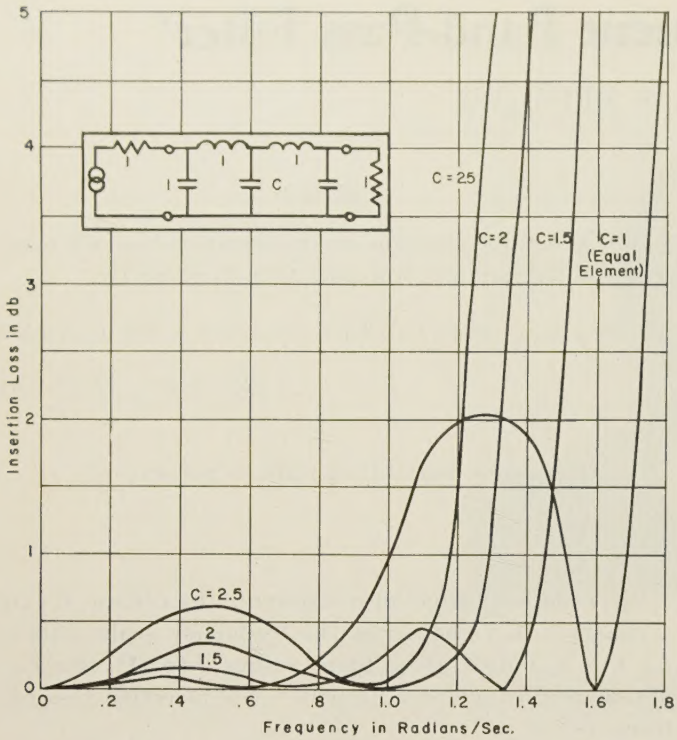

Fig. 1—Theoretical response of a five-section, low-pass filter for various values of the center element.

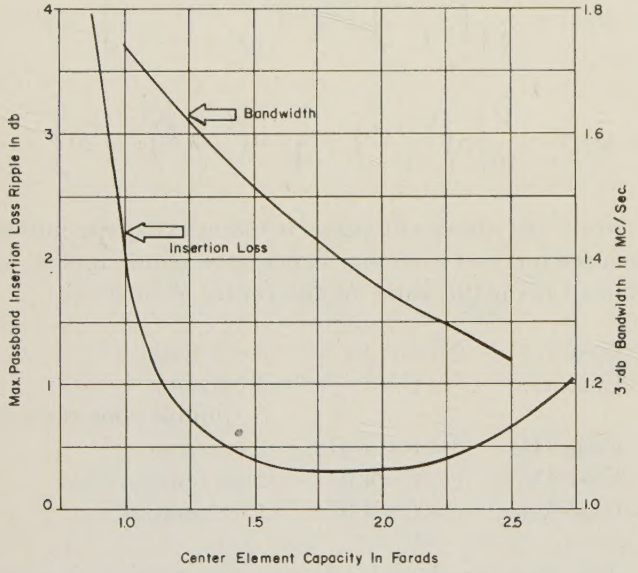

Fig. 2—Maximum pass band insertion loss ripple and a 3-db bandwidth of five-section, low-pass filter for various values of the center element.

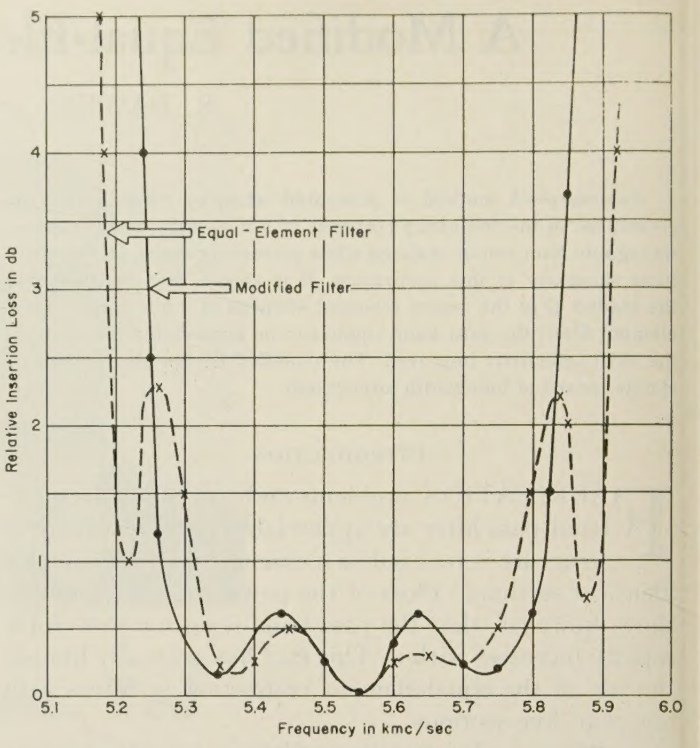

Fig. 3—Experimental response curves of a five-section, equal-element filter illustrating the effect of increasing the center resonant loaded Q.

Tchebycheff response so closely that no useful purpose is served by reproducing the curve.

A typical response of a modified five-section, equal-element band-pass filter is shown in Fig. 3. The improved response was obtained by simply replacing the inductive posts forming the center resonant element with posts of larger diameter.

Conclusion

In addition to retaining nearly all the simplicity of the equal-element realization, the modified design affords a convenient means for simply, accurately, and systematically varying the bandwidth with negligible pass band distortion. As seen in Fig. 2, the bandwidth may be varied as much as ± 10 per cent while still maintaining a ripple of less than $\frac{1}{2}$ db.

Although this technique has not been applied to higher order equal-element filters, it is felt that the general approach is applicable.

Application of Rayleigh-Ritz Method to Dielectric Steps in Waveguides*

R. E. COLLIN† AND R. M. VAILLANCOURT†

Summary—**The Rayleigh-Ritz method is applied to obtain approximations to the first N eigenfunctions and corresponding eigenvalues in an inhomogeneously filled rectangular waveguide. These approximate eigenfunctions are then used to obtain a solution for the reflection and transmission coefficients at the junction of an empty and partially filled waveguide. Theoretical and experimental results are given for a dielectric slab which extends completely across the broad dimension of the guide, but only partially across the narrow dimension. The experimental values are within the experimental error of the computed values obtained by considering the dominant mode and only two evanescent modes.**

Introduction

WAVE propagation in a waveguide inhomogeneously filled with a dielectric has been studied by many authors.[1] As a general rule, the modes are more complex and transcendental equations have to be solved, in order to find the propagation constants of the various modes. This has led several authors to consider the application of variational methods for obtaining approximations to the eigenvalues.[2–4] By means of the Rayleigh-Ritz method (hereafter called the R-R method), one may obtain approximations for the first N eigenvalues, and also for the first N eigenfunctions.[5,6] In this paper, the discontinuity between an empty and an inhomogeneously filled rectangular guide will be studied using the R-R method. The following procedure is used:

1) The first N eigenfunctions in the inhomogeneously filled guide are approximated by the Rayleigh-Ritz method.
2) Equations expressing the continuity of the tangential field components at the junction are then easily written down and solved for the reflection and transmission coefficients.

In a rectangular guide inhomogeneously filled with a dielectric slab, as in Fig. 1, the two sets of fundamental modes are the longitudinal section electric and magnetic modes (LSE and LSM modes), having the electric and magnetic vector, respectively, contained entirely within a longitudinal section. In an empty guide, the TE and TM modes may be derived from a magnetic and an electric Hertzian potential having only a longitudinal component respectively.[7] By analogy with this problem, it is readily seen that the LSE and LSM modes may be derived from a magnetic and an electric Hertzian potential, respectively and having a single component directed normal to the dielectric-empty guide interface. These two sets of modes form a complete set in which any arbitrary field distribution may be expanded.[8]

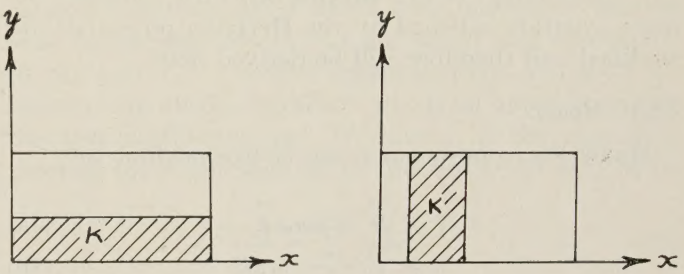

Fig. 1—Inhomogeneously filled rectangular waveguide.

For a general inhomogeneously filled cylindrical guide, the division into LSE and LSM modes is not possible.

When an H_{10} mode is incident at the junction of an empty rectangular guide and a guide partially filled, as in Fig. 1(a), both LSE and LSM modes are excited. In the case of Fig. 1(b) with an H_{10} mode incident, only H_{no} modes are excited. The case of Fig. 1(a) is considerably more complex and, therefore, was chosen as a good example to which the R-R method could be applied.

This same type of dielectric step discontiuity has been treated in a recent paper by Angulo, using the correct expressions for the eigenfunctions and a variational method for evaluation of the equivalent circuit parameters.[9] However, the coupling of the LSE modes by the

* Manuscript received by the PGMTT, October 16, 1956.
† Canadian Armament Res. and Dev. Establishment, Valcartier, P. Q.

[1] L. G. Chambers, "Propagation in waveguides filled longitudinally with two or more dielectrics," *Brit. J. Appl. Phys.*, vol. 4, pp. 39–45; February, 1953. (This is a review article containing sixteen references.)

[2] L. G. Chambers, "Compilation of the propagation constants of an inhomogeneously filled waveguide," *Brit. J. Appl. Phys.*, vol. 3, pp. 19–21; January, 1952.

[3] L. G. Chambers, "An approximate method for the calculation of propagation constants for inhomogeneously filled waveguides," *Quart. J. Mech. and Appl. Math.*, vol. 7, pt. 3, pp. 299–316; September, 1954.

[4] A. D. Berk, "Variational principles for electromagnetic resonators and waveguides," IRE TRANS., vol. AP-4, pp. 104–111; April, 1956.

[5] R. Courant and D. Hilbert, "Methods of Mathematical Physics," Interscience Publishing Co., New York, N. Y., 1st English ed., p. 175; 1953.

[6] R. Weinstock, "Calculus of Variations," McGraw-Hill Book Co., Inc., New York, N. Y., 1st ed., chs. 7–9; 1952.

[7] J. A. Stratton, "Electromagnetic Theory," McGraw-Hill Book Co., Inc., New York, N. Y., sec. 6.1; 1941.

[8] J. Van Bladel, "Field expandibility in normal modes for a multilayered rectangular or circular waveguide," *J. Franklin Inst.*, vol. 253, pp. 313–321; April, 1952.

[9] C. M. Angulo, "Discontinuities in a rectangular waveguide partially filled with dielectric," IRE TRANS., vol. MTT-5, pp. 68–74; January, 1957.

step when a LSM mode is incident is neglected. Therefore, the results obtained are only approximate and valid for small discontinuities; *i.e.* ($t \ll b$ or $t \approx b$, where t is the slab thickness and b the waveguide height) when the amplitudes of the coupled LSE modes are small.

This same step has been analyzed by R. E. Collin (unpublished work) as well as the simpler case of the H-plane dielectric step.[10]

Use of the R-R method has the great advantage of avoiding evaluation of many complicated expressions, especially for cases where a waveguide cross section is divided into more than two regions by dielectric media of different dielectric constant.

Wave Equation for the Modes

In order to bring the problem being studied into the class that can be handled by the normal Sturm-Liouville theory, the rectangular guide will be considered as filled with a lossless dielectric material with a dielectric constant which is a continuous function of the coordinate y, but independent of x and z. From the theory for the continuous case, one may readily pass to the case where the dielectric constant is a discontinuous function of y; *e.g.*, a slab filling. With a varying dielectric constant, the wave equation satisfied by the Hertzian potentials are modified and therefore will be derived here.

LSM Modes

Maxwell's equations in a source free medium are

$$\nabla \times \vec{H} = j\omega\epsilon_0\kappa\vec{E}, \tag{1a}$$

$$\nabla \times \vec{E} = -j\omega\mu\vec{H}, \tag{1b}$$

$$\nabla \cdot \vec{B} = 0, \tag{1c}$$

$$\nabla \cdot \kappa E = 0, \tag{1d}$$

where κ is the relative dielectric constant and here is considered as a function of y.

By virtue of (1c), one may take

$$\vec{H} = j\omega\epsilon_0 \nabla \times \vec{\Pi}_E \tag{2}$$

where $\vec{\Pi}_E$ is an electric Hertzian potential with a y component only. From (1b)

$$\nabla \times \vec{E} = k_0^2 \nabla \times \vec{\Pi}_E$$

which integrates to

$$\vec{E} = k_0^2 \vec{\Pi}_E + \nabla\phi. \tag{3}$$

From (1a)

$$\begin{aligned} \nabla \times \nabla \times \vec{\Pi}_E &= \nabla\nabla \cdot \vec{\Pi}_E - \nabla^2\vec{\Pi}_E = \kappa k_0^2 \vec{\Pi}_E + \kappa\nabla\phi \\ &= \kappa k_0^2 \vec{\Pi}_E + \nabla\kappa\phi - \phi\nabla\kappa. \end{aligned} \tag{4}$$

[10] R. E. Collin and J. Brown, "The calculation of the equivalent circuit of an axially unsymmetrical waveguide junction," *Proc. IEE*, vol. 103, pt. C, pp. 121–128; March, 1956.

As yet $\nabla\phi$ and $\nabla \cdot \vec{\Pi}_E$ are unspecified and one may, therefore, put

$$\nabla\nabla \cdot \vec{\Pi}_E = \nabla\kappa\phi$$

which apart from an irrelevant constant integrates to

$$\nabla \cdot \vec{\Pi}_E = \kappa\phi. \tag{5}$$

From (5), $\phi = \kappa^{-1}\nabla \cdot \vec{\Pi}_E$ and hence the wave equation for $\vec{\Pi}_E$, *i.e.*, (4) becomes

$$\nabla^2\vec{\Pi}_E + \kappa k_0^2 \vec{\Pi}_E - \kappa^{-1}\nabla\kappa\nabla \cdot \vec{\Pi}_E = 0 \tag{6}$$

while (3) for the electric field becomes

$$\begin{aligned} \vec{E} &= k_0^2 \vec{\Pi}_E + \nabla(\kappa^{-1}\nabla \cdot \vec{\Pi}_E) \\ &= \nabla \cdot \vec{\Pi}_E \nabla\kappa^{-1} + \kappa^{-1}\nabla\nabla \cdot \vec{\Pi}_E + \kappa k_0^2 \vec{\Pi}_E \\ &= \kappa k_0^2 \vec{\Pi}_E + \kappa^{-1}\nabla\nabla \cdot \vec{\Pi}_E - \kappa^{-2}\nabla \cdot \vec{\Pi}_E \nabla\kappa \\ &= \kappa^{-1}\nabla \times \nabla \times \vec{\Pi}_E, \end{aligned} \tag{7}$$

this latter result following from the wave equation. From (7), one sees at once that (1d) is satisfied, since

$$\nabla \cdot \kappa\vec{E} = \nabla \cdot (\nabla \times \nabla \times \vec{\Pi}_E) \equiv 0.$$

For a variation with x according to $\sin \pi x/a$ and exponential z dependence, the solutions to (6) are of the form

$$\vec{\Pi}_E = \vec{i}_y \sin\frac{\pi x}{a} \psi_E(y) e^{\pm\gamma z} \tag{8}$$

where ψ_E is a solution of the Sturm-Liouville equation

$$\frac{d^2\psi_E}{dy^2} - \kappa^{-1}\frac{d\kappa}{dy}\frac{d\psi_E}{dy} + \left(\kappa k_0^2 - \frac{\pi^2}{a^2} + \gamma^2\right)\psi_E = 0, \tag{9}$$

or equivalently

$$\frac{d}{dy}\frac{1}{\kappa}\frac{d\psi_E}{dy} + \frac{1}{\kappa}\left(\kappa k_0^2 - \frac{\pi^2}{a^2} + \gamma^2\right)\psi_E = 0.$$

Eq. (9) has an infinite number of solutions ψ_{En} with corresponding eigenvalues γ_n^2. These solutions form an orthogonal set with respect to the weighting function κ^{-1} and may be normalized so that

$$\int_0^b \psi_{En}\psi_{Es}\kappa^{-1}dy = \delta_{ns} \tag{10}$$

where δ_{ns} is the Kronecher delta and is equal to unity, if $n = s$ and zero otherwise. When κ is a continuous function, both ψ_{En} and $d\psi_{En}/dy$ are continuous.

When κ is the discontinuous function,

$$\kappa(y) = \kappa_0 - (\kappa_0 - 1)U(y - t) \tag{11}$$

where $U(y-t)$ is the step function

$$U(y - t) = \begin{cases} 0, & y < t, \\ 1, & y \geqq t, \end{cases} \tag{12}$$

ψ_{En} and $\kappa^{-1}(d\psi_{En}/dy)$ are continuous in order that the tangential field components should be continuous at the interface. At $y=o,\ b,\ d\psi_{En}/dy$ vanishes. The term

$$\kappa^{-1}\frac{d\kappa}{dy}\frac{d\psi_E}{dy}$$

in the differential equation (9) becomes

$$\kappa^{-1}(1-\kappa_0)\delta(y-t)\frac{d\psi_E}{dy},$$

where $\delta(y-t)$ is the Dirac impulse function. The term $d\psi_E/dy$ is discontinuous at $y=t$ and hence, the second derivative also has an impulse discontinuity at $y=t$. The physical reason for these discontinuities is the polarization charge in the dielectric.

LSE Modes

The longitudinal section electric modes do not have a component of electric field parallel to $\nabla\kappa$ and, therefore,

$$\nabla\cdot\kappa\vec{E} = \kappa\nabla\cdot\vec{E} + \vec{E}\cdot\nabla\kappa = 0$$

gives $\nabla\cdot\vec{E}=0$. For these modes, one may take

$$\vec{E} = -j\omega\mu\nabla\times\vec{\Pi}_M \tag{13}$$

where $\vec{\Pi}_M$ is a magnetic Hertzian potential with only a y component. From (1a),

$$\nabla\times\vec{H} = \kappa k_0^2\nabla\times\vec{\Pi}_M = k_0^2\nabla\times\kappa\vec{\Pi}_M,$$

since

$$\nabla\times\kappa\vec{\Pi}_M = \kappa\nabla\times\vec{\Pi}_M - \vec{\Pi}_M\times\nabla\kappa = \kappa\nabla\times\vec{\Pi}_M.$$

This equation integrates to

$$\vec{H} = \kappa k_0^2\vec{\Pi}_M + \nabla v.$$

From (1b),

$$\nabla\nabla\cdot\vec{\Pi}_M - \nabla^2\vec{\Pi}_M = \kappa k_0^2\vec{\Pi}_M + \nabla v.$$

Let $\nabla\nabla\cdot\vec{\Pi}_M=\nabla v$ and the wave equation for $\vec{\Pi}_M$ becomes

$$\nabla^2\vec{\Pi}_M + \kappa k_0^2\vec{\Pi}_M = 0, \tag{14}$$

while the equation for $\vec{H}$ becomes

$$\vec{H} = \kappa k_0^2\vec{\Pi}_M + \nabla\nabla\cdot\vec{\Pi}_M = \nabla\times\nabla\times\vec{\Pi}_M. \tag{15}$$

With an x variation according to $\cos\pi x/a$ and exponential z variation, the solution to (14) is of the form

$$\vec{\Pi}_M = \vec{i}_y\cos\frac{\pi x}{a}\psi_M(y)e^{\pm\beta z}, \tag{16}$$

where ψ_M is a solution of

$$\frac{d^2\psi_M}{dy^2} + \left(\kappa k_0^2 - \frac{\pi^2}{a^2} + \beta^2\right)\psi_M = 0. \tag{17}$$

Eq. (17) has an infinite number of solutions, ψ_{Mn}, with corresponding eigenvalues, β_n^2, and these solutions can be chosen to form an orthonormal set such that

$$\int_0^b \psi_{Mn}\psi_{Ms}dy = \delta_{ns}. \tag{18}$$

Both ψ_{Mn} and $d\psi_{Mn}/dy$ are continuous, irrespective of whether κ is continuous or not. At $y=0,\ b,\ \psi_{Mn}$ vanishes.

Minimum Characterization of the Eigenvalues

LSM Modes

If (9) is multiplied by $\kappa^{-1}\psi_E$ and the term involving the second derivative integrated by parts once (this term vanishes, since ψ_E and $\kappa^{-1}(d\psi_E/dy)$ are both continuous and $d\psi_E/dy$ vanishes at $y=0,\ b$), one gets

$$\gamma^2\int_0^b\kappa^{-1}\psi_E^2dy - \int_0^b\left\{\left(\frac{d\psi_E}{dy}\right)^2 - \left(\kappa k_0^2 - \frac{\pi^2}{a^2}\right)\psi_E^2\right\}\kappa^{-1}dy = 0. \tag{19}$$

Eq. (19) is a variational expression for the propagation constant γ^2. An extremisation of this equation by that class of functions $\phi(y)$, which are continuous with at least a piecewise continuous derivative and orthogonal to the first $K-1$ correct eigenfunctions ψ_{Ei}, with respect to the weight factor κ^{-1}, yields an upper bound on the true eigenvalue γ_K^2. By means of the expansion theorem for a complete set of functions, one may write

$$\phi = \sum_0^\infty a_n\psi_{En}. \tag{20}$$

The orthogonalization conditions give

$$a_n = 0; \qquad n = 0, 1, \cdots K-1. \tag{21}$$

Substituting into (19), gives

$$\begin{aligned}\gamma^2\sum_K^\infty a_n^2 &= \int_0^b\kappa^{-1}\sum_{s=K}^\infty\sum_{n=K}^\infty\left\{\frac{d\psi_{Es}}{dy}\frac{d\psi_{En}}{dy} - \left(\kappa k_0^2 - \frac{\pi^2}{a^2}\right)\psi_{Es}\psi_{En}\right\}a_na_sdy\\ &= \sum_{s=K}^\infty\sum_{n=K}^\infty a_sa_n\left\{\left(\kappa^{-1}\psi_{Es}\frac{d\psi_{En}}{dy}\right)\Big|_0^b - \int_0^b\kappa^{-1}\left[\psi_{Es}\frac{d^2\psi_{En}}{dy^2} + \left(\kappa k_0^2 - \frac{\pi^2}{a^2}\right)\psi_{Es}\psi_{En}\right]dy\right\}.\end{aligned}$$

The integrated term vanishes and, using (9) and (10), the result is

$$\gamma^2\sum_{n=K}^\infty a_n^2 = \sum_{n=K}^\infty a_n^2\gamma_n^2. \tag{22}$$

Assuming that the eigenfunctions ψ_{En} have been ordered so that $\gamma_0^2<\gamma_1^2<\gamma_2^2 \cdots <\gamma_K^2$, the result (22) may be written as

$$\gamma^2 = \frac{\sum_{n=K}^{\infty} a_n^2\gamma_n^2}{\sum_{n=K}^{\infty} a_n^2} = \gamma_K^2 + \frac{\sum_{n=K+1}^{\infty} a_n^2(\gamma_n^2 - \gamma_K^2)}{\sum_{n=K}^{\infty} a_n^2} \geq \gamma_K^2, \quad (23)$$

since $\gamma_n^2>\gamma_K^2$ for $n>K$. Only when $\phi\equiv\psi_{EK}$, will $\gamma^2=\gamma_K^2$. In general, the approximate eigenvalue is too large. A suitable series of functions to use for this extremisation are the corresponding eigenfunctions for the empty guide. For the LSM modes these are

$$\phi_{En} = \sqrt{\frac{\epsilon_{on}}{b}} \cos \frac{n\pi}{b} y, \quad n = 0, 1, 2, \cdots, \quad (24)$$

where ϵ_{on} is the Neumann factor,

$$\epsilon_{on} = \begin{cases} 1, & n = 0 \\ 2, & n > 0. \end{cases}$$

LSE Modes

For the LSE modes, the variational expression corresponding to (19) is

$$\beta^2 \int_0^b \psi_M^2 dy - \int_0^b \left\{ \left(\frac{d\psi_M}{dy}\right)^2 - \left(\kappa k_0^2 - \frac{\pi^2}{a^2}\right)\psi_M^2 \right\} dy = 0. \quad (25)$$

As for the previous case, the approximation to the Kth eigenvalue by that class of functions which are continuous and vanish at $y=0$, b, and are orthogonal to the first $K-1$ eigenfunctions ψ_{Mi} is from above. A suitable set of functions for this extremisation are again the corresponding functions for the empty guide, *i.e.*,

$$\phi_{Mn} = \sqrt{\frac{2}{b}} \sin \frac{n\pi}{b} y, \quad n = 1, 2, \cdots. \quad (26)$$

The above variational expressions are also valid when κ is a discontinuous function of y.

The Approximate Eigenfunctions

This section will consider the solution for the first $N+1$ approximate eigenvalues and corresponding approximate eigenfunctions for the case of the LSM modes. In the previous section, it was shown that the extremisation of (19), with respect to functions which were orthogonal to the first $K-1$ true eigenfunctions, gave an upper bound on the Kth eigenvalue. Since one does not know the true eigenfunctions, the class of functions to be used for the Kth extremisation will be made orthogonal to the first $K-1$ approximate eigenfunctions. It may be shown that this procedure also yields an upper bound on the Kth eigenvalue.[11] The proof is based essentially on the principle that the class of functions which are used for the first $N+1$ approximate eigenfunctions is a narrower class of functions than the complete set of true eigenfunctions.

The substitution of a series of the functions ϕ_{En} into (19) and subsequent extremisation leads to a matrix eigenvalue problem. The resultant matrix is a symmetrical real matrix whose eigenvalues are approximations from above to the first $N+1$ eigenvalues. For each eigenvalue, a solution for an eigenvector exists and the totality of eigenvectors obtained form an orthogonal set with respect to suitable weighting factors. This latter result follows from the well-known theory of real symmetrical matrices.[12] For this reason, the orthogonalization conditions, which were originally imposed upon the functions ϕ_{En}, may be dispensed with.

From this point on, ψ_{En} and γ_n^2 will be used to denote the nth approximate eigenfunction and eigenvalue, respectively. For the Kth approximate eigenfunction take

$$\psi_{EK} = \sum_{n=0}^{N} a_{nK}\phi_{En} \quad (27)$$

where a_{nk} are unknown coefficients to be determined subject to the normalization condition

$$\int_0^b \kappa^{-1}\psi_{EK}^2 dy = \sum_{s=0}^{N}\sum_{n=0}^{N} a_{nK}a_{sK}P_{sn} = 1 \quad (28)$$

where

$$P_{sn} = P_{ns} = \int_0^b \kappa^{-1}\phi_{En}\phi_{Es} dy.$$

Substituting into (19) gives

$$\sum_{n=0}^{N}\sum_{s=0}^{N}\int_0^b \kappa^{-1}\left\{\frac{d\phi_{Es}}{dy}\frac{d\phi_{En}}{dy} - \left(\kappa k_0^2 - \frac{\pi^2}{a^2} + \gamma_K^2\right)\phi_{Es}\phi_{En}\right\} dy = \text{stationary quantity.} \quad (29)$$

Let

$$\int_0^b \kappa^{-1}\left\{\frac{d\phi_{Es}}{dy}\frac{d\phi_{En}}{dy} - \left(\kappa k_0^2 - \frac{\pi^2}{a^2}\right)\phi_{Es}\phi_{En}\right\} dy = T_{sn} = T_{ns}. \quad (30)$$

Thus,

$$\sum_{s=0}^{N}\sum_{n=0}^{N} a_{sK}a_{nK}(T_{sn} - \gamma_K^2 P_{sn}) = \text{stationary quantity.} \quad (31)$$

Equating all $\partial/\partial a_{nk}$ equal to zero for $n=0, 1, \cdots, N$, yields the following set of homogeneous equations

$$\sum_{n=0}^{N} a_{nK}(T_{sn} - \gamma_K^2 P_{sn}) = 0, \quad s = 0, 1, \cdots N. \quad (32)$$

[11] Courant and Hilbert, *op. cit.*, ch. 6.

[12] C. G. Montgomery, R. H. Dicke, and E. M. Purcell, "Principles of Microwave Circuits," M.I.T. Rad. Lab. Ser., McGraw-Hill Book Co., Inc., New York, N. Y., vol. 8, pp. 405–409; 1948.

For a solution, the determinant must vanish and this results in $N+1$ roots for γ_K^2 which are the $N+1$ approximate eigenvalues. For each root, say γ_K^2, a solution for a_{nK} can be obtained, this solution is unique when subjected to the normalization conditions (28). The set of coefficients a_{nK} are orthogonal to the set a_{nR} with respect to the weighting factors P_{sn} for $K \neq R$, *i.e.*,

$$\sum_{n=0}^{N} \sum_{s=0}^{N} a_{nR} a_{sK} P_{sn} = \delta_{RK}. \tag{33}$$

The proof is given in the Appendix.

For the LSE modes, the set of homogeneous equations obtained are

$$\sum_{n-1}^{N} b_{nK}(Q_{sn} - \beta_K^2 \delta_{sn}) = 0, \qquad s = 1, 2, \cdots N, \tag{34}$$

where

$$Q_{sn} = Q_{ns} = \int_0^b \left\{ \frac{d\phi_{Ms}}{dy} \frac{d\phi_{Mn}}{dy} - \left(\kappa k_0^2 - \frac{\pi^2}{a^2} \right) \phi_{Ms} \phi_{Mn} \right\} dy. \tag{35}$$

The vanishing of the determinant yields the first N approximate eigenvalues. The corresponding eigenvectors define the corresponding approximate eigenfunctions. The coefficients b_{nk} are subjected to the normalization condition

$$\sum_{n=1}^{N} b_{nK}^2 = 1, \qquad K = 1, 2, \cdots N,$$

and satisfy the orthogonality conditions

$$\sum_{n=1}^{N} b_{nK} b_{nR} = 0, \qquad R \neq K.$$

Matching of Fields at Junction

Consider the junction of an empty and inhomogeneously filled rectangular guide as illustrated in Fig. 2.

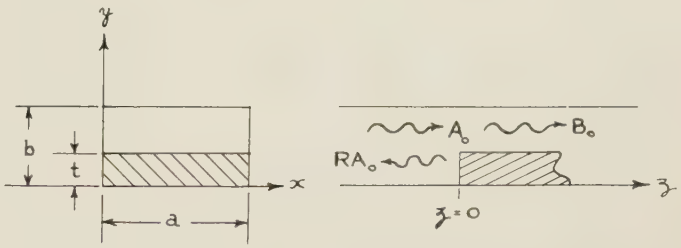

Fig. 2—Junction of an empty and partially filled rectangular guide.

Let an H_{10} mode be incident from the empty guide. The higher order modes excited will consist of an infinite number of the LSM and LSE modes. It will be assumed that only the dominant mode, *i.e.*, the first LSM mode, propagates in either the empty or partially filled guide. For an approximate solution, only a finite number of modes are considered and in the partially filled guide these will be taken as the approximate eigenfunctions as obtained by the R-R method. At the junction $z=0$, the tangential field components are made continuous and this leads to four simultaneous equations which must be solved for the reflection and transmission coefficients. The fields are obtained from the two Hertzian potentials $\vec{\Pi}_E$ and $\vec{\Pi}_M$ by means of (2), (7), (13), and (15). There are two different expressions for E_y and H_y which, however, yield the same results. In writing the continuity equations for the transverse field components, the functions of x and other common factors will be deleted to save space. The following equations, expressing continuity of E_y, H_x, E_x, and H_y, respectively, are obtained

$$\sqrt{\frac{1}{b}} \left(\Gamma_0^2 - \frac{\pi^2}{a^2} \right) (1 + R) A_0 + \sum_{n=1}^{N} A_n \left(\Gamma_n^2 - \frac{\pi^2}{a^2} \right) \sqrt{\frac{2}{b}} \cos \frac{n\pi}{b} y = \sum_{K=0}^{N} B_K \left(\gamma_K^2 - \frac{\pi^2}{a^2} \right) \sum_{n=0}^{N} a_{nK} \kappa^{-1} \sqrt{\frac{\epsilon_{0n}}{b}} \cos \frac{n\pi}{b} y, \tag{36}$$

$$j\omega\epsilon_0 \Gamma_0 (1 - R) \sqrt{\frac{1}{b}} A_0 - j\omega\epsilon_0 \sum_{n=1}^{N} A_n \Gamma_n \sqrt{\frac{2}{b}} \cos \frac{n\pi}{b} y - \sum_{s=1}^{N} \frac{s\pi^2}{ab} C_s \sqrt{\frac{2}{b}} \cos \frac{s\pi}{b} y = j\omega\epsilon_0 \sum_{K=0}^{N} B_K \gamma_K \sum_{n=0}^{N} a_{nK} \sqrt{\frac{2}{b}} \cos \frac{n\pi}{b} y - \sum_{K=1}^{N} \frac{\pi}{a} D_K \sum_{s=1}^{N} \frac{s\pi}{b} b_{sK} \sqrt{\frac{2}{b}} \cos \frac{s\pi}{b} y, \tag{37}$$

$$j\omega\mu \sum_{n=1}^{N} C_n \Gamma_n \sqrt{\frac{2}{b}} \sin \frac{n\pi}{b} y - \sum_{n=1}^{N} \frac{n\pi^2}{ab} A_n \sqrt{\frac{2}{b}} \sin \frac{n\pi}{b} y = -j\omega\mu \sum_{K=1}^{N} D_K \beta_K \sum_{n=1}^{N} b_{nK} \sqrt{\frac{2}{b}} \sin \frac{n\pi}{b} y - \sum_{K=0}^{N} B_K \sum_{n=1}^{N} \frac{n\pi^2}{ab} a_{nK} \kappa^{-1} \sqrt{\frac{2}{b}} \sin \frac{n\pi}{b} y, \tag{38}$$

$$\sum_{n=1}^{N} C_n \left(\Gamma_n^2 - \frac{\pi^2}{a^2} \right) \sqrt{\frac{2}{b}} \sin \frac{n\pi}{b} y = \sum_{K=1}^{N} D_K \left(\beta_K^2 - \frac{\pi^2}{a^2} \right) \sum_{n=1}^{N} b_{nK} \sqrt{\frac{2}{b}} \sin \frac{n\pi}{b} y, \tag{39}$$

where R is the complex reflection coefficient, A_n, B_n, C_n, and D_n are unknown amplitude coefficients, and

$$\Gamma_n^2 = \frac{n^2\pi^2}{a^2} + \frac{n^2\pi^2}{b^2} - k_0^2.$$

The amplitude of the dominant mode on the output side of the junction, *i.e.*, for $z>0$, is B_0.

Multiplying (36) and (37) by

$$\sqrt{\frac{\epsilon_{0n}}{b}} \cos \frac{n\pi}{b} y$$

and (38) and (39) by

$$\sqrt{\frac{2}{b}} \sin \frac{n\pi}{b} y$$

for $n=0, 1, \cdots, N$, in turn, and integrating from $y=0$ to $y=b$, converts these equations to the following algebraic equations

$$\left.\begin{aligned} -k_0^2(1+R)A_0 &= \sum_{K=0}^{N} B_K\left(\gamma_K^2 - \frac{\pi^2}{a^2}\right)\sum_{n=0}^{N} a_{nK}P_{n0}, \\ \left(\Gamma_n^2 - \frac{\pi^2}{a^2}\right)A_n &= \sum_{K=0}^{N} B_K\left(\gamma_K^2 - \frac{\pi^2}{a^2}\right)\sum_{s=0}^{N} a_{sK}P_{sn}, \quad n = 1, 2, \cdots N, \end{aligned}\right\} \tag{40}$$

$$\left.\begin{aligned} \Gamma_0(1-R)A_0 &= \sum_{K=0}^{N} B_K\gamma_K a_{0K}, \\ j\omega\epsilon_0\Gamma_n A_n + \frac{n\pi^2}{ab}C_n &= -j\omega\epsilon_0\sum_{K=0}^{N} B_K\gamma_K a_{nK} + \frac{n\pi^2}{ab}\sum_{K=1}^{N} D_K b_{nK}, \quad n = 1, 2, \cdots N, \end{aligned}\right\} \tag{41}$$

$$\left.\begin{aligned} j\omega\mu C_n\Gamma_n - \frac{n\pi^2}{ab}A_n &= -j\omega\mu\sum_{K=1}^{N} D_K\beta_K b_{nK} - \frac{n\pi^2}{ab}\sum_{K=0}^{N} B_K\sum_{s=1}^{N} a_{sK}J_{sn} \end{aligned}\right\} \tag{42}$$

where

$$\left.\begin{aligned} J_{sn} &= \frac{b^2}{n^2\pi^2}\left[T_{sn} + k_0^2\delta_{sn} - \frac{\pi^2}{a^2}P_{sn}\right], \quad n = 1, 2, \cdots N, \end{aligned}\right\}$$

$$C_n\left(\Gamma_n^2 - \frac{\pi^2}{a^2}\right) = \sum_{K=1}^{N} D_K\left(\beta_K^2 - \frac{\pi^2}{a^2}\right)b_{nK}, \quad n = 1, 2, \cdots N, \tag{43}$$

This latter system of equations may be written in matrix form as a set of four homogeneous matrix equations. For a solution for the amplitude coefficients, the resultant determinant of the over-all system must vanish and this gives the value of the reflection coefficient directly. Alternatively, A_n and C_n may be eliminated by means of (40) and (43), leaving a system of two sets of equations involving B_k and D_k. The required solution for any particular case is obtained in a straightforward manner, but the general details are too lengthy for inclusion here.

An Example

The reflection and transmission coefficients were calculated for an H_{10} mode incident on a partially filled guide, as illustrated in Fig. 2, for values of t/b ranging from 0 to 1. The free space wavelength was 3.14 cm, the dielectric constant was 2.52, and the internal waveguide dimensions were 0.9×0.4 inch. The dominant mode and two evanescent modes (one LSE and one LSM mode) were taken into account in both the empty and partially filled guide. This led to a sixth-order determinant which, however, had fifteen of its elements equal to zero, and was readily reduced to a third-order determinant. This latter determinant gave $(1-R)/(1+R)$ as the ratio of two second-order determinants. In Fig. 3 opposite, the modulus and phase angle of the reflection coefficient are plotted, while the phase angle of the transmitted wave is plotted in Fig. 4. The computed values of the transmission coefficient phase angle are not very accurate, because of their small absolute value. The measured values are also plotted in the above figures and in all cases are within the estimated experimental error from the computed values. The measured values were obtained by the usual tangent method, *i.e.*, by plotting the field minimum position in the partially filled guide vs short circuit position in the empty guide and subsequent analysis of the resultant curve. The dielectric slab was located in the slotted standing-wave detector section.

It is interesting to note that the modulus of the reflection coefficient is within one or two per cent of what

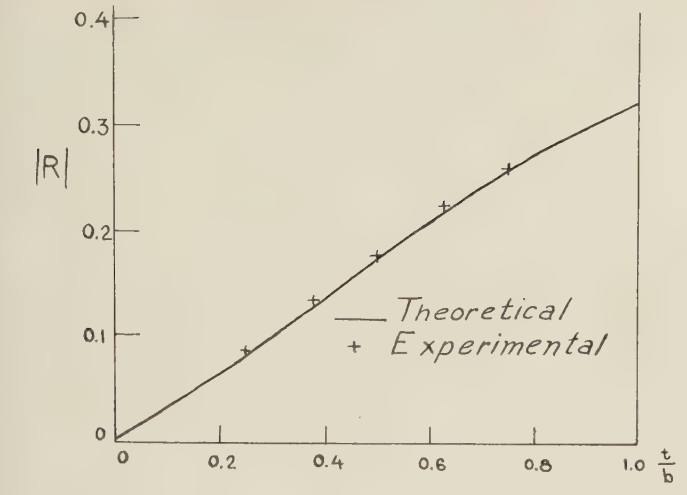

(a)

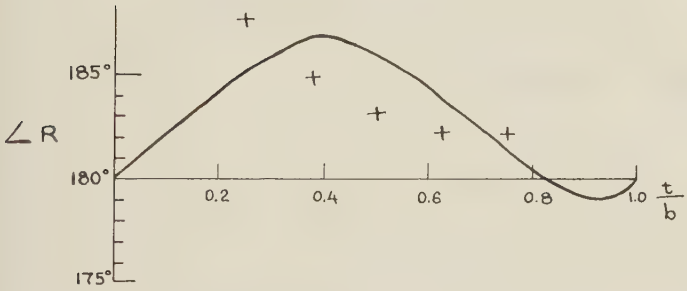

(b)

Fig. 3—(a) Modulus of reflection coefficient, (b) phase angle of reflection coefficient.

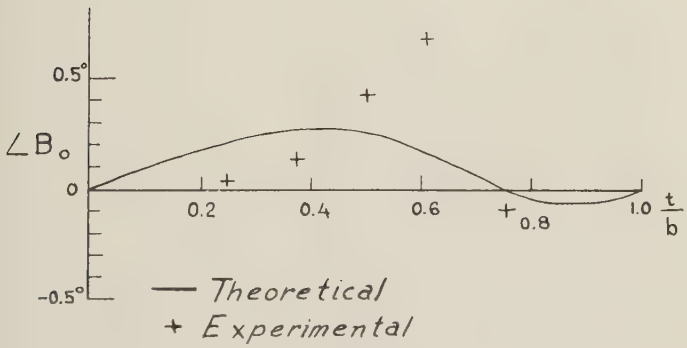

Fig. 4—Phase angle of transmitted wave.

one would compute by assuming that the junction is equivalent to a junction of two transmission lines with characteristic impedances proportional to the respective wavelengths in the empty and partially filled guides. From Fig. 3(b), it is seen that for values of $t/b<0.82$, the phase angle of the reflection coefficient is greater than π radians, while for values of $t/b>0.82$ the phase angle is less than π radians, corresponding respectively to more electric energy than magnetic energy stored in the evanescent modes at the junction and vice versa. The evanescent LSE modes store more magnetic energy, while the evanescent LSM modes store more electric energy, except when the modes are close to propagating, so that

$$\gamma_n^2 < \frac{\pi^2}{a^2} \quad \text{and} \quad \beta_n^2 < \frac{\pi^2}{a^2}.$$

For values of

$$\frac{t}{b} > 0.85, \qquad \gamma_1^2 < \frac{\pi^2}{a^2}$$

and the first evanescent LSM mode stores an excess of magnetic energy at the junction, resulting in a phase angle of less than π radians for the reflection coefficient.

These results are obtained by considering only a small number of modes. If a larger number of modes are taken into account, sufficient compensation may take place so that the phase angle of the reflection coefficient does not become less than π radians for this particular sample. Further calculations are required to clarify this behavior.

The modulus of the transmission coefficient can be computed only when the characteristic impedances of the empty and partially filled guide have been specified. Since these may be specified in any convenient way, the modulus of the transmission coefficient is not unique, the only restriction being that the transmitted power must be equal to the difference between the incident and reflected power.

Conclusion

The use of the R-R method for obtaining approximations to the first N eigenfunctions in a partially filled guide permits one to evaluate, in a straightforward manner, the junction discontinuity existing between an empty and partially filled guide. The reduction in computational labor is considerable, and the solution of transcendental equations and the evaluation of many complex expressions is avoided. The method outlined here may equally well be applied to the evaluation of the parameters of a slotted dielectric interface in free space.

Appendix

Eq. (32) in the text may be written in matrix form as follows

$$\begin{bmatrix} T_{00} & T_{01} \cdots T_{0N} \\ \vdots & \\ T_{N0} & \cdots \quad T_{NN} \end{bmatrix} \begin{bmatrix} a_{0K} \\ \vdots \\ a_{NK} \end{bmatrix} = \gamma_K^2 \begin{bmatrix} P_{00} & \cdots P_{0N} \\ \vdots & \\ P_{N0} & \cdots P_{NN} \end{bmatrix} \begin{bmatrix} a_{0K} \\ \vdots \\ a_{NK} \end{bmatrix} \tag{44}$$

or more briefly as

$$[T_{ij}][a_{jK}] = \gamma_K{}^2[P_{ij}][a_{jK}] \tag{45}$$

and for the Rth solution as

$$[T_{ij}][a_{jR}] = \gamma_R{}^2[P_{ij}][a_{jR}]. \tag{46}$$

Take the transpose of (2) to get

$$\{a_{jK}\}[T_{ji}] = \gamma_K{}^2\{a_{jK}\}[P_{ji}],$$

or

$$\{a_{jK}\}[T_{ij}] = \gamma_K{}^2\{a_{jK}\}[P_{ij}], \tag{47}$$

since $T_{ij}=T_{ji}$ and $P_{ij}=P_{ji}$ and where $\{a_{jk}\}$ is a row matrix. Postmultiply (4) by $[a_{jR}]$, premultiply (3) by $\{a_{jk}\}$, and subtract to get

$$(\gamma_K{}^2 - \gamma_R{}^2)\{a_{jK}\}[P_{ij}][a_{jR}] = 0. \tag{48}$$

When $\gamma_K{}^2 \neq \gamma_R{}^2$, (5) gives

$$\sum_{n=0}^{N}\sum_{s=0}^{N} a_{nK}a_{sR}P_{sn} = 0,$$

upon development of the matrix product. This proves the orthogonality of the eigenvectors.

Coupling Through an Aperture Containing an Anisotropic Ferrite*

DONALD C. STINSON†

Summary—**Coupling through an aperture containing anisotropic ferrites is investigated theoretically by a simple extension of Bethe's small-hole coupling theory to include the dipole moment of the body in the aperture. The magnetic dipole moment of the ferrite body is ordinarily a vector but becomes a tensor upon the application of a magnetostatic field. This new theory is applicable to any situation where Bethe's small-hole coupling theory is valid. Experimental verification was quite satisfactory and was obtained on two Bethe-hole type couplers: one with the waveguides parallel, and the other with the waveguides perpendicular.**

Introduction

THE THEORY of coupling through small windows was formulated by Bethe more than a decade ago.[1] Initially, he found that the amplitudes of the modes excited in a waveguide by a window were proportional to

$$\int \bar{E}_1 \times \bar{H}_2 \cdot \bar{n} ds$$

where field 1 is the excited field, field 2 is a normal mode of the guide, and $\bar{n}$ is the inward normal. Later, he evaluated the integral over the window by developing a lumped-constant theory[2] for small windows and then applied this lumped-constant theory to side windows[3] in waveguides.

Bethe's coupling theory depends upon his lumped-constant theory for small windows, which in turn depends upon replacing the excitation caused by the window by a quantity which is proportional to the following parameters: 1) frequency; 2) the normal electric or tangential magnetic field (exciting field) which would exist at the center of gravity of the window if the window were replaced by a solid metal wall; 3) the corresponding fields (induced fields) of the normal modes which are excited by the window; and 4) lumped constants (polarizabilities) which are functions only of the shape and dimensions of the window. The basis of his lumped-constant theory depends upon the fact that the excitation of the window can be replaced by "equivalent" electric and magnetic dipole moments. These "equivalent" electric and magnetic dipole moments lead him to consider the polarizabilities (which are defined as the "equivalent" dipole moments per unit incident field) as the true lumped constants of the window. This is logical since a window may act as either an inductive or capacitive element, depending upon its location and the propagating mode in the waveguide.

Since his coupling theory applies only to cases where the window and the waveguides are filled with the same isotropic and homogeneous material, it is the purpose of this paper to extend his theory to include cases where the window is completely filled with an anisotropic ferrite. The ferrite involved is anisotropic in the sense that its permeability becomes a tensor upon the application of a magnetostatic field. This extension will be made by adding the "equivalent" magnetic dipole moment of the ferrite to that of the window.

* Manuscript received by the PGMTT, November 7, 1956. This work was supported by the U. S. Navy at the Univ. of Calif. under contract N7-ONR-29529 and is based on a thesis submitted in partial fulfillment of the requirements for the Ph.D. degree, Dept. of Elec. Eng., Univ. of Calif., 1956.

† Lockheed Aircraft Corp., Sunnyvale, Calif.

[1] H. A. Bethe, "Formal Theory of Waveguides of Arbitrary Cross Section," M.I.T. Rad. Lab. Rep. 43-26; March 16, 1943.

[2] H. A. Bethe, "Lumped Constants for Small Irises," M.I.T. Rad. Lab. Rep. 43-22; March 24, 1943.

[3] H. A. Bethe, "Theory of Side Windows in Wave Guides," M.I.T. Rad. Lab. Rep. 43-27; April 4, 1943.

Dipole Moments

The ferrite in the window will affect both the electric and magnetic dipole moments. It is assumed that the isotropic permeability of the ferrite is real and unity for microwaves, and that the dielectric constant is different from unity. The anisotropic permeability of the ferrite is a tensor and is given by expressions in the Appendix. Further, it is postulated that the dipole moment of the filled aperture can be replaced by two other dipole moments: one to account for the aperture itself and the other to account for the material in the aperture. From Bethe[4] it is known that the "equivalent" dipole moments of the empty window are given as

$$-\Pi_w = \mathfrak{M}_1 H_{0l}\bar{l} + \mathfrak{M}_2 H_{0m}\bar{m} \tag{1a}$$

$$\Phi_w = \epsilon_0 \mathcal{P}\bar{n}\cdot\overline{E}_0 \tag{1b}$$

where ϵ_0 is the electric inductive capacity of free space; $\overline{E}_0$, $\overline{H}_0$ are the fields that would exist at the center of gravity of the window if the window were replaced by a metal wall; and $\mathfrak{M}_1$, $\mathfrak{M}_2$, and $\mathcal{P}$ are the magnetic and electric polarizabilities, respectively.

Since the material in the window introduces a magnetization and a polarization, assume that the "equivalent" dipole moments of the body in the window are given as

$$\Pi_b = \mathfrak{M}_1 M_{0l}\bar{l} + \mathfrak{M}_2 M_{0m}\bar{m} \tag{2a}$$

$$\Phi_b = \mathcal{P}\bar{n}\cdot\overline{P}. \tag{2b}$$

Eqs. (2a) and (2b) are deduced by noting that, in general, the electric or magnetic dipole moment of a material is the product of its volume and the polarization or magnetization. Since the polarizabilities $\mathfrak{M}_1$, $\mathfrak{M}_2$, and $\mathcal{P}$ have the dimensions of a volume and depend upon the shape of the window, it is assumed that the volume of the material can be replaced by the polarizabilities of the window when the material is located in the window.

The total "equivalent" magnetic dipole moment of the filled aperture is the sum of (1a) and (2a); the total "equivalent" electric dipole moment of the filled aperture is the sum of (1b) and (2b). Thus, the following expressions are obtained for the total "equivalent" magnetic and electric dipole moments:

$$-\mu_0\overline{\Pi} = \mathfrak{M}_1 B_{0l}{}^{\#}\bar{l} + \mathfrak{M}_2 B_{0m}{}^{\#}\bar{m} \tag{3a}$$

$$\Phi = \mathcal{P}\bar{n}\cdot\overline{D}_0 \tag{3b}$$

where

$$B_0{}^{\#} = \mu_0(\overline{H}_0 - \overline{M}_0)$$

$$\overline{D}_0{}^{\#} = \epsilon_0 Q\overline{E}_0.$$

The quantity Q is a number greater than unity and expresses the fact that the polarization increases the magnitude of the electric dipole moment. The value of Q is determined from experiment and the quantity $\overline{H}_0 - \overline{M}_0$ is determined from the theory of the anisotropic magnetization of a ferrite. This is considered briefly in the Appendix. However, the result is that

$$B_{0l}{}^{\#} = \mu_{ll}{}^{\#}H_{0l} + \mu_{lm}{}^{\#}H_{0m}$$

$$B_{0m}{}^{\#} = \mu_{ml}{}^{\#}H_{0l} + \mu_{mm}H_{0m} \tag{4}$$

where

$$\mu_{ll}{}^{\#} = \mu_{mm}{}^{\#} = \mu_0(1 - \chi_{ll})$$

$$\mu_{lm}{}^{\#} = -\mu_{ml}{}^{\#} = -\mu_0\chi_{lm}.$$

The magnetostatic field is applied in the n direction, while the microwave field is applied in the plane normal to $\bar{n}$.

General Coupling Expressions

In this section, the expressions for the amplitudes of the normal modes coupled by a window between two waveguides is derived. Since this theory is well known, the presentation is brief.

Silver[5] gives the following expressions for the field components of freely propagating modes in waveguides of arbitrary but uniform cross section:

TE waves:

$$H_z = jH_{az}\exp(\mp j\beta_a z); \qquad H_{az} = K_a{}^2(\omega\mu)^{-1}\psi_a$$

$$\overline{E}_t = \overline{E}_{at}\exp(\mp j\beta_a z); \qquad \overline{E}_{at} = \nabla_t\psi_a \times \bar{i}_z$$

$$\overline{H}_t = \pm H_{at}\exp(\mp j\beta_a z); \qquad \overline{H}_{at} = \beta_a(\omega\mu)^{-1}\nabla_t\psi_a. \tag{5}$$

TM waves:

$$E_z = \pm jE_{az}\exp(\mp j\beta_a z); \qquad E_{az} = K_a{}^2\beta_a{}^{-1}\phi_a$$

$$\overline{E}_t = \overline{E}_{at}\exp(\mp i\beta_a z); \qquad \overline{E}_{at} = \nabla_t\phi_a$$

$$\overline{H}_t = \pm \overline{H}_{at}\exp(\mp j\beta_a z); \qquad \overline{H}_{at} = \omega\epsilon\beta_a{}^{-1}\bar{i}_z \times \nabla_t\phi_a. \tag{6}$$

Also,

$$P_{aa} = \frac{1}{2}S_a = \frac{1}{2}\int \overline{E}_{at} \times \overline{H}_{at}\cdot\bar{i}_z ds$$

$$P_{ab} = 0.$$

The functions $\overline{H}_{az}$, E_{at}, E_{az}, $\overline{H}_{at}$ are all real. Further, β_a is the phase constant; ω is the angular frequency; μ and ϵ are the magnetic and electric inductive capacities, respectively; K is the eigenvalue of $(\nabla_t{}^2 + K_a{}^2)F = 0$, where F is ψ_a or ϕ_a as the case may be; and $\omega^2\mu\epsilon = K_a{}^2 + \beta_a{}^2$. Exp $(j\omega t)$ time dependence is assumed and mks units are used throughout. The subscripts a and b in (5) and (6) designate the pair of mode indices mn and should not be confused with the transverse dimensions of rectangular waveguides.

Also needed are expressions for the fields (5) and (6) when the waveguide is shorted at an arbitrary location:

Short at $z = d$, $-\infty \leq z \leq d$:

$$H_z = 2H_{az}\exp(-j\beta_a d)\sin\beta_a(z - d)$$

$$E_z = 2jE_{az}\exp(-j\beta_a d)\cos\beta_a(z - d)$$

$$\overline{E}_t = -2j\overline{E}_{at}\exp(-j\beta_a d)\sin\beta_a(z - d)$$

$$\overline{H}_t = 2\overline{H}_{at}\exp(-j\beta_a d)\cos\beta_a(z - d). \tag{7}$$

[4] Bethe, footnote 2, see (18) and (25).

[5] S. Silver, "Microwave Antenna Theory and Design," McGraw-Hill Book Co., Inc., New York, N. Y., art. 7.3; 1949.

Short at $z=-d$, $-d\leq z\leq\infty$:

$$\begin{aligned} H_z &= -2H_{az}\exp(-j\beta_a d)\sin\beta_a(z+d)\\ E_z &= -2jE_{az}\exp(-j\beta_a d)\cos\beta_a(z+d)\\ \overline{E}_t &= 2j\overline{E}_{at}\exp(-j\beta_a d)\sin\beta_a(z+d)\\ \overline{H}_t &= -2\overline{H}_{at}\exp(-j\beta_a d)\cos\beta_a(z+d). \end{aligned} \tag{8}$$

It has been shown by Bethe[1] and by Silver[6] that the modal amplitudes of the fields set up in an infinite waveguide by a window in the wall are the following:

$$2A_aS_a = -\int_w \overline{E}_1\times\overline{H}_2^-\cdot\bar{n}ds \tag{9}$$

$$2B_aS_a = -\int_w \overline{E}_1\times\overline{H}_2^+\cdot\bar{n}ds. \tag{10}$$

The + and − superscripts on the field $\overline{H}_2$ indicate waves going in the direction of positive or negative z, respectively. The field $\overline{E}_1$ is the electric field set up in the guide by the window. The field $\overline{H}_2$ is a normal mode field of the waveguide when the window is absent. The surface integral is over the window, and the set of axes l, m, n are fixed in the aperture. Further, the l direction is always parallel to the long dimension of the aperture, the m direction is always parallel to its narrow dimension, and n points away from the source of excitation.

Eqs. (9) and (10) are also valid when the excited waveguide is semi-infinite and when either side-window or end-window coupling (iris coupling) is being considered. In either case, it is only necessary to obtain the field $\overline{H}_2$ in (9) and (10) from (7) or (8), rather than from (5) or (6).

The integrals in (9) and (10) have been evaluated by Bethe[7] when the window is empty. When the window is filled with a ferrite, they become

$$\begin{matrix} 2A_aS_a \\ 2B_aS_a \end{matrix} = -j\omega(\mp\mathfrak{M}_1B_{0l}{}^{\#}H_{2l}+\mathfrak{M}_2B_{0m}{}^{\#}H_{2m} + \mathcal{P}D_{0n}{}^{\#}E_{2n}). \tag{11}$$

The fields $\overline{B}_0{}^{\#}$ and $\overline{D}_0{}^{\#}$ are defined in (3) and (4). The upper signs in (11) refer to A_a; the lower signs refer to B_a. For a circular window of radius r, $\mathfrak{M}_1=\mathfrak{M}_2=(4/3)r^3$ and $\mathcal{P}=(2/3)r^3$. For apertures of other shapes, $\mathfrak{M}_1$ always corresponds to an incident magnetic field parallel to the long dimension of the aperture, while $\mathfrak{M}_2$ refers to the narrow dimension of the aperture. It should be noted that $\mathfrak{M}_1$ and $\mathfrak{M}_2$ are functions only of the shape of the window and are not to be confused with the fields 1 and 2. For a specific application, the fields $\overline{E}_2$, $\overline{H}_2$ will be defined by one of the expressions (5)–(8); the fields $\overline{E}_0$, $\overline{H}_0$ will be defined by one of the same expressions except that the mode index a is replaced by b. Eq. (11) is also valid when the waveguides are semi-infinite and for iris coupling between waveguides.

[6] *Ibid.*, art. 9.10.
[7] Bethe, footnote 2, see (51) and (55).

Coupling Through Side Windows

In this section, the general expression (11) is evaluated for two particular cases: 1) the axis of the primary guide (source of excitation) is parallel to the axis of the secondary guide (excited guide), and 2) the axis of the primary guide is perpendicular to that of the secondary guide.[8] The first device is designated as a parallel coupler,[9] and the second device as a perpendicular coupler. The set of axes fixed in the primary waveguide is denoted by ξ, η, ζ; the set of axes fixed in the secondary waveguide is denoted by x, y, z. As mentioned before the set of axes l, m, n are fixed in the aperture. The orientation of the three sets of axes is illustrated in Fig. 1. However, m and z are made parallel for the two

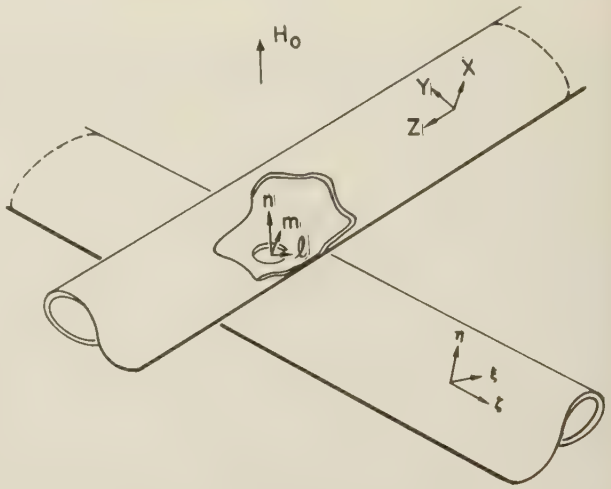

Fig. 1—Orientation of axes.

couplers under consideration. Also, the mode index a applies to the secondary guide, and the mode index b applies to the primary guide. Case A is defined as the situation where identical rectangular waveguides are joined on their broad sides, the TE_{10} mode is propagated, and the window is centered.

[8] Both of these waveguide configurations were considered by A. D. Berk and E. Strumwasser, "Ferrite directional couplers," Proc. IRE, vol. 44, pp. 1439–1446; October, 1956. However, their work was based on the theory of scattering by an obstacle in a waveguide. Further, they considered only ferrite cylinders extending into both waveguides with the coupling holes located at positions of circular polarization of the magnetic field. The theory presented in this paper is also applicable to these situations and is sufficiently different, it is felt, to warrant a paper on these configurations. Such a paper is nearing completion.

[9] This particular waveguide configuration was also studied by R. W. Damon, "Magnetically controlled microwave directional coupler," *J. Appl. Phys.*, vol. 26, pp. 1281–1283; October, 1955. His work is of a qualitative nature and considers a ferrite cylinder located at the position of circular polarization of the magnetic field. Furthermore, his theory is also based upon an extension of Bethe's coupling theory. However, his theory is not of a general nature but merely replaces the magnetic dipole moment of the hole by the magnetic dipole moment of the ferrite body in the hole.

It would seem that we conceived the idea of extending Bethe's coupling theory about the same time. The author originally felt that Bethe's method could be extended to treat the case of an anisotropic ferrite filling the coupling hole (Inst. of Eng. Res., Progress Rep. Ser. No. 60, Issue No. 7, Electronics Res. Lab., Univ. of Calif., Berkeley, Calif., p. 11; January 15, 1955) and later developed such a theory during the summer of 1955 (Progress Rep. Ser. No. 60, Issue No. 10, p. 9; October 15, 1955).

Parallel Coupler, Primary and Secondary Waveguides Infinite

Expressions for A_a and B_a are obtained from (11), where the fields $\overline{E}_2$, $\overline{H}_2$ are specified in (5) or (6). The fields $\overline{D}_0{}^{\#}$, $\overline{B}_0{}^{\#}$ are given in (3) and (4); the fields $\overline{E}_0$, $\overline{H}_0$ are given by (1) or (2). This results in

$$2A_aS_a$$
$$2B_aS_a$$
$$= -j\omega[(\mp\mathfrak{M}_1H_{al}\mu_{ll}{}^{\#} + j\mathfrak{M}_2H_{az}\mu_{ml}{}^{\#})H_{bl} + j(\mp\mathfrak{M}_1H_{al}\mu_{lm}{}^{\#} + j\mathfrak{M}_2H_{az}\mu_{mm}{}^{\#})H_{bz} + \epsilon_0\mathcal{P}QE_{an}E_{bn}]. \quad (12)$$

It should be noted that the transverse components of the fields with the mode indices a and b have been left in the aperture coordinates, since all that was specified thus far is that m and z and ζ are parallel. However, once the orientations of the ln, $\xi\eta$, and xy axes are prescribed, one should insert the field components in their proper coordinate systems. Therefore, if (5) is used in (12), the following expression results for Case A:

$$2A_aS_a$$
$$= -j\omega[\mp\mathfrak{M}_1\pi^2\beta^2(\omega^2\mu^2a^2)^{-1}\mu_{ll}{}^{\#} + \epsilon_0\pi^2a^{-2}Q\mathcal{P}]. \quad (13)$$
$$2B_aS_a$$

In (13), use has been made of the fact that $H_{al} = -H_{az}$, $H_{bl} = -H_{b\xi}$, $E_{an} = E_{a\eta}$, and $E_{bn} = E_{b\eta}$.

If a round coupling hole of diameter d and thickness t is considered, (13) reduces to the following:

$$\begin{matrix} A_aS_a \\ \\ B_aS_a \end{matrix} = -j\omega \exp(-j\beta_bd)\{-(\mp\mathfrak{M}_1H_{al}\mu_{lm}{}^{\#} + j\mathfrak{M}_2H_{az}\mu_{mm}{}^{\#})H_{b\xi}\cos\beta_bd - [(\pm\mathfrak{M}_1H_{al}\mu_{ll}{}^{\#} - j\mathfrak{M}_2H_{az}\mu_{ml}{}^{\#})H_{b\zeta} - j\epsilon_0\mathcal{P}QE_{an}E_{b\eta}]\sin\beta_bd\}. \quad (19)$$

$$A_a$$
$$= -j\pi d^3(3ab\lambda_g)^{-1}F_H[\mp(1-\chi_{zz}) + 1/2(\lambda_g/\lambda_0)^2QF_EF_H{}^{-1}] \quad (14)$$
$$B_a$$

where $F_E = F_H = \exp\{-2\pi t\lambda_c{}^{-1}[1-(\lambda_c/\lambda_0)^2]^{1/2}\}$; λ_c is different for F_E and F_H,[10] since the electric and magnetic fields (although below cutoff) in the window propagate as different modes. It was assumed that the terms F_E and F_H are not affected by the presence of the material in the hole.

Perpendicular Coupler, Primary and Secondary Waveguides Infinite

Expressions for A_a and B_a are again obtained from (11), and the fields $\overline{E}_2$, $\overline{H}_2$ are specified in (5) or (6). However, the fields $\overline{B}_{0\#}$ must be made proportional to the proper fields in the primary waveguide. Thus,

$$B_{0l}{}^{\#} = -\mu_{ll}{}^{\#}H_\zeta - \mu_{lm}{}^{\#}H_\zeta$$
$$B_{0m}{}^{\#} = -\mu_{ml}{}^{\#}H_\zeta - \mu_{mm}{}^{\#}H_\zeta. \quad (15)$$

[10] C. G. Montgomery, "Technique of Microwave Measurements," McGraw-Hill Book Co., Inc., New York, N. Y., p. 862; 1947.

If $\overline{B}_0{}^{\#}$ from (15) and $\overline{D}_0$ from (3) are substituted into (11) after using the proper field components from (1) or (2), the following expression results:

$$2A_aS_a$$
$$= -j\omega[j(\pm\mathfrak{M}_1H_{b\xi}H_{al}\mu_{ll}{}^{\#} - \mathfrak{M}_2H_{b\xi}H_{az}\mu_{mm}{}^{\#})$$
$$2B_aS_a$$
$$\pm\mathfrak{M}_1H_{b\xi}H_{al}\mu_{lm}{}^{\#} + \mathfrak{M}_2H_{b\xi}H_{az}\mu_{ml}{}^{\#} + \epsilon_0\mathcal{P}QE_{b\eta}E_{an}]. \quad (16)$$

With the field components in (16) given by (5), the following expression results for Case A:

$$2A_aS_a$$
$$= -j\omega[\mp\mathfrak{M}_1\pi^2\beta^2(\omega^2\mu^2a^2)^{-1}\mu_{lm}{}^{\#} + \epsilon_0\pi^2a^{-2}\mathcal{P}Q]. \quad (17)$$
$$2B_aS_a$$

For a round coupling hole of diameter d, (17) simplifies to

$$A_a$$
$$= -j\pi d^3(3ab\lambda_g)^{-1}F_H[\mp\chi_{xy} + 1/2(\lambda_g/\lambda_0)^2QF_EF_H{}^{-1}]. \quad (18)$$
$$B_a$$

Perpendicular Coupler, Primary Waveguide Semi-Infinite, Secondary Waveguide Infinite

This situation is the same as the preceding case, except that the fields H_ξ, H_ζ, and E_η are given by (7) with the mode index a replaced by b, instead of by (5) or (6). Thus, for a short at $z=d$, $-\infty \leq z \leq d$, and window at the origin:

Using the field values from (5) in (19), the following relation is obtained for Case A and $\beta_bd = q\pi$, where q is an integer:

$$A_aS_a = -B_aS_a = j\omega\mathfrak{M}_1\pi^2\beta^2(\omega^2\mu^2a^2)^{-1}\mu_{lm}{}^{\#}. \quad (20)$$

For a round coupling hole of diameter d, (20) reduces to

$$A_a = -B_a = -j2\pi d^3(3ab\lambda_g)^{-1}F_H\chi_{xy}. \quad (21)$$

Experimental Results for Side-Window Coupling

In the last section, the amplitudes of the modes coupled by the parallel and perpendicular coupler were evaluated. Here, the coupled power for Case A conditions and for a round coupling hole is calculated. The power coupled into the secondary waveguide by the window is equal to the square of A_a or B_a, since these amplitudes have been derived for unit amplitude incident fields in the primary waveguide.

The coupled power for (14) becomes

$$C_{\parallel}{}^{\pm} = C_0 + 10\log\{[\mp(1 - C'A) + 1/2(\lambda_g/\lambda_0)^2QF\,F_H{}^{-1}]^2 + (C'B)^2\} \quad (22)$$

where

$$C_0 = 20 \log \left[\pi d^2 (3ab\lambda_g)^{-1} F_H\right].$$

The upper and lower signs refer to the mode coupled in the same and opposite directions, respectively, as that of the incident mode. The quantities A, B, and C' are defined in the Appendix. For $d = 0.1235''$, $t = 0.020''$, $F_H = 0.555$, and $f = 9.350$ kmc, the unperturbed magnetic coupling (C_0) is -55.3 db. Thus, (22) becomes

$$C_{\parallel}^{\pm} = -55.3 + \log \left\{ \left[\mp (1 - C'A) + 0.8189Q \right]^2 + (C'B)^2 \right\}. \quad (23)$$

When no magnetostatic field is applied, the ferrite is isotropic, and C' vanishes. Consequently, the factor Q can be evaluated experimentally from the zero magnetostatic field expressions. The value used here in comparing theory and experiment will be an average value rather than one which gives the best agreement. Therefore, the resultant curves will not agree exactly at the zero magnetostatic field point, but this is acceptable since the interest here is in qualitative agreement.

Comparison of the theoretical expression (23) with experimental results is offered in Fig. 2 for a Ferramic A sphere. (Parameter λ_1, is proportional to the damping constant and is defined in the Appendix.) According to theory, the diagonal susceptibility is an even function of the applied magnetostatic field. Since the experimental curves for both directions of magnetostatic field were the same within the limits of experimental error, only the experimental curves for one direction of the applied magnetostatic field is presented.

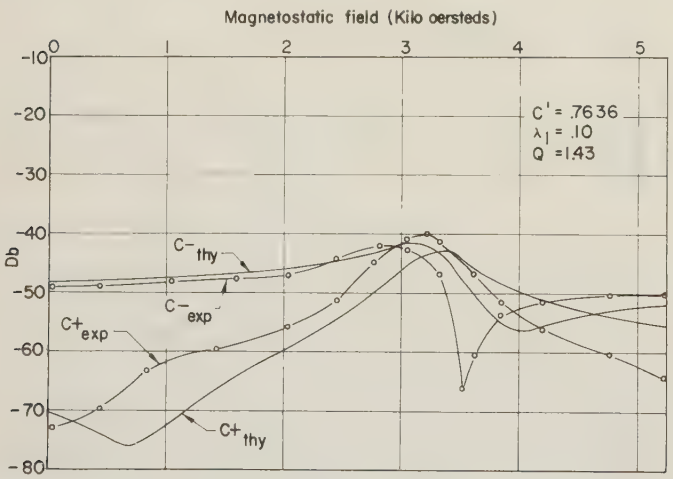

Fig. 2—Forward and reverse coupling in parallel coupler, Ferramic A sphere, both waveguides infinite.

The effect on the reverse coupling of a variation in Q is shown in Fig. 3 for a Ferramic A sphere. Note that an increase in Q increases the initial coupling slightly and also reduces the variation between the maximum values of coupling. This is correct since an increase in Q corresponds to an increase in the dielectric constant, which in turn corresponds to an increase in electric coupling.

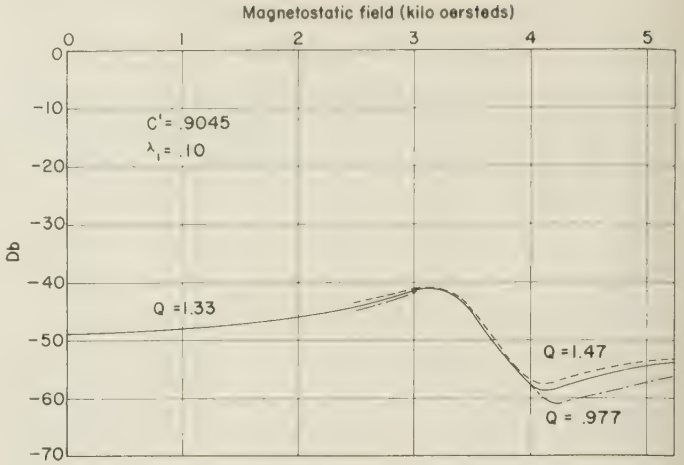

Fig. 3—Reverse coupling in parallel coupler as function of dielectric properties of Ferramic A sphere, both waveguides infinite.

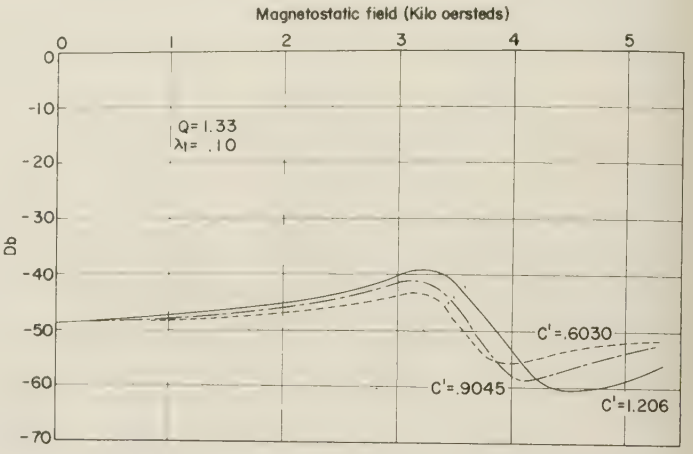

Fig. 4—Reverse coupling in parallel coupler as function of saturation magnetization of Ferramic A sphere, both waveguides infinite.

Fig. 4 shows the effect on the reverse coupling of a variation in saturation magnetization. A reduction of this parameter causes a reduction of the coupled magnetic field, thereby reducing the perturbing effect of the ferrite.

The third parameter of the ferrite studied is the damping constant. The behavior of the reverse coupling for various reduced damping constants is shown in Fig. 5. It should be remembered that the reduced damping constant is the ratio of the actual damping constant to the magnetization (saturation magnetization here). This parameter is the most critical of the three, as one would expect in a resonance-type phenomenon. Note that a reduction of the damping constant causes an increase of the perturbing effect of the ferrite.

The coupled power for (18) becomes

$$C_{\perp}^{\pm} = -49.4 + 10 \log \left[(\pm EF + 0.845Q)^2 + (EG)^2 \right] \quad (24)$$

where $d = 0.1495$ inch, $t = 0.020$ inch, F_H-0.617, $f = 9.350$ kmc, and the unperturbed coupling (C_0) is -49.4 db.

The quantities EF and EG are defined in the Appendix and are odd functions of the applied magnetostatic field. This means that a reversal of the direction of the magnetostatic field results in an interchange of the forward and reverse couplings: that is, $C^+(+) = C^-(-)$ and

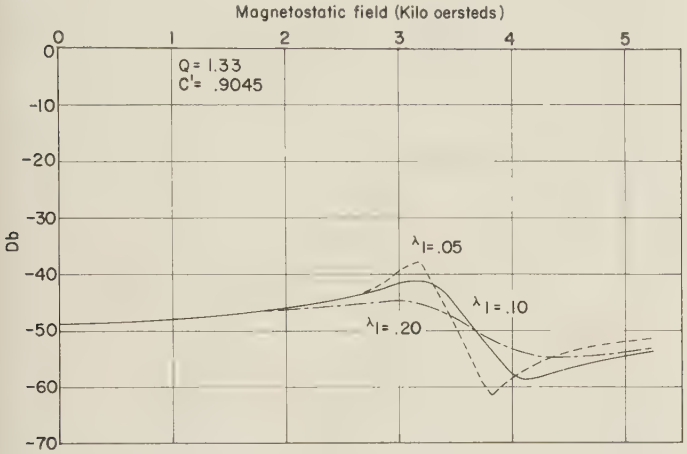

Fig. 5—Reverse coupling in parallel coupler as function of reduced damping constant of Ferramic A sphere, both waveguides infinite.

$C^+(-) = C^-(+)$, where, for instance, $C^+(-)$ indicates the forward coupling for negative values of the applied magnetostatic field. Comparison of theory and experiment for positive values of the applied magnetostatic field is illustrated in Fig. 6 for a Ferramic A sphere. The agreement between theory and experiment is acceptable, although it is felt that better quantitative agreement can be obtained by choosing a smaller value for the reduced damping constant.

The coupled power for (21) becomes

$$C_{\perp}^{\pm} = -43.4 + 10 \log [E^2(F^2 + G^2)] \qquad (25)$$

where C_0 is 6 db larger because of the short in the primary waveguide. The constants of the window are the same as for (24). Since the short in the primary waveguide is located so as to annul the electric coupling, there is no coupling into the secondary waveguide until the ferrite becomes anisotropic. Note in Fig. 7, for Ferroxcube 4-A, that a small value of the magnetostatic field is sufficient to increase the coupling to the value it would normally be when only the electric field couples. Agreement is quite satisfactory except for small values of applied magnetostatic field. One sees very clearly that the theoretical curve predicts too large a coupling initially. This is probably caused by the fact that the actual magnetization has been replaced by the saturation magnetization. The agreement at resonance could also be improved by using a smaller reduced damping constant.

Although the theory derived is valid only when the coupling aperture is completely filled with a material, it is of interest to examine experimentally the effect on

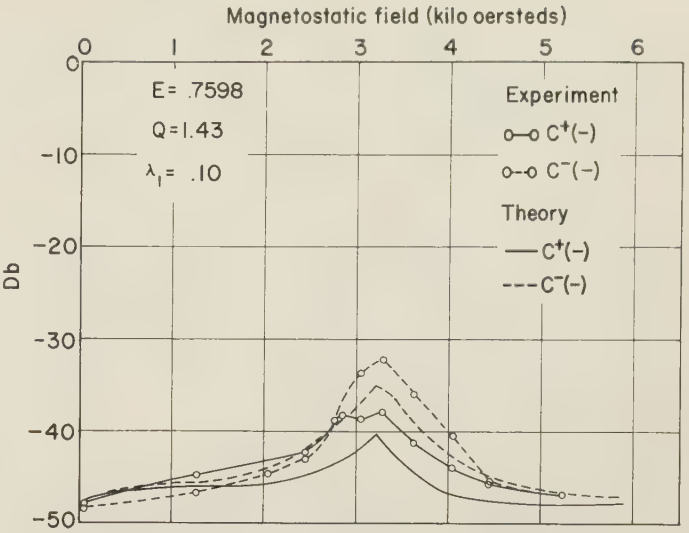

Fig. 6—Forward and reverse coupling in perpendicular coupler, Ferramic A sphere, both waveguides infinite.

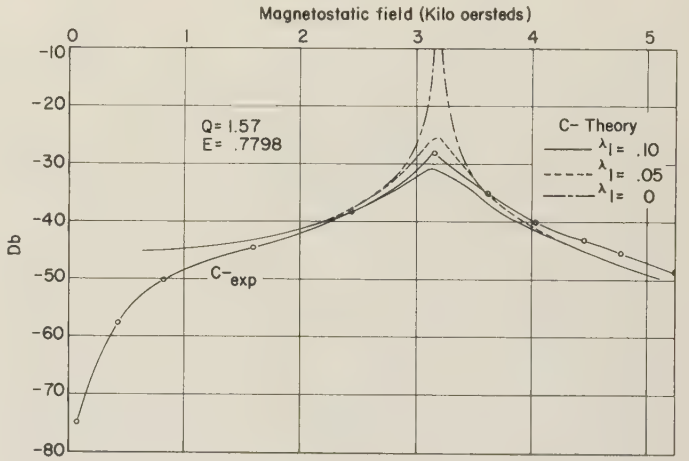

Fig. 7—Reverse coupling in perpendicular coupler as function of reduced camping constant of Ferroxcube 4-A sphere, primary waveguide semi-infinite, secondary waveguide infinite.

the magnetic coupling of partially filling the aperture with a ferrite. In this case, shorts were used to annul the electric coupling. However, the electric coupling could also be excluded by properly choosing the location of the window. For comparison purposes, the magnetic coupling curves for a spherical, a rectangular, and a disk-shaped Ferroxcube 4-A sample are shown in Fig. 8. The spherical and disk-shaped samples were placed in a round aperture; the rectangular sample was placed in a rectangular aperture with the long dimension parallel to the axis of the primary waveguide. These were all obtained with the perpendicular coupler and for Case A conditions. The curves for the rectangular and disk-shaped samples are very similar. However, the curve for the spherical sample has a much larger amplitude at resonance than either of the other curves, and its resonance also occurs for a much smaller value of applied magnetostatic field.

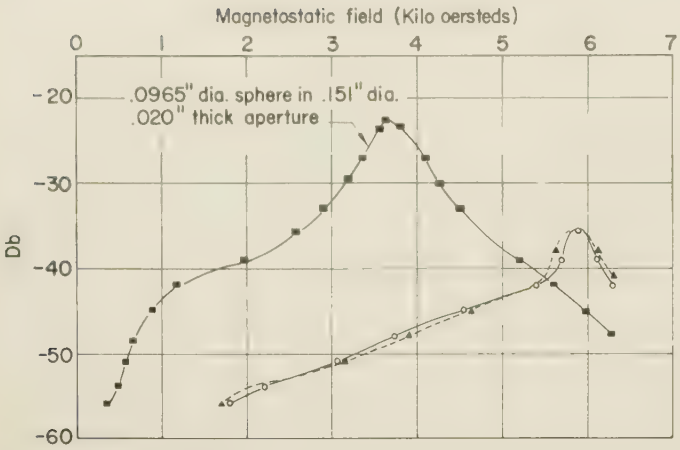

Fig. 8—Effect on magnetic coupling in perpendicular coupler by partially filling aperture with various shaped Ferroxcube 4-A samples. ■ 0.0965 inch dia. sphere in 0.151 inch dia., 0.020 inch thick aperture. ▲ 0.250 inch×0.075 inch×0.020 inch thick sample in aperture of same size and 0.010 inch thick. ○ 0.100 inch dia., 0.021 inch thick disk in 0.151 inch dia., 0.020 inch thick aperture.

Conclusion

The theory presented is satisfactory for small samples, although the sample sizes used here are near the upper size limit for these materials. For materials with smaller losses, it would be necessary to use even smaller sample sizes in order to avoid dimensional effects.

The theory of the magnetization of the ferrite is the weak link in this coupling theory. Consequently, any effort to apply this coupling theory to larger samples would require a proper modification of the magnetization expressions. It is felt that the dimensional effects in the sample enter in two ways. The first occurs because of the inhomogeneity in magnetization and can be accounted for by properly choosing the constants of the ferrite. In other words, we can choose values for the constants in such a manner as to obtain good agreement between theory and experiment but these values will not necessarily be the true constants of the material. The other effect occurs when the sample becomes electrically large and acts as a resonator. The present coupling theory does not account for this.

Appendix

Tensor Magnetization of a Ferrite

The purpose here is to evaluate the susceptibilities defined in (4). These susceptibilities result when a ferrite is made anisotropic by the application of a magnetostatic field in the n direction. Although this has been done by several authors,[11,12] part of the work is repeated here for continuity. The form followed is that given by Beljers.[11]

The fundamental equation for the magnetization, $\overline{M}$, is the following:

$$\dot{\overline{M}}\gamma^{-1} = \overline{M} \times \overline{B} - \lambda(\overline{B} - \overline{B}\cdot\overline{M}M^{-2}\overline{M}) \qquad (26)$$

where $\gamma = -ge/2m$ (the magnetomechanical ratio, a negative quantity for an electron); e and m are the electron charge and mass, respectively; g is the spectroscopic splitting factor; λ is a damping constant; and $\overline{B} = \mu_0(\overline{H} + \overline{M})$. The damping constant can be introduced in different manners, but the two commonly used forms both give identical results for the order of approximation used here.[13]

For the problem under consideration, the following is chosen:

$$\begin{aligned} H_l &= h_l - (N_l - 1/3)M_l \\ H_m &= h_m - (N_m - 1/3)M_m \\ H_n &= H - (N_n - 1/3)M \end{aligned}$$

where the N_i's are the demagetizing factors, the quantities h_l and h_m are the applied microwave magnetic fields, and H is the applied magnetostatic field.

Consistent with the usual assumption, the microwave magnetizations are as follows:

$$\begin{aligned} M_l = \gamma M L^{-1}[h_l\{\mu_0^2\gamma(1+\lambda_1^2)[H + M(N_m - N_n)] \\ - j\omega\mu_0\lambda_1\} - j\omega\mu_0 h_m] \\ M_m = \gamma M L^{-1}[h_m\{\mu_0^2\gamma(1+\lambda_1^2)[H + M(N_l - N_n)] \\ - j\omega\mu_0\lambda_1\} + j\omega\mu_0 h_l] \end{aligned} \qquad (27)$$

where

$$\begin{aligned} L = &-\omega^2 + \mu_0^2\gamma^2(1+\lambda_1^2)[H + M(N_l - N_m] \\ &\cdot [H + M(N_n - N_m)] - 2j\omega\mu_0\gamma\lambda_1 H \\ &- j\omega\mu_0\gamma\lambda_1 M(N_l - N_m - 2N_n), \end{aligned}$$

$\lambda_1 = \lambda/M$ is a reduced damping constant, and M is the saturation magnetization in the n direction. When the ferrite sample is spherical, the magnetizations simplify considerably to the following:

$$\begin{aligned} M_l &= \chi_{ll}h_l + \chi_{lm}h_m \\ M_m &= \chi_{ml}h_l + \chi_{mm}h_m \end{aligned} \qquad (28)$$

where

$$\begin{aligned} \chi_{ll} &= \chi_{llr} + j\chi_{lli} \\ \chi_{lm} &= \chi_{lmr} + j\chi_{lmi}. \end{aligned}$$

For computational purposes, the following substitutions are made:

$$\begin{aligned} \gamma' &= -\gamma \\ x &= \mu_0\gamma' H\omega^{-1}(1+\lambda_1^2)^{1/2}. \end{aligned} \qquad (29)$$

[11] H. G. Beljers, "Measurements on gyromagnetic resonance of a ferrite using cavity resonators," *Physica*, vol. 14, pp. 629–641; Februrary, 1949.

[12] C. L. Hogan, "The microwave gyrator," *Bell Sys. Tech. J.*, vol. 31, pp. 1–31; January, 1952.

[13] We introduce our damping constant according to Landau and Lifschitz (see Beljers, *op. cit.*).

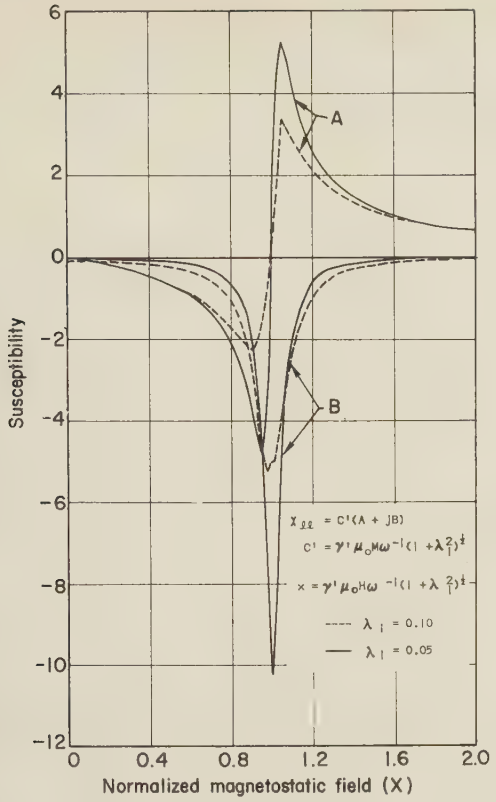

Fig. 9—Diagonal susceptibility of small ferrite sphere as function of normalized applied magnetostatic field.

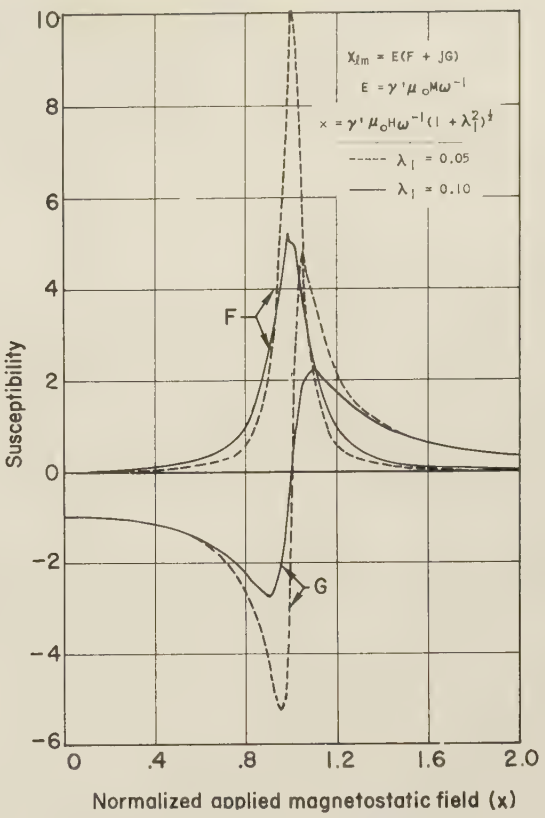

Fig 10—Nondiagonal susceptibility of small ferrite sphere as function of normalized applied magnetostatic field.

Thus, the components of the susceptibilities become

$$\begin{aligned} \chi_{llr} &= C'A \\ \chi_{lli} &= C'B \\ \chi_{lmr} &= EF \\ \chi_{lmi} &= EG \end{aligned} \tag{30}$$

where

$$\begin{aligned} C' &= \gamma'\mu_0 M\omega^{-1}(1+\lambda_1^2)^{1/2} \\ A &= a/b \\ B &= -a'/b \\ E &= \gamma'\mu_0 M\omega^{-1} \\ F &= c/b \\ G &= -c'/b \\ a &= x\{x^2 - [1 - 2\lambda_1^2(1+\lambda_1^2)^{-1}]\} \\ a' &= \lambda_1(x^2+1)(1+\lambda_1^2)^{-1/2} \\ c' &= 1 - x^2 \\ c &= 2\lambda_1 x(1+\lambda_1^2)^{-1/2} \\ b &= x^4 - 2x^2[1 - 2\lambda_1^2(1+\lambda_1^2)^{-1}] + 1. \end{aligned}$$

Note also that $\chi_{mm} = \chi_{ll}$, and $\chi_{lm} = -\chi_{ml}$.

In most ferrite work the susceptibilities are defined so that

$$\begin{aligned} M_l &= \chi h_l - jKh_m \\ M_m &= jKh_l + \chi h_m \end{aligned} \tag{31}$$

where

$$\begin{aligned} \chi &= \chi' - j\chi'' \\ K &= K' - jK''. \end{aligned}$$

Using this notation,

$$\begin{aligned} \chi' &= C'A \\ \chi'' &= -C'B \\ K' &= -EG \\ K'' &= -EF. \end{aligned} \tag{32}$$

For the simple case of no damping, the imaginary parts of both χ and K vanish. Eq. (33) then reduces to the one that is characteristic of a gyrotropic medium.

In order to understand better the behavior of the permeability of the ferrite when it is anisotropic, several families of curves of χ_{ll} and χ_{lm} are plotted as a function of x, with M and λ_1 as parameters; Fig. 9 is a plot of χ_{ll} vs x for $\lambda_1 = 0.05$ and $\lambda_1 = 0.10$. Similarly, Fig. 10 is a plot of χ_{lm} vs x for $\lambda_1 = 0.05$ and $\lambda_1 = 0.10$. In both figures, the coefficients C' and E were set equal to unity. It should also be noted that χ_{ll} is an even function of the applied magnetostatic field, whereas χ_{lm} is an odd function of the applied magnetostatic field.

Acknowledgment

I would like to thank Dr. D. J. Angelakos for his aid with the theoretical aspects of this work and Seymon Hersh for his help with the manuscript.

An Adjustable Sliding Termination for Rectangular Waveguide*

ROBERT W. BEATTY†

Summary—A new adjustable sliding termination for rectangular waveguide has been developed. The termination is of simple design and can easily be adjusted to have reflection coefficients from zero to nearly unity in magnitude and any desired phase. In addition to the usual applications of adjustable sliding terminations for rectangular waveguide, it provides a suitable design for an adjustable transfer or secondary standard of impedance for rectangular waveguide systems.

Introduction

ADJUSTABLE sliding terminations for rectangular waveguide are useful for a variety of purposes, including calibration of microwave impedance measuring devices, obtaining the directivity of directional couplers, and determining the parameters of waveguide junctions.

An adjustable sliding termination for rectangular waveguide was described by Grantham in 1951.[1] Several years later, a similar termination was produced commercially. This termination[2] differed from its predecessor in details of construction of the dissipative element and the reflecting antenna. Both of these terminations were designed primarily to provide minimum reflection and could not be adjusted over a wide range of vswr (voltage standing-wave ratio). The commercial termination has a vswr range of 1.005 to 1.15. The principle of the double slug tuner was used[3] to obtain an adjustable sliding termination with a somewhat greater range of adjustment. An adjustable sliding termination having a wide range of vswr was described by Kato and Sakai,[4] but it was not possible to adjust this termination for cancellation of reflections.

Principle of Operation

As shown in the diagram of Fig. 1, this termination slides inside a rectangular waveguide and consists of a short-circuiting piston to which is attached a dissipative strip supported by a dielectric rod, which can rotate and slide relative to the piston. The phase of the reflection from the strip can be varied by sliding the strip, while the magnitude of the net reflection from the short circuit can be varied by rotating[5] the strip. With independent control of these two motions, complete cancellation of reflections can be obtained. On the other hand, with the strip surface perpendicular to the electric field, minimum losses occur in the strip and almost perfect reflection is obtained. It is possible to adjust the termination to any intermediate condition, then to slide the entire assembly, to obtain almost any reflection coefficient desirable.

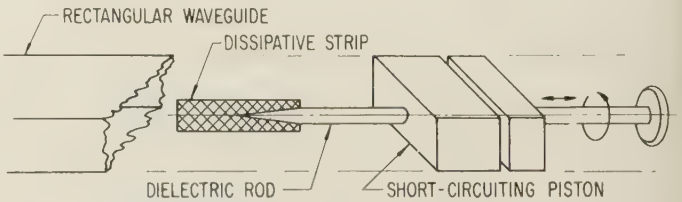

Fig. 1—Essential features of termination.

Theory

Apparently, the analysis of the fields inside a rectangular waveguide containing an arbitrarily positioned dissipative strip has not yet been published. Lacking this basic information, a rigorous analysis of the action of this termination has not been attempted. An approximate study based upon microwave circuit theory is given below.

As shown in Fig. 2, the termination can be regarded as an attenuator terminated in a short-circuited line of variable length. In terms of the scattering coefficients[6] S_{11}, S_{12}, and S_{22} of the attenuator, the input voltage reflection coefficient is

$$\Gamma_1 = S_{11} - \frac{S_{12}^2}{S_{22} + e^{j2\beta l}}, \tag{1}$$

where $\beta = 2\pi/\lambda_G$, and λ_G equals the wavelength in the waveguide. The condition for cancellation of reflections ($\Gamma_1 = 0$) is

$$S_{12}^2 = S_{11}e^{j2\beta l}(1 + S_{22}e^{-j2\beta l}). \tag{2}$$

* Manuscript received by the PGMTT, November 19, 1956.

† Natl. Bur. of Standards, Boulder, Colo.

[1] R. E. Grantham, "A reflectionless wave-guide termination," *Rev. Sci. Instr.*, vol. 22, pp. 828–834; November, 1951.

[2] W. A. Andrews, U. S. Patent No. 2,701,861.

[3] R. C. Ellenwood and W. E. Ryan, "A uhf and microwave matching termination," PROC. IRE, vol. 41, pp. 104–107; January, 1953.

[4] N. Kato and T. Sakai, "Waveguide Type Variable Impedance Circuit and its Application for Rieke Diagram," Rep. of the Microwave Communication Res. Committee in Japan, p. 7; December, 1955.

[5] G. C. Southworth, "Principles and Applications of Waveguide Transmission," D. Van Nostrand Co., Inc., New York, N. Y., pp. 374–376; 1950. An attenuator employing a rotating strip is described.

[6] Scattering coefficients are the elements of the scattering matrix. See C. G. Montgomery, R. H. Dicke, and E. M. Purcell, "Principles of Microwave Circuits," M.I.T. Rad. Lab. Ser., McGraw-Hill Book Co., Inc., New York, N. Y., vol. 8, pp. 146–149; 1948.

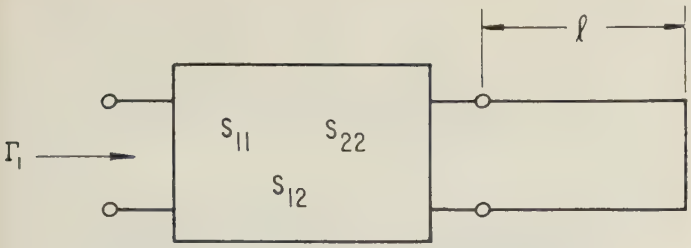

Fig. 2—Approximate equivalent circuit representation.

Normally, $|S_{11}|$ and $|S_{22}|$ are much less than unity, and the approximate condition for cancellation of reflections is

$$S_{12}^2 \approx S_{11}e^{j2\beta l}. \tag{3}$$

Rotation of the strip will, in general, change both $|S_{12}^2|$ and $|S_{11}|$. A typical variation of these quantities with θ (the angle between the electric field direction and the normal to the surface of the strip) is shown in Fig. 3(a). At the angle θc, the magnitudes of S_{12}^2 and S_{11} are equal, and it is possible to obtain cancellation of reflections by sliding the strip, varying l. If the strip is too short, $|S_{12}^2|$ will not decrease enough to equal $|S_{11}|$, as shown in Fig. 3(b). However, it is possible to increase $|S_{11}|$ by adding a reflecting object at the end of the strip, so that cancellation of reflections can again be obtained as in Fig. 3(c).

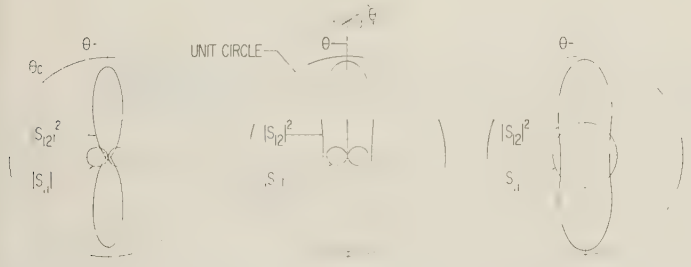

Fig. 3—Dependence of $|S_{11}|$ and $|S_{12}^2|$ upon rotation of thin rectangular strip: (a) rectangular strip 0.35 inch×1.5 inches, (b) rectangular strip 0.35 inch×0.75 inch, and (c) metal reflector added to increase $|S_{11}|$.

Design

A number of considerations can influence the design of the termination. If the primary need is for a reflection-free termination, with no need for a wide range of vswr, it seems advisable to use a thicker strip of dissipative material such as Synthane. The extra thickness can give added strength to a long, tapered strip, which will require less rotation to achieve cancellation of reflection, and give a smoother adjustment which is less frequency sensitive than with shorter strips. Examples of such a design are shown in Fig. 4, and a diagram of typical variation of $|S_{12}^2|$ and $|S_{11}|$ is shown in Fig. 5.

If a wide range of adjustment of vswr is desired, a thin strip is required. IRC resistance strip may be used

Fig. 4—Adjustable sliding loads for different waveguide sizes.

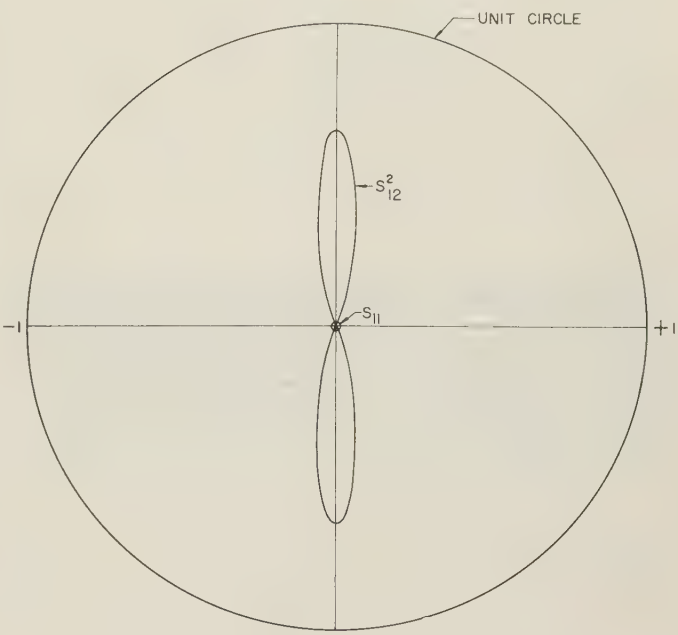

Fig. 5—Variation of $|S_{11}|$ and $|S_{12}^2|$ with rotation of thick tapered strip.

to obtain fairly high ranges, but a dissipative film on a thin mica strip is capable of greater range. A thin film has little strength and it may be desirable to add a reflecting disk or rod as shown in Fig. 6. The disk or rod permits a shorter strip to be used, while retaining the ability to cancel reflections.

Control of the mechanical motion required may be achieved by the arrangements shown in Figs. 7 and 8, next page. Independent control of the sliding and rotation of the strip is achieved in both arrangements, but in Fig. 8, the strip may be rotated and slid by hand until the clamping screw is used, which clamps the dielectric rod supporting the strip so that it can only be moved by the limited fine adjustments A and B. One adjustment of sliding (knob A) and an independent adjustment of rotation (knob B) are provided.

As a matter of practical interest, an adjustable load having satisfactory performance over the recommended frequency range of RG-52/U waveguide was constructed, using a rectangular IRC resistance strip 200 ohms per square, 0.35 inch×1.50 inches. The strip was not tapered, but mounted on a dielectric rod as was shown in Fig. 1.

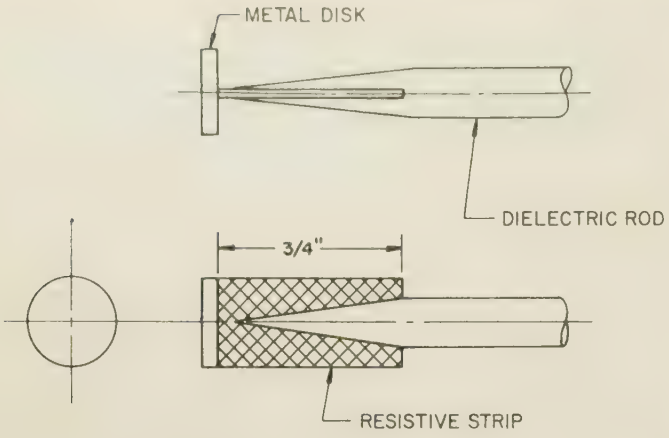

Fig. 6—Short strip and reflecting disk.

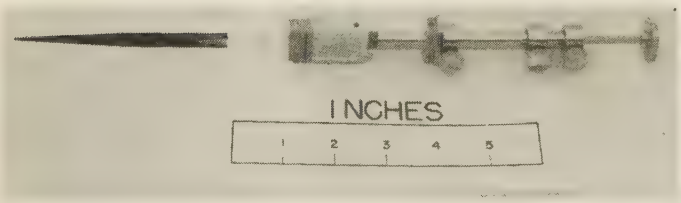

Fig. 7—Mechanical controls permitting independent adjustment of rotation and sliding, with control locking.

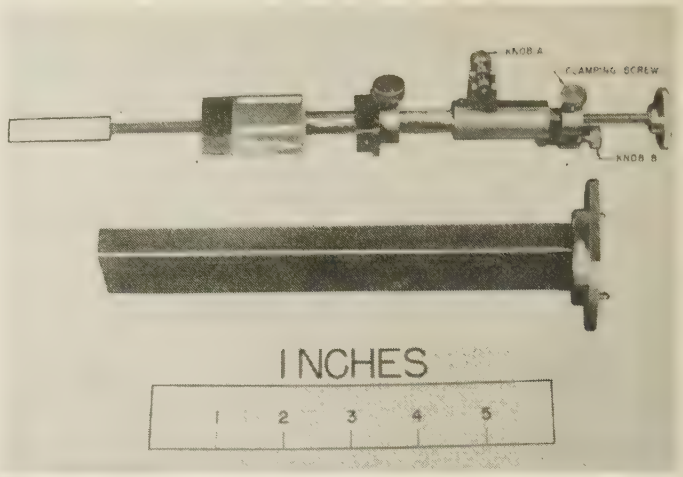

Fig. 8—Mechanical controls permitting coarse manual adjustment and locking, followed by fine independent adjustments of rotation and sliding.

Acknowledgment

The writer is indebted to J. Lowenbach, W. Foote, and W. Clore of the Instrument Shop, who made experimental models and contributed to the mechanical design, to E. Niesen, who made the measurements upon which Figs. 3 and 5 are based, and to Dr. D. M. Kerns and Dr. D. G. Burkhard, who reviewed the paper.

Field Displacement Isolators at 4, 6, 11, and 24 KMC*

S. WEISBAUM† AND H. BOYET‡

Summary—**Performance of ferrite field displacement isolators at various frequency bands is described. Single and double-slab isolators have been constructed in rectangular waveguide. Four single-slab isolators are reported in the following frequency bands: 3700–4200 mc; 5925–6425 mc; 10,700–11,700 mc and 23,500–24,470 mc; one double-slab isolator is described in the frequency range 10,700–11,700 mc.**

Introduction

THE field displacement isolator consists of a rectangular slab of ferrite partially filling a rectangular waveguide.[1] The ferrite slab is transversely magnetized and has resistance material appropriately disposed on one of its sidefaces (see Fig. 1, opposite). Basically, this device produces isolation for the following reasons: When a microwave travels through the device in a given direction, the polarization of the rf magnetic field in the plane perpendicular to the biasing magnetic field is opposite in sense to that which it would be for the reverse direction of propagation. As a result, the rf magnetic field interacts differently with the spin precessions of the electronic magnetic moments for the two directions of propagation, and this leads to different electric field distributions across the waveguide for the two directions of propagation[2] (see Fig. 2). If this difference in electric field strengths at one face of the ferrite can be made large, resistance material, suitably placed on the ferrite, will attenuate reverse traveling waves to a much larger degree than forward traveling waves, and isolation is thereby effected.

The above principles have been applied with success to an isolator at 6 kmc (0.2-db forward loss, 30-db reverse loss, 1.06 vswr over the band 5925–6425 mc). The

* Manuscript received by the PGMTT, December 5, 1956.

† RCA, New York, N. Y. Formerly with Bell Telephone Labs., Murray Hill, N. J.

‡ Bell Telephone Labs., Murray Hill, N. J.

[1] A. G. Fox, S. E. Miller, and M. T. Weiss, "Behavior and applications of ferrites in the microwave region," *Bell Sys. Tech. J.*, vol. 34, pp. 5–103; January, 1955.

[2] B. Lax, H. J. Button, and L. M. Roth, "Ferrite phase shifters in rectangular waveguide," *J. Appl. Phys.*, vol. 25, pp. 1413–1419; November, 1954.

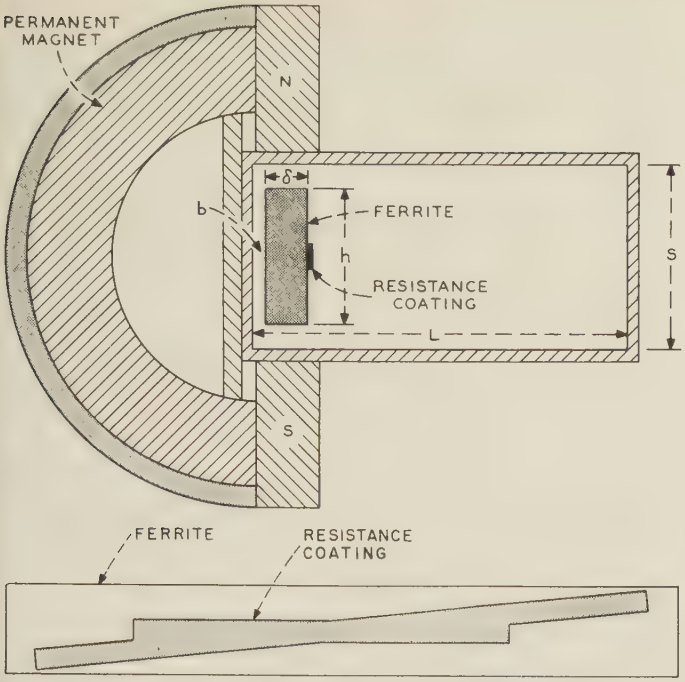

Fig. 1—Assembly of ferrite, resistance material, magnet, and waveguide in single-slab ferrite field displacement isolator and disposition of resistance material on ferrite slab.

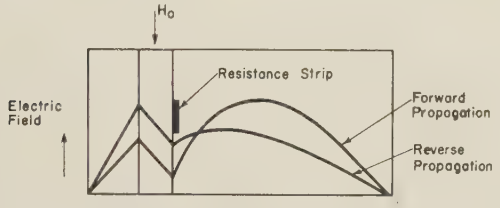

Fig. 2—Theoretical transverse electric field distribution in single-slab isolator, full height ferrite.

experimental, theoretical, and design details for this device have been elaborated upon elsewhere.[3] Subsequent work with the field displacement isolator has met with success at other frequency bands: 3700–4200 mc; 10,700–11,700 mc; and 23,500–24,470 mc. The purpose of this paper is to summarize the performance of field displacement isolators developed to date in the various frequency bands at Bell Telephone Laboratories.

Before doing so, it is desirable to discuss briefly two important features of the field displacement isolator: the partial height ferrite geometry used, and the disposition of the resistance material. Less than full height ferrite slabs are used to insure good match into the isolator. With such partial height slabs the boundary requirements on the top and bottom faces of the ferrite are less stringent and a smaller portion of the incident wave needs to be converted into a reflected wave to satisfy the boundary conditions. This results in considerably smaller vswr for the partial height ferrite than for the full height ferrite.

A disposition of the resistance material was conceived which makes use of the nonreciprocal nature of the longitudinal components of electric field set up by the partial height ferrite.[3] Resistance material is placed in a region where both the fundamental transverse component and longitudinal component of electric field are small for the forward direction but, as a result of the nonreciprocity of both components, both may be large at the resistance material for the backward direction of propagation. This configuration of resistance material is shown in Fig. 1. The actual resistance material is a baked resistance coating of graphite and resin covered by a baked clear coating, similar to that used in attenuator vanes. The length of the resistance strips is critical in determining the forward and reverse attenuations. Experiments indicate that the attenuation is not a linear function of length of resistance strip.

As an aid in the design of isolators at various frequency bands, we have relied to a first approximation on a scaling[3] of transverse geometric quantities and magnetic quantities. Thus starting from a frequency ω, we may scale to a new frequency $f\omega$ (f any number) by changing all waveguide and ferrite geometries and spacings by a factor $1/f$ and all magnetic quantities by a factor f (see Appendix).

Performance

In Figs. 3, 4, 5, and 6, next page, we show graphically the performance of the field displacement isolator at 4 kmc, 6 kmc, 11 kmc, and 24 kmc, respectively, together with the values of the operating parameters. $4\pi M_s$ denotes the saturation magnetization of the ferrite. The other symbols are defined in Fig. 1. The length of ferrite is 5 inches in each isolator, but shorter lengths are currently being investigated.

In the 24-kmc case the largest $4\pi M_s$ ferrite available was 4900 Gauss.

A double-slab field displacement isolator[4] was constructed at 11 kmc. In this construction the two slabs are located symmetrically with respect to the center line of the rectangular waveguide. The two slabs are magnetized by equal but oppositely directed magnetic fields so that the spin precessions in each interact equally with the rf magnetic fields at each slab. Each slab has a resistance strip configuration identical with that shown in Fig. 1. The length of ferrite slabs is 5 inches. Performance and operating conditions are shown in Fig. 7.

Table I, p. 197, summarizes performance of most recent isolator models. All isolators are single slab except where noted.

[3] S. Weisbaum and H. Seidel, "The field displacement isolator," *Bell Sys. Tech. J.*, vol. 35, pp. 877–898; July, 1956.

[4] S. Weisbaum and H. Boyet, "A double slab ferrite field displacement isolator at 11 kmc," Proc. IRE, vol. 44, pp. 554–555; April, 1956.

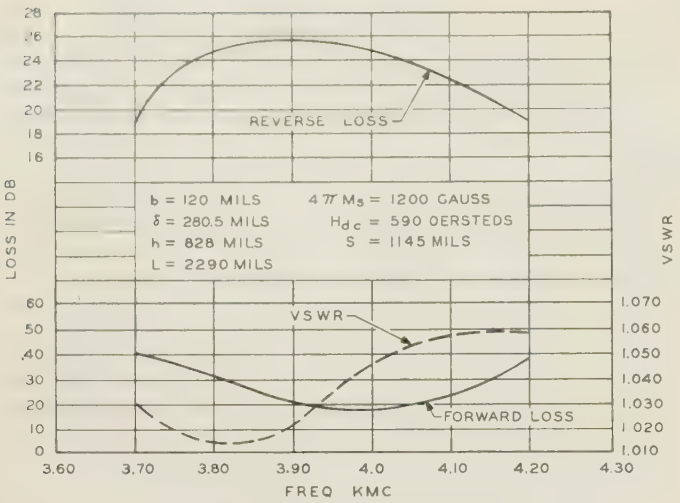

Fig. 3—Performance of single-slab field displacement isolator at 4 kmc.

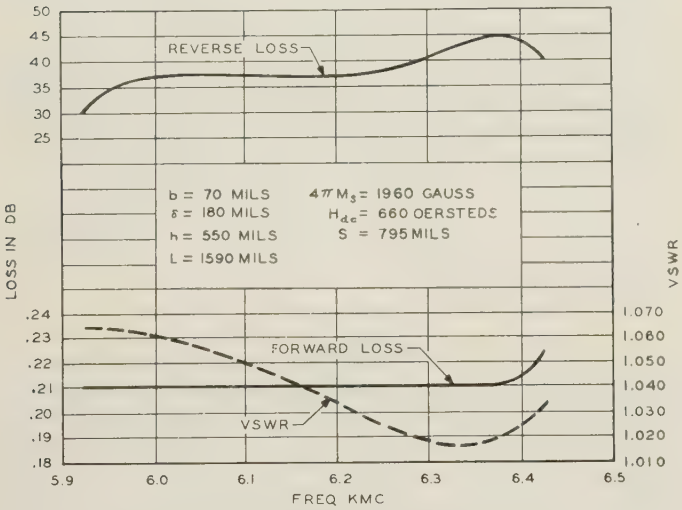

Fig. 4 Performance of single-slab field displacement isolator at 6 kmc.

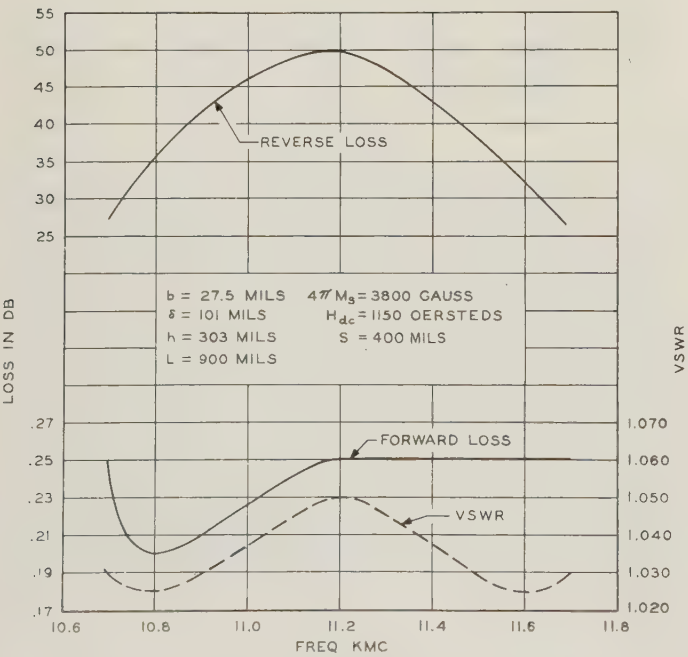

Fig. 5—Performance of single-slab field displacement isolator at 11 kmc.

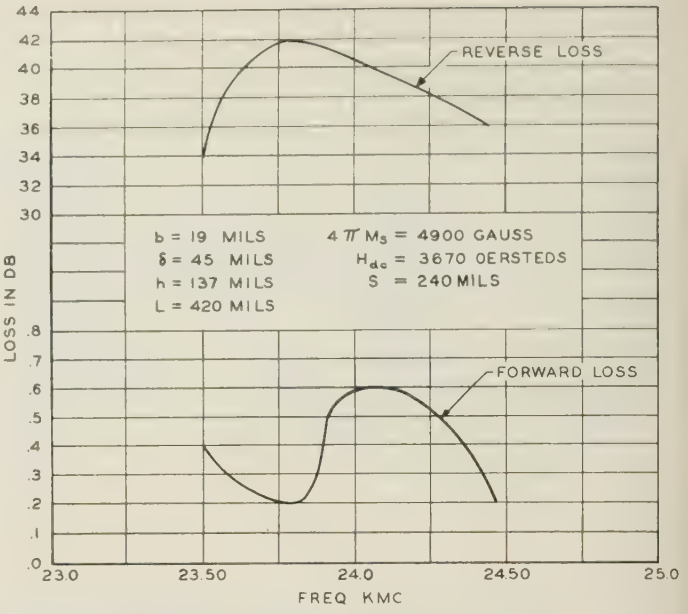

Fig. 6—Performance of single-slab displacement isolator at 24 kmc. VSWR was not measured in this case.

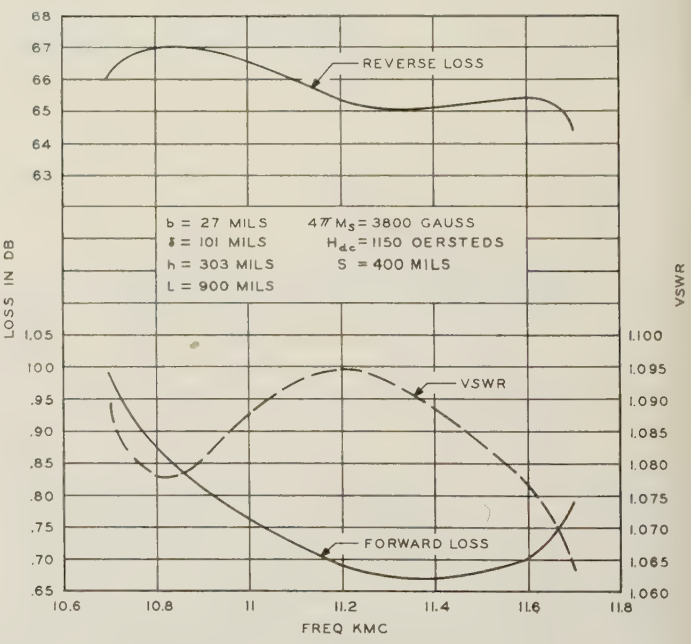

Fig. 7—Performance of double-slab field displacement isolator at 11 kmc.

Discussion

The theoretical basis of scaling to other frequencies is presented in the Appendix. Table II opposite presents the geometrical and magnetic operating conditions to be expected in the various frequency band isolators, using the 6-kmc isolator as a basis and scaling the parameters up (or down) to the other frequency band isolators (4 kmc, 11 kmc, 24 kmc). The values in parentheses are the values expected from scaling, the others are the values used in the actual device.

In all cases, the cross sections of the waveguides available at the various frequencies did not scale exactly from the 6-kmc case. In addition, for convenience the length of ferrite in the various isolators were exactly the same (5 inches) so as to make use of the same magnet

TABLE I

PERFORMANCE OF FIELD DISPLACEMENT ISOLATORS

Frequency range (mc)	Maximum forward loss (db)	Minimum reverse loss (db)	Minimum return loss (db)	Ferrite description		Applied dc magnetic field (oersteds)
				Composition	Magnetization (Gauss)	
3700–4200	0.41	19.2	30	$Mg_{.9}Cu_{.1}Al_{.35}Fe_{1.4}Mn_{.04}$	1200	590
5925–6425	0.22	30	30	$Mg_{.9}Mn_{.1}Fe_{1.2}$	1960	660
10,700–11,700 single slab	0.25	28	32	$Ni_{.8}Cu_{.1}Zn_{.1}Fe_{1.9}Mn_{.02}$	3800	1150
double slab	0.99	65	27		3800	1150
23,500–24,470	0.60	34	—	$Ni_{.6}Zn_{.4}Fe_{1.9}Mn_{.02}$	4900	3670

TABLE II

SCALED AND ACTUAL VALUES OF GEOMETRIC AND MAGNETIC PARAMETERS IN ISOLATORS AT VARIOUS FREQUENCY BANDS; 6-KMC ISOLATOR IS USED AS BASIS. QUANTITIES IN PARENTHESES ARE SCALED VALUES

Frequency mc	δ mils	b mils	h mils	L mils	$4\pi M_s$ Gauss	H applied oersteds
5925–6425	180	70	550	1590	1960	660
3700–4200	280.5, (288)	120, (112)	828, (880)	2290, (2544)	1200, (1225)	590, (412)
10,700–11,700	101, (100)	27.5, (39)	303, (305)	900, (883)	3800, (3528)	1150, (1188)
23,500–24,470	45, (45)	19, (17)	137, (137)	420, (397)	4900, (7840)	3670, (2640)

assembly in all cases. Naturally, as a result of starting out with these two nonscaled quantities, we had to compensate the other geometric and magnetic quantities so as to bring performance at all frequency bands into line. This partly accounts for the discrepancies between scaled and actual operating conditions shown in Table II.

In addition, the bandwidth over which the 4-kmc isolator was tested was considerably greater (on a scaled basis) than that for the 6-kmc isolator. Thus to obtain good performance over the relatively greater band, the geometric quantities had to be altered somewhat from their scaled values.

In the 11-kmc isolator, the best ferrite available at the time was one with a saturation magnetization approximately 300 Gauss away from the scaled value. We see from Table II that the position of the slab, b, was quite different from the scaled value to compensate for this.

The largest $4\pi M_s$ ferrite available at 24 kmc was 4900 Gauss, considerably away from the 7840 Gauss required by scaling. While we used approximate scaled values for the transverse geometric parameters, we note the applied magnetic field is quite far from the required scaled value. Indeed, Table I shows the forward loss for this isolator to be quite out of line with forward losses obtained in the other cases. We may understand this on the basis of the theory of the electric field null developed[3] for the case of a full height ferrite. There it is shown that an electric field null is obtained at the ferrite face for the forward direction of propagation if the geometric and magnetic quantities satisfy

$$\frac{\frac{\pi}{b}(\mu^2 - k^2)\tan k_m\delta}{\mu k_m - k\beta \tan k_m\delta} + \tan k_a(L - b - \delta) = 0$$

where all quantities are defined in the Appendix. Clearly if the geometric quantities are scaled in going from 6 kmc to 24 kmc (*i.e.*, k_a, k_m, $\beta \rightarrow fk_a$, fk_m, $f\beta$ and L, b, $\delta \rightarrow (L/f)$, b/f, δ/f, f being the scaling factor), while the magnetic quantities are not, so that μ and k are different at 24 kmc than at 6 kmc, then the equation is not preserved and the electric field null is destroyed. Hence the higher forward loss in the 24-kmc isolator.

Finally, the applied fields would not be expected to scale if the internal anisotropy fields are different from their scaled values in the various ferrites used. While we have no data on the anisotropy fields in the various ferrites employed, it is unlikely that they scale according to frequency.

We have made use of scaling only as a guide in obtaining isolators at other frequency bands. It is highly likely, however, that if all geometric and magnetic parameters were perfectly scaled, comparable performance could be obtained in each scaled frequency band.

APPENDIX

Scaling for a rectangular waveguide containing a full height ferrite slab may be seen from the following considerations: the phase constant β satisfies the transcendental equation[2]

$$\frac{1}{2}\left(\frac{k_a^2}{\rho^2} + \frac{\beta^2}{\theta^2} - k_m^2\right)\cos k_a(L - \delta - 2b) + \frac{j\beta k_a}{\rho\theta}\sin k_a(L - \delta - 2b)$$
$$+ \frac{1}{2}\left(\frac{k_a^2}{\rho^2} - \frac{\beta^2}{\theta^2} + k_m^2\right)\cos k_a(L - \delta) + \frac{k_a k_m}{\rho}\cot(k_m\delta)\sin k_a(L - \delta) = 0$$

where

$$\rho = \frac{\mu}{\mu^2 - k^2}$$

$$\theta = \frac{\mu}{jk}$$

$$\mu = 1 + \frac{4\pi M_s \gamma \omega_0}{\omega_0^2 - \omega^2}$$

$$k = -\frac{4\pi M_s \gamma \omega}{\omega_0^2 - \omega^2}$$

Suppose the loaded waveguide produces a phase constant β at the frequency ω. We assert that the phase constant at a new frequency $f\omega$ (f any number) is $f\beta$ provided the geometric and magnetic quantities are changed from their old values b, δ, L, $4\pi M_s$, H_0 to the new values b/f, δ/f, L/f, $f4\pi M_s$, and fH_0 at the new frequency $f\omega$. For then, μ, k, ρ, and θ remain unchanged while k_a and k_m become fk_a and fk_m provided β becomes $f\beta$ at the new frequency. Indeed, with these changes, $f\beta$ satisfies the transcendental equation at the new frequency, as is readily observed. A typical component of field is given by[2]

$$E_z = A \sin k_a x e^{-j\beta y}$$

$$A = \frac{\left[\left(1 - \frac{\beta}{k_m \theta}\right) \sin k_a(L - b - \delta) + \frac{jk_a}{k_m \rho} \cos k_a(L - b - \delta)\right] e^{-jk_m \delta}}{\left(1 - \frac{\beta}{k_m \theta}\right) \sin k_a b - j \frac{k_a}{k_m \rho} \cos k_a b},$$

$4\pi M_s$ = saturation magnetization of ferrite

γ = gyromagnetic ratio of electron

ω = angular frequency of wave

$\omega_0 = \gamma H_0$

H_0 = internal dc magnetic field

$k_a^2 = \omega^2 \epsilon_0 \mu_0 - \beta^2$

$k_m^2 = \frac{\omega^2 \epsilon \mu_0}{\rho} - \beta^2$

ϵ_0, μ_0 = dielectric constant and permeability of free space

ϵ = dielectric constant of ferrite.

and thus the fields are unchanged in value and distribution at the new frequency, phase constant, and operating conditions provided the geometry x, y is scaled down (or up) to x/f, y/f.

Acknowledgment

We should like to thank F. J. Sansalone, J. J. Kostelnik, and J. D. Apgar for aid in the measurement program.

We are greatly indebted to L. G. Van Uitert for the development of the suitable ferrites in each of the various frequency ranges.

A Method of Producing Broad-Band Circular Polarization Employing an Anisotropic Dielectric*

H. S. KIRSCHBAUM† AND S. CHEN†

Summary—A procedure is described whereby it is possible to design circular polarizers for both waveguides and in window form to be used over a broad band of frequencies. The difference in phase constants for two mutually orthogonal *E* fields while propagating in an anisotropic dielectric is combined with the effect due to guide wall spacing to obtain a reasonably constant differential phase constant for the two fields over a broad frequency band. By properly choosing the length of the anisotropic dielectric in the direction of propagation, and orienting this dielectric properly with respect to an incident linearily-polarized wave, the transmitted wave is circularly polarized over a correspondingly broad band of frequencies.

Introduction

VARIOUS methods[1–4] have been proposed for obtaining circular polarization of an electromagnetic wave in a waveguide or in free space. Some of these methods are frequency sensitive while others are not. This paper describes a method for obtaining circular polarization over a broad band of frequencies by making use of an artificial anisotropic dielectric.

A wave in a waveguide may be said to be circularly polarized if the following conditions are met. The wave shall consist of two equal components in space quadrature (each being a dominant mode) traveling in the same direction. The electric vectors of the two components shall be 90° out of phase with each other. The equality of the two electric field vectors is necessitated by the fact that a circularly-polarized wave can be propagated in a waveguide without loss of circularity only if the two components that go to make it up are propagated with the same velocity. In other words, what is required is a guide that is doubly symmetric in cross section such as either a square or a circle.

The method described here makes use of a section containing an artificial anisotropic dielectric in the waveguide (which is not necessarily doubly symmetric), disposed in such a way as to produce circular polarization at the interface furthest from the source of energy. If this interface is followed by a perfectly square or round guide, the circularly-polarized wave will propagate unaltered.

The use of an anisotropic dielectric is further extended to produce a polarizing window which can control the polarization emanating from a linearly-polarized antenna.

Analysis

Consider a rectangular waveguide as in Fig. 1, which is capable of transmitting both the TE_{10} and TE_{01} modes. This waveguide is filled with an anisotropic dielectric having the property that the dielectric constant for the electric vector in the y direction is greater than the dielectric constant for the electric vector in the x direction. If it is assumed that only the TE_{10} and TE_{01} modes are transmitted, then the x-polarized wave will "see" only ϵ_z and the y-polarized wave will "see" only ϵ_x.

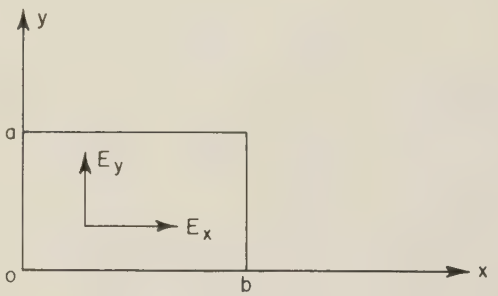

Fig. 1—Coordinate system and waveguide dimensions.

These two waves will behave as though the guide were filled with an isotropic dielectric having dielectric constants ϵ_x and ϵ_y, respectively. For these two polarizations, the propagation constants are, respectively,

$$\beta_x = \beta_0 \sqrt{k_x - \left(\frac{\lambda}{2a}\right)^2} \tag{1}$$

$$\beta_y = \beta_0 \sqrt{k_y - \left(\frac{\lambda}{2b}\right)^2} \tag{2}$$

where $\beta_0 = \omega\sqrt{\mu_0\epsilon_0}$, k_x and k_y are the relative dielectric constants of the anisotropic medium in the directions indicated by the subscript, and λ is the free-space wavelength of the wave.

For the case where $\epsilon_y > \epsilon_x$ and $b > a$, the above relations plot as shown in Fig. 2. At some frequency ω_0 the slopes of the two curves are equal, and this frequency can be

* Manuscript received by the PGMTT, December 7, 1956. The research reported was sponsored in part by the Signal Corps Eng. Labs., U. S. Army Signal Corp., through a contract with the Ohio State University Research Foundation.

† Antenna Lab., Dept. of Elec. Eng., The Ohio State University, Columbus, Ohio.

[1] "Preliminary Instruction Book for the M4902 Airborne 'S' Band Circularly-Polarized Radiator," Radio Res. Lab., Harvard University Rep. No. 411-1B-71; March 12, 1945.

[2] "Quarter-Wave Plate for Broad-Band Circular Polarization," M.I.T. Rad. Lab. Ser., Rep. No. 769, McGraw-Hill Book Co., Inc., New York, N. Y.; January 28, 1946.

[3] R. M. Brown and A. J. Simmons, "Dielectric Quarter-Wave and Half-Wave Plates in Circular Waveguide," Naval Res. Lab. Rep. No. 4218; November 10, 1953.

[4] A. J. Simmons, "A Method of Producing Broad-Band Circular Polarization in Square Waveguide," Naval Res. Lab. Rep. No. 4286; January 28, 1954.

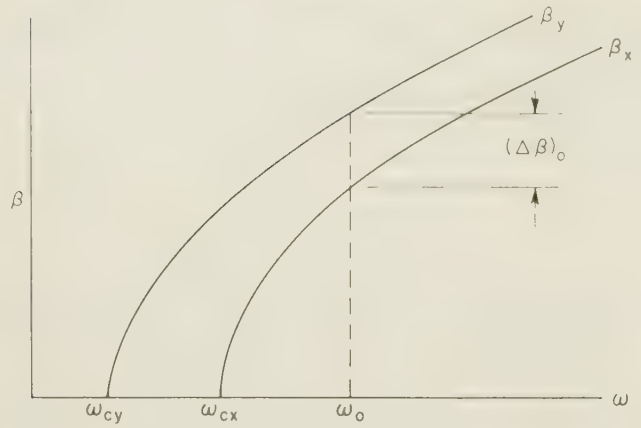

Fig. 2—Phase constant vs frequency.

taken as the center of a band of frequencies over which $(\beta_y - \beta_x)$ remains very nearly constant. Upon solving for the frequency at which the slopes of the two propagation functions are equal, there is obtained

$$\omega_0 = \frac{\pi}{\sqrt{\mu_0\epsilon_0(k_y - k_x)}} \sqrt{\frac{1}{a^2}\frac{k_y}{k_x} - \frac{1}{b^2}\frac{k_x}{k_y}}. \tag{3}$$

From (3) it follows that

$$\frac{4(k_y - k_x)}{\lambda^2} = \frac{1}{a^2}\frac{k_y}{k_x} - \frac{1}{b^2}\frac{k_x}{k_y} \tag{4}$$

where λ_0 is the free-space wavelength corresponding to ω_0. If λ_0 is fixed at some particular value, then a curve such as Fig. 3 can be drawn showing the relationship between a and b required to satisfy (4).

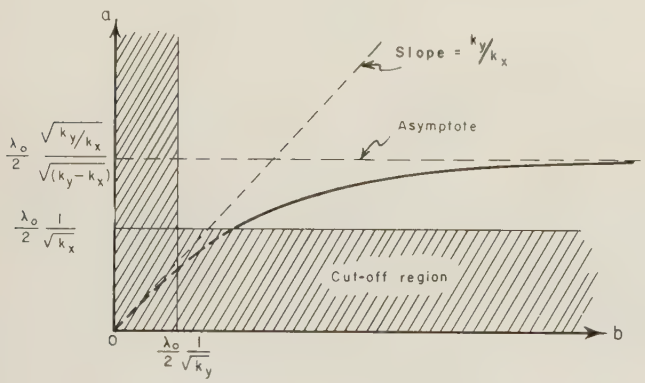

Fig. 3—Usable range of guide dimensions.

It should be noted that this curve is asymptotic to

$$\frac{\lambda_0}{2}\frac{\sqrt{k_y/k_x}}{\sqrt{k_y - k_x}}$$

as b becomes infinitely large. The case for b = infinity will be taken up in greater detail later when the subject of a polarizing window is discussed.

Eq. (4) is good provided neither a nor b becomes so small as to result in the guide's being cut off at the wavelength λ_0. Since a practical design requires $b > a$, and since $\epsilon_y > \epsilon_x$, the guide will cut off first for the x-polarized wave. The cutoff wavelength for the x-polarized wave is

$$\lambda_{cx} = 2a\sqrt{k_x}, \tag{5}$$

from which it can be seen that the dimension a cannot be less than $\lambda_0/2\sqrt{k_x}$. Hence in Fig. 3, only the solid portion of the a vs b curve can be used. From the point of view of the simplicity of the transition pieces from rectangular to round or square guide, it would be best to choose a square cross section for the quarter-wave plate. However, with the k_y and k_x available, such a choice would either result in a quarter-wave plate of large cross section or it would put ω_0 too close to the cutoff region. To permit ω_0 to be somewhere near the center of the band of frequencies to be considered, it is usually necessary to choose a point on the curve of Fig. 3 such that at the lowest frequency to be considered the quarter-wave plate is not cut off.

Having established the dimensions of the cross section, a curve of $\Delta\beta$ vs frequency can be computed for the frequency band under consideration. From the average value of $\Delta\beta$ over this band, a length can be chosen for the quarter-wave plate such that $(\Delta\beta)_{ave}$ times the length l equals $\pi/2$ radians.

Up to this point, no consideration has been given to the problem of internal reflections within the quarter-wave plate due to mismatches at the two interfaces. If it is assumed that the guide walls are continued unbroken on either side of the quarter-wave plate, as would probably be the case for a round or square guide, then the complex transmission coefficients through the quarter-wave plate for the x and y polarizations of the wave are

$$\dot{k}_{tx} = \frac{1}{\cos\beta_x l + j\frac{1}{2}\left(\frac{Z_{0x}}{Z_{1x}} + \frac{Z_{1x}}{Z_{0x}}\right)\sin\beta_x l} \tag{6}$$

$$\dot{k}_{ty} = \frac{1}{\cos\beta_y l + j\frac{1}{2}\left(\frac{Z_{0y}}{Z_{1y}} + \frac{Z_{1y}}{Z_{0y}}\right)\sin\beta_y l}, \tag{7}$$

where $\dot{k}_{tx}$ and $\dot{k}_{ty}$ are the complex transmission coefficients for the x- and y-polarized waves. The quantities Z_{0x} and Z_{0y} are the guide impedances for the air-filled guide and Z_{1x} and Z_{1y} are the guide impedances in the region filled with the anisotropic dielectric. From (6) and (7) the actual differential phase shift between the incident waves and emergent waves will be

$$\Delta\phi = (\phi_y - \phi_x) = \arctan\left\{\frac{1}{2}\left[\frac{Z_{1y}}{Z_{0y}} + \frac{Z_{0y}}{Z_{1y}}\right]\tan\beta_y l\right\} - \arctan\left\{\frac{1}{2}\left[\frac{Z_{1x}}{Z_{0x}} + \frac{Z_{0x}}{Z_{1x}}\right]\tan\beta_x l\right\}. \tag{8}$$

The ratio of the absolute values of $\dot{k}_{tx}$ and $\dot{k}_{ty}$ when averaged over the frequency band under consideration will serve to determine the relative magnitudes of the incident x- and y-polarized waves necessary to produce circular polarization in the emerging wave. The incident waves must meet the following requirement in order to produce circular polarization, namely,

$$\left|\frac{E_{ix}}{E_{iy}}\right| = \left|\frac{\dot{k}_{ty}}{\dot{k}_{tx}}\right|_{\text{ave}} \tag{9}$$

where the average is taken over the frequency band under consideration.

This requirement follows from the fact that the transmitted waves must be equal in magnitude in order to have circular polarization.

This same anisotropic material when placed in a round guide leads to a problem, the exact solution of which is intractable. However, as shown later under the experimental work, such a round guide behaves qualitatively in the same manner as a square guide having the same cutoff wavelength in the dominant mode.

The Polarizing Window

As stated above, when b is allowed to approach infinity the dimension a approaches

$$\frac{\lambda_0}{2}\frac{\sqrt{k_y/k_x}}{\sqrt{k_y - k_x}},$$

and for the y-polarized wave, the guide would become a parallel-plate transmission line. For the x-polarized wave, the guide would be infinitely deep. If a number of these guides were stacked above each other, there would result a configuration as shown in Fig. 4. This could be made to serve as a polarizing window when placed in front of a linearly-polarized antenna. In Fig. 2, the cutoff frequency for the y-polarized wave would become zero and the phase constant through the material would become a straight line function of frequency. As in the case of the quarter-wave plate in the waveguide, (6), (7), and (8) apply with Z_{0x} and Z_{0y} equal to the impedance of free space. The impedances Z_{1x} and Z_{1y} are, respectively,

$$Z_{1x} = \frac{\sqrt{\mu_0/\epsilon_0}}{\sqrt{k_x - \left(\frac{\lambda}{2a}\right)^2}} \tag{10}$$

$$Z_{1y} = \frac{1}{\sqrt{k_y}}\sqrt{\frac{\mu_0}{\epsilon_0}}. \tag{11}$$

The Anisotropic Dielectric

The anisotropic dielectric used in the quarter-wave plates described in this paper is an artificial one composed of alternate sheets of polystyrene and air (or polyfoam). The sheets of polystyrene and air are of equal thickness as shown in Fig. 5. If the wavelength used in the quarter-wave plates is very much greater than the thickness of the sheets of the anisotropic dielectric, the dielectric constants of the anisotropic dielectric can be computed on the basis of a dc field. Upon doing this it is found that

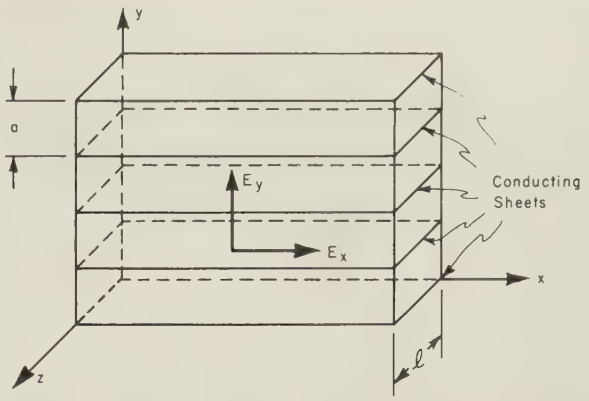

Fig. 4—Construction details of polarizing window.

$$\epsilon_x = \frac{2\epsilon_p\epsilon_f}{\epsilon_p + \epsilon_f} \tag{12}$$

$$\epsilon_y = \frac{\epsilon_p + \epsilon_f}{2}, \tag{13}$$

where ϵ_x and ϵ_y are the dielectric constants for x- and -polarized fields, respectively, and ϵ_p and ϵ_f are the dielectric constants of polystyrene and air (or polyfoam) respectively. These equations are obviously applicable to relative dielectric constants also. Tests on the quarter-wave window placed in front of a horn antenna up to frequencies where the thickness of the polystyrene was about $\frac{1}{3}$ of a wavelength indicate that the use of these dc dielectric constants is justifiable.

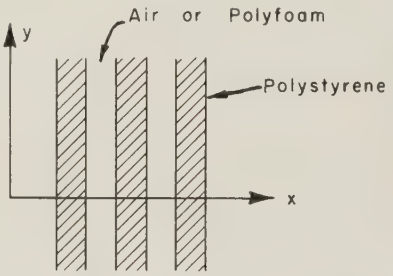

Fig. 5—Artificial anisotropic dielectric.

For a polystyrene and air anisotropic dielectric, the ϵ_x and ϵ_y are 1.438 ϵ_0 and 1.780 ϵ_0, respectively. If polyfoam is used instead of air, they are 1.470 ϵ_0 and 1.795 ϵ_0, respectively.

Experimental Results

Quarter-Wave Plates

A number of quarter-wave plates embodying the principles stated above were built and tested. The first of these, shown in the photographs of Fig. 6, had the di-

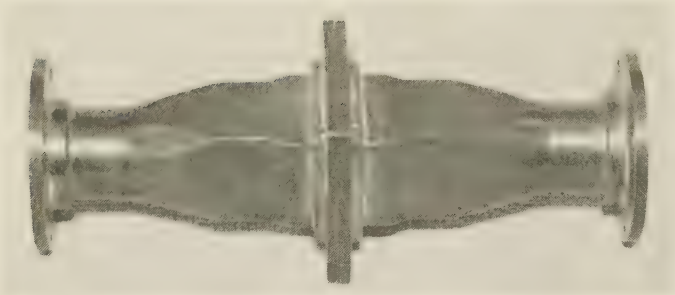

(a)

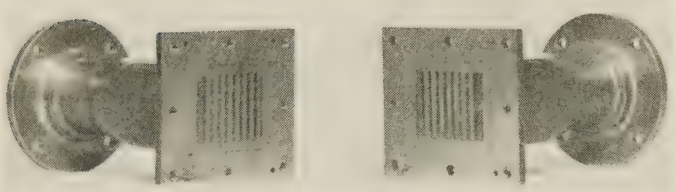

(b)

Fig. 6—Photographs of quarter-wave plate.

mensions listed in Table I, below. This quarter-wave plate was designed for a rectangular guide so that advantage could be taken of the differential phase shift inherent in a rectangular guide regardless of the presence of an anisotropic medium.

TABLE I

Dimension a	$=2.30$ cm
Dimension b	$=2.80$ cm
Length l	$=3.30$ cm
Dielectric thickness	$=0.159$ cm
Air thickness	$=0.159$ cm
ϵ_y	$=1.780\ \epsilon_o$
ϵ_z	$=1.438\ \epsilon_o$

This quarter-wave plate was tested for axial ratio vs frequency using the circuit of Fig. 7. The results obtained are shown in Fig. 8, the anomalous behavior at 11.1 and 12.45 kmc being caused by resonance within the transition pieces. The theoretical performance is drawn on the figure as a comparison.

In order to eliminate the transition pieces, a quarter-wave plate, employing the same artificial anisotropic dielectric, was built into a round guide of 15/16-inch nominal inside diameter. This plate was 4.83 cm long, this length being based on the calculated performance of a hypothetical square guide having the same cutoff wavelength as the actual round guide used. In actuality an error in calculation resulted in the length of 4.83 cm being about 10 per cent longer than it should have been. The axial ratio vs frequency obtained for this quarter-wave plate is shown in Fig. 9. In this case, excellent results were obtained over a 1.56 to 1 frequency band. The theoretical performance of the hypothetical square guide quarter-wave plate of length 4.37 cm is shown for comparison. These measurements show that less differential phase shift per cm of dielectric is obtainable in the

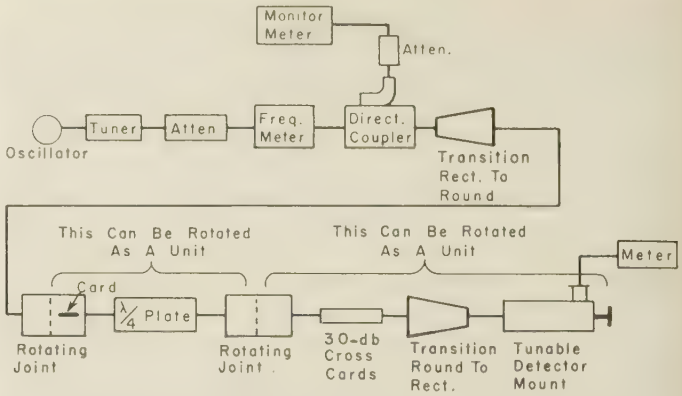

Fig. 7—Test equipment used to measure axial ratio of quarter-wave plates in a guide.

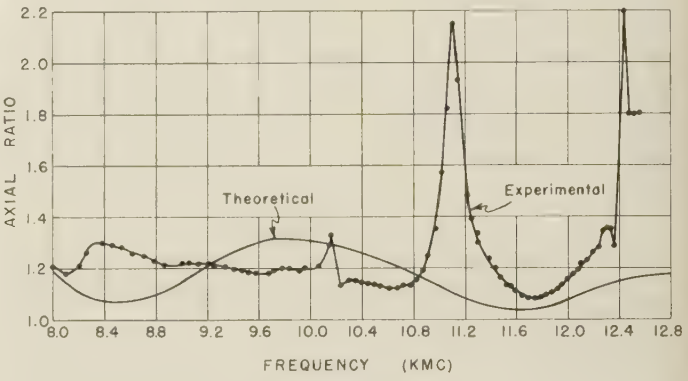

Fig. 8—Axial ratio vs frequency for λ/4 plate in 2.8×2.3-cm guide.

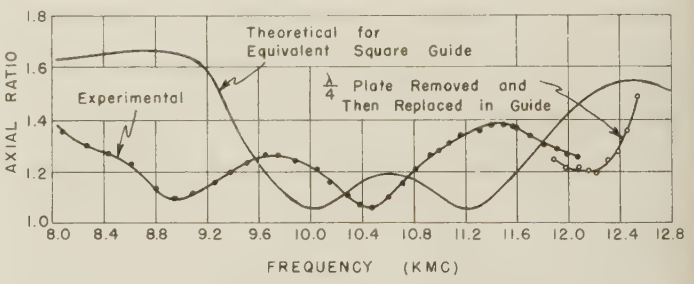

Fig. 9—Axial ratio vs frequency for λ/4 plate in 15/16-inch circular guide.

round guide than in the square guide, and that the mismatch at the interfaces does not seem to be as poor as in the case of the square guide. This may be explained qualitatively as follows. Consider the case of both guides transmitting waves polarized along the axis of greatest dielectric constant (the y axis in these reports). In the case of the square guide, there are no field components in the x direction and so the wave "sees" only ϵ_y. In the case of the round guide, off the diameter, there are components of electric field in both the x and y directions, the field in the y direction predominating. In any event, for the purposes of determining the propagation constant for this wave, the wave "sees" a dielectric constant somewhat less than ϵ_y. In a similar manner an x-oriented wave propagating in the circular guide will "see" a dielectric constant somewhat greater than ϵ_x. Hence the

differential phase shift between x- and y- oriented waves will not be as great as it would in the perfectly square guide. On the other hand, this effect should improve the variation of the ratio of transmission coefficients, and result in a better axial ratio over the frequency band than would be obtainable in square guide.

Polarizing Windows

In Fig. 10 is shown a photograph of a polarizing window built in accordance with the above theory. The dimensions of the window are given in Table II. Measurements were made on this window by illuminating it with a 6×6 inch horn in which were placed several 700-ohm absorbing cards perpendicular to the incident polarization. This was done to absorb any cross-polarized reflections from the window. The incident polarization is inclined at an angle of 42.5° with respect to the metal strips of the window. This angle was determined by test and deviates from 45° because the average transmission coefficients for the x- and y- polarized waves are not equal to each other over the frequency band under consideration. The beam from the window was directed into a 7-foot cube "dark room" in which was placed a polarization-sensitive detector. Measurements were made, directly on the beam axis, of axial ratio over a band of frequencies extending from 8.2 kmc to 17.2 kmc. The results plotted in Fig. 11 show that the axial ratio does not exceed 1.5 over a 2.1 to 1 frequency band. It further appears that the useful bandwidth of the window has not been realized.

Conclusion

By means of the foregoing design procedure, it is possible to build circular polarizers for both waveguides and in the form of windows which will operate over a very broad band of frequencies. The design procedure did not take into account either impedance matching or "end effects" in the case of the window. If both of these were taken into account either analytically or experimentally, it should be possible to secure even better results than those obtained here.

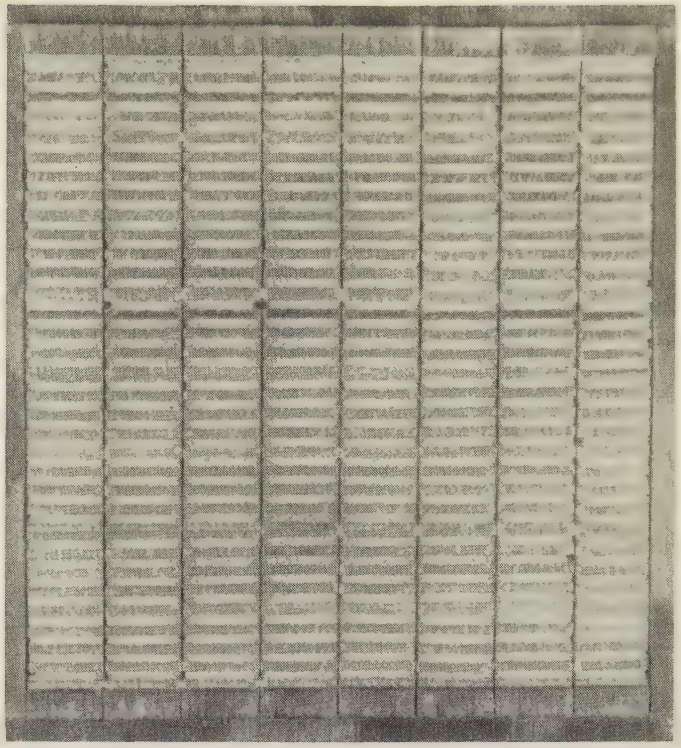

Fig. 10—Photograph of polarizing window.

TABLE II

Dimensions of Polarizing Window

$a=2.64$ cm $l=2.60$ cm	$\epsilon_y=1.79$ $\epsilon_x=1.47$	$\lambda_o=2.71$ cm $f_o=11.$ kmc $(\Delta\beta)_o\, l=82.5°$

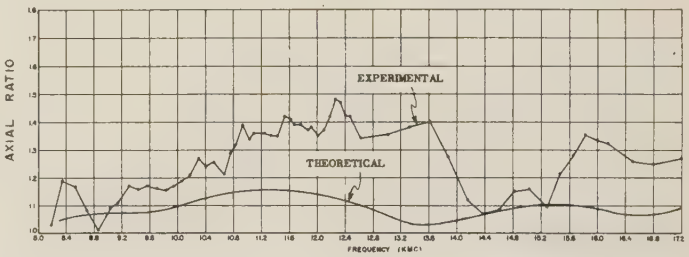

Fig. 11—Axial ratio vs frequency for polarizing window.

Errors in a Magic-Tee Phase Changer*

RAYMOND M. VAILLANCOURT†

Summary—This paper recalls the basic properties of a magic-tee and how it can be used as a linear phase changer. An analysis of the symmetrical magic-tee phase changer is made, which shows that nonlinearities of the phase shift and amplitude modulation are second and higher order effects caused by small mismatches of the structure. Also, some qualitative comments are made on the errors of an asymmetrical phase changer. Measurements on a phase changer assembled from ordinary laboratory equipment show that the phase shift is linear to better than 1°.

Introduction

THE PRINCIPLE of operation of the ideal magic-tee phase changer[1] is readily understood from a consideration of the properties of a magic-tee. Many microwave structures have the properties of a magic-tee[2,3] but for the sake of simplicity, the most familiar device, *i.e.*, the side outlet "*E*" and "*H*" plane tee is used to visualize the principle of operation. The side outlet tee shown in Fig. 1, which is assumed to be symmetrical with respect to the plane which contains the axis of arms 3 and 4, is called a magic-tee when the structure is completely matched, *i.e.*, when a matched load is seen looking into any one of the four arms if the other are terminated in reflectionless loads. For this case, the total power a generator feeds into any one arm couples in equal amounts into the two adjacent arms and not into the opposite arm. If a generator is connected to arm 4, the coupled waves into arms 1 and 2 have the same phase in planes equidistant from the symmetry plane, but are π radians out of phase if the generator feeds arm 3. Now, if two variable short circuits are inserted into arms 1 and 2 at a distance L_1, and $L_2 = L_1 + (\lambda g/4)$ respectively from the symmetry plane, all the power going into arm 4 will appear at the output of arm 3. The wave launched at input 4 splits into two equal and in phase waves in arms 1 and 2. Because arm 2 is $\lambda g/4$ longer than arm 1, these two waves are reflected back in the symmetry plane with a phase difference of π radians and will cancel each other in arm 4 but reinforce each other in arm 3. If the lengths of arms 1 and 2 are both increased by ΔL, the total path length of the structure has changed by $2\Delta L$, and the phase of the output wave in arm 3 has changed by $(2\Delta L/\lambda g)2\pi$.

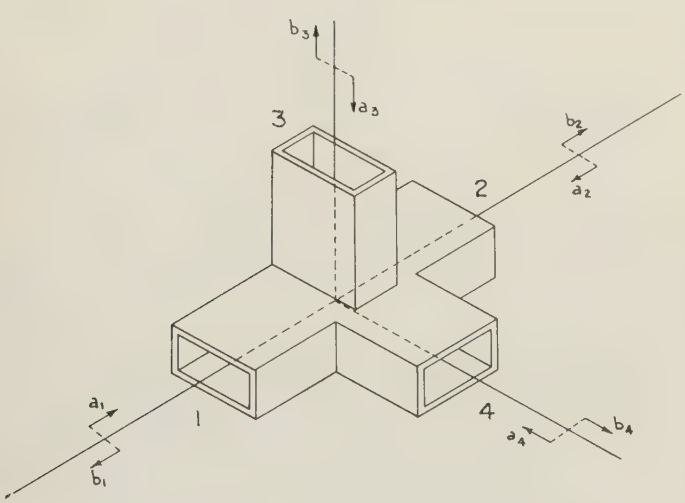

Fig. 1—Side outlet "*E*" and "*H*" plane arm tee.

It should be added that the variable short circuits can also be inserted in arms 3 and 4 instead of arms 1 and 2 and will give a similar relative phase change of the output in arm 2 when arm 1 is connected to a generator.

Ten independent equations are available to fix the relationship between the 16 parameters required to describe the behavior of an unmatched and asymmetrical hybrid tee. The relations between the various parameters are not linear, and solutions for the dependent parameters in terms of a suitably chosen set of six independent parameters are practically untractable. On the other hand, for an unmatched symmetrical tee, only nine parameters are required, and three of them can be chosen independently.

The resulting simplification is such that an analysis of the errors in the linearity of the phase change caused by reflections is possible. Thus the main part of this paper is concerned with the analysis of the errors in a symmetrical hybrid tee phase changer. Some qualitative remarks on the effects of small asymmetries are made at the end of the paper. Experimental results on a typical phase changer assembled from commercial components are also included.

Scattering Matrix of Side-Outlet Tee[4]

The reference planes in each arm (see Fig. 1) are chosen far enough from the junction to be out of the diffraction field. It is assumed that only the fundamental H_{10} mode can be propagated in the waveguides and that the guides have the same uniform cross section and negligible losses.

* Manuscript received by the PGMTT, December 17, 1956.

† Canadian Armament Res. and Dev. Establishment, Valcartier, Quebec, Canada.

[1] G. Saxton and C. W. Miller, "Magic-tee waveguide junction," *Wireless Eng.*, vol. 25, pp. 138–147; May, 1948.

[2] C. G. Montgomery, R. H. Dicke, and E. M. Purcell, "Principles of Microwave Circuits, M.I.T. Rad. Lab. Ser., McGraw-Hill Book Co., Inc., New York, N. Y., vol. 8, ch. 12; 1948.

[3] W. K. Kahn, "*E*-plane forked hybrid-T junction," IRE Trans., vol. MTT-3, pp. 52–58; December, 1955.

[4] C. G. Montgomery, "Technique of Microwave Measurements," McGraw-Hill Book Co., Inc., New York, N. Y., sec. 9.2; 1947.

The amplitudes of emergent and incident waves are related as follows:

$$\begin{bmatrix} b_1 \\ b_2 \\ b_3 \\ b_4 \end{bmatrix} = \begin{bmatrix} S_{11} & S_{12} & S_{13} & S_{14} \\ S_{21} & S_{22} & S_{23} & S_{24} \\ S_{31} & S_{32} & S_{33} & S_{34} \\ S_{41} & S_{42} & S_{43} & S_{44} \end{bmatrix} \begin{bmatrix} a_1 \\ a_2 \\ a_3 \\ a_4 \end{bmatrix}. \tag{1}$$

a_n and b_n are so normalized that $|a_n|^2$ and $|b_n|^2$ are respectively proportional to the incident and emergent power at terminal n. Since the structure is assumed lossless, its scattering matrix has the properties of a unitary matrix, *i.e.*,

$$\sum_{j=1}^{4} S_{ij}S_{sj}^* = \begin{cases} 1 & \text{for } i = s \\ 0 & \text{for } i \neq s. \end{cases} \tag{2}$$

The application of these conditions to the scattering matrix (1) together with the reciprocity conditions

$$S_{ij} = S_{ji}, \quad i, j, = 1, 2, 3, 4 \tag{3}$$

gives 10 independent equations. But in general, $S_{mn} = U_{mn} + jV_{mn}$, and hence there are 20 unknown parameters. Without loss in generality, the four reference planes can always be chosen so that the diagonal elements S_{mm} are pure real numbers.[5] This choice of reference planes reduces the number of unknown parameters to 16. This implies that at least six unknowns must be measured to evaluate all the others. The above properties of the scattering matrix will be used in the analysis of the magic-tee phase changer.

Analysis of Magic-Tee Phase Changer

Consider a tee with variable plungers inserted in arms 1 and 2 at θ_1 and θ_2 electrical degrees from their respective reference planes. If a generator is connected to arm 4 with arm 3 terminated in a matched load, it follows that

$$\begin{aligned} a_1 &= -b_1e^{-2j\theta_1} \\ a_2 &= -b_2e^{-2j\theta_2} \\ a_3 &= 0 \end{aligned} \tag{4}$$

and the expression for b_3 as a function of a_4 is

$$\begin{aligned} b_3 = a_4\Big[S_{34} - \frac{1}{\Delta}\{&S_{13}S_{14}e^{-2j\theta_1} + S_{23}S_{24}e^{-2j\theta_2} \\ &+ (-S_{12}S_{13}S_{24} - S_{12}S_{14}S_{23} + S_{13}S_{14}S_{22} \\ &+ S_{23}S_{24}S_{11})e^{-2j(\theta_1+\theta_2)}\}\Big] \end{aligned} \tag{5}$$

where

$$\Delta = (1 + S_{11}e^{-2j\theta_1})(1 + S_{22}e^{-2j\theta_2}) - S_{12}^2e^{-2j(\theta_1+\theta_2)}. \tag{6}$$

Any actual tee should have very little asymmetry in order to have a simple calibration law when used as a phase changer. Assuming perfect symmetry makes the analysis possible and yet gives a good theoretical insight to the actual performance of a good magic-tee phase changer.

From symmetry considerations it follows that

$$\begin{aligned} S_{23} &= -S_{13} & S_{22} &= S_{11} \\ S_{24} &= S_{14} & S_{34} &= 0. \end{aligned} \tag{7}$$

S_{34} must be equated to zero since, for the H_{10} mode of propagation, the electric field distribution in the cross sections of arms 3 and 4 are asymmetrical and symmetrical respectively and hence there is no coupling between these arms. Substitution of (7) in (5) and (6) gives

$$b_3 = \frac{-a_4S_{13}S_{14}(e^{-2j\theta_1} - e^{-2j\theta_2})}{1 + S_{11}(e^{-2j\theta_1} + e^{-2j\theta_2}) + (S_{11}^2 - S_{12}^2)e^{-2j(\theta_1+\theta_2)}}. \tag{8}$$

The phase and amplitude of b_3/a_4 can be evaluated from (8), but simpler expressions follow without loss in generality if the diagonal elements of the scattering matrix are made pure real numbers. The Appendix gives the derivation of $|S_{12}|$, $|S_{13}|$, and $|S_{14}|$ as functions of U_{11}, U_{33}, and U_{44}, *i.e.*,

$$|S_{13}|^2 = \frac{1 - U_{33}^2}{2}; \qquad |S_{14}|^2 = \frac{1 - U_{44}^2}{2}$$

$$U_{12} = \frac{U_{44}^2 - U_{33}^2}{4U_{11}};$$

$$V_{12}^2 = \frac{U_{33}^2 + U_{44}^2}{2} - U_{11}^2 - U_{12}^2.$$

Substituting these values in (8) the phase of b_3/a_4 is then expressible as

$$\measuredangle \frac{b_3}{a_4} = \phi_0 - \left(\theta_1 + \theta_2 - \frac{\pi}{2}\right) - \psi \tag{9}$$

where

$$\psi = \tan^{-1} - \frac{[U_{11}(\sin 2\theta_1 + \sin 2\theta_2) + \alpha \sin 2(\theta_1 + \theta_2) + \beta \cos 2(\theta_1 + \theta_2)]}{[1 + U_{11}(\cos 2\theta_1 + \cos 2\theta_2) + \alpha \cos 2(\theta_1 + \theta_2) - \beta \sin 2(\theta_1 + \theta_2)]}$$

with

$$\alpha = U_{11}^2 - U_{12}^2 + V_{12}^2$$

and

$$\beta = 2U_{12}V_{12}.$$

The constant phase angle ϕ_0 is the phase of $S_{13}S_{14}$. The modulus of b_3/a_4 is given by

[5] Montgomery, Dicke, and Purcell, *op. cit.*, p. 149.

$$\left|\frac{b_3}{a_4}\right| = \frac{2\,|S_{13}|\,|S_{14}|\,|\sin(\theta_1-\theta_2)|}{\{(1-\alpha)^2+\beta^2+4U_{11}\cos(\theta_1-\theta_2)\cos(\theta_1+\theta_2) + 4[[\cos(\theta_1+\theta_2)+U_{11}\cos(\theta_1-\theta_2)][\alpha\cos(\theta_1+\theta_2)-\beta\sin(\theta_1+\theta_2)]]\}^{1/2}} \cdot \quad (10)$$

Substitution of $\theta_2=\theta_1+(\pi/2)+t$, ($t$ is a small angular error which may arise in the initial setting of the plungers in arms 1 and 2) in (9) and (10) gives

$$\not\propto \frac{b_3}{a_4} = \phi_0 - (2\theta_1 + t) - \psi_1 = \phi \quad (11)$$

where

$$\psi_1 = \tan^{-1}\frac{-U_{11}[\sin 2\theta_1 - \sin 2(\theta_1+t)] + \alpha\sin 2(2\theta_1+t) + \beta\cos 2(2\theta+t)}{1+U_{11}[\cos 2\theta_1 - \cos 2(\theta_1+t)] - \alpha\cos 2(2\theta+t) + \beta\sin 2(2\theta_1+t)}$$

$$\left|\frac{b_3}{a_4}\right| = \frac{2\,|S_{13}|\,|S_{14}|\cos t}{\{(1-\alpha)^2+\beta^2+4U_{11}\sin t\sin(2\theta_1+t)+4[\sin(2\theta_1+t)+U_{11}\sin t][\alpha\sin(2\theta_1+t)+\beta\cos(2\theta_1+t)]\}^{1/2}} \cdot \quad (12$$

Since α^2 and β^2 are small quantities of fourth order, the square root is of second order and hence the modulation amplitude $\sqrt{\alpha^2+\beta^2}$ of the output is of second order. The output varies at twice the rate of the phase shift of the principal wave. For the particular values of U_{11}, U_{33}, U_{44} used above the modulation of the output is 1 per cent.

The third term, ψ_1, of (11) is a contribution of second order provided t, U_{11}, U_{12}, and V_{12} are small. Moreover, if t is a small error, its variation δt with plunger setting will be of second order. Thus to a second order of approximation, the phase of b_3/a_4 is a linear function of θ_1 since ϕ_0 is constant. The extrema of the third term should be very near and of the order of magnitude of those obtained for the case $t=0$. For $t=0$

$$\psi_1 = \tan^{-1}\frac{\alpha\sin 4\theta_1 + \beta\cos 4\theta_1}{1-\alpha\cos 4\theta_1+\beta\sin 4\theta_1} \quad (13)$$

and ψ_1 has extrema for

$$\theta_1 = \frac{1}{4}\cos^{-1}\left\{\alpha \pm \beta\left[\frac{1}{\alpha^2+\beta^2}-1\right]^{1/2}\right\}. \quad (14)$$

To give an order of magnitude of the expected error due to ϕ_1, let $U_{11}=U_{33}=U_{44}=0.1$ (this implies a residual vswr $=1.22$) and ϕ_1 max$\simeq 0.57°$. When $t=0$

$$\left|\frac{b_3}{a_4}\right| = \frac{2\,|S_{13}|\,|S_{14}|}{\{1+\alpha^2+\beta^2-2\alpha\cos 4\theta_1+2\beta\sin 4\theta_1\}^{1/2}}$$

$$= 2\,|S_{13}|\,|S_{14}|\left\{1-\frac{1}{2}(\alpha^2+\beta^2)+\sqrt{\alpha^2+\beta^2}\cdot\left[\frac{\alpha}{\sqrt{\alpha^2+\beta^2}}\cos 4\theta_1 - \frac{\beta}{\sqrt{\alpha^2+\beta^2}}\sin 4\theta_1\right]+\cdots\right\}$$

$$\approx 2\,|S_{13}|\,|S_{14}|\,[1+\sqrt{\alpha^2+\beta^2}\cos(4\theta_1+\phi_1) \quad (15)$$

where

$$\phi_1 = \tan^{-1}\beta/\alpha.$$

Experimental Verification

To use a side outlet tee as a phase changer it is necessary to match it reasonably well (vswr <1.3) and to have the plungers in the "through" arms respectively at θ_1 and θ_1+90 electrical degrees from the symmetry plane.

For narrow-band operation, traveling screw tuners may be used in the "E" and "H" plane arms. A residual vswr$\simeq$1.03 is readily obtained provided the load terminations in the other three arms have small "phasable" reflection coefficients. Long tapered wood loads which can be slid in the waveguides do very well.

To fix the respective locations of the plungers in the "through" arms, one reflectionless load termination of the through arms is replaced by a plunger and the position of one minimum of the electric field in the input slotted line is measured. Repeating the same experiment for the other arm with another plunger gives the difference in the electrical length of the two through arms. From this result and the measure of the guide wavelength (not the slotted guide wavelength), one of the two plunger arms can be made 90 electrical degrees longer than the other.

Because the structure was not perfectly matched, the locations of the electric field minima in the slotted line were averaged for open and short-circuit conditions at the output by moving the output plunger a quarter of a guide wavelength away from its initial position for every setting of the plungers in the through arms.

The results of the measurements are shown in Table I. The maximum variation of the incremental phase shift

TABLE I

$2L_1$ cm	ϕ	$\Delta\phi$
0.000	0.00	
0.254	19.6	19.6
0.508	39.5	19.9
0.752	58.8	19.3
1.016	77.9	19.1
1.270	97.7	19.8
1.524	117.5	19.8
1.753	137.3	19.8
2.032	156.8	19.5
2.286	176.4	19.6
2.540	195.8	19.4

$f=9193\pm5$ mc.
$\frac{1}{2}\lambda gs=2.327\pm0.002$-cm wavelength in the guide.
$\frac{1}{2}\lambda gD=2.340\pm0.005$-cm wavelength in the slotted line.
vswr for "E" and "H" arms≈1.03
$2L_1$=incremental path length of the through arms.
ϕ=relative phase shift in the slotted line.
$\Delta\phi$=incremental phase shift in the slotted line.

is within 0.8°. The estimated maximum error in the plunger setting L_1 is ±0.001 cm and in the location of the field minimum ±0.005 cm. Thus the estimated maximum error in ϕ is $\pm0.4°$. In view of this limited accuracy in the measurements it would seem that the phase shift was linear to better than 0.8°.

Conclusion

It has been shown that the symmetrical magic-tee makes a lossless linear phase changer whose phase linearity is affected to a second order for reflection coefficients equal to or less than 0.1.

The fact that isolation between the "E" and "H" plane arms is not infinite although usually greater than 40 db ($|S_{34}|<0.01$) introduces additional errors. This coupling is caused by a certain amount of asymmetry for which S_{34} may be considered as a measure. Reference to (5)–(7) shows that when the tee is not perfectly symmetrical, $S_{34}\neq0$ and the term $(S_{13}S_{14}S_{22}+S_{23}S_{24}S_{11}-S_{12}S_{13}S_{24}-S_{12}S_{14}S_{23})$ does not completely cancel. This term may however be expected to be small for slight asymmetry since it does cancel for a symmetrical tee. The main effect of small asymmetry is then to introduce two additional terms the order of magnitude of which is 0.02 and varying in phase with respect to the dominant term $S_{13}S_{14}(e^{-2j\theta_1}-e^{-2j\theta_2})$ in the numerator of (8). The dominant term has a magnitude of approximately unity, so the beating of these terms could be expected to produce an additional phase error of around $\pm\tan^{-1}0.02$ or $\pm1.14°$ if both perturbing terms add in phase. Thus a maximum phase error or departure from linearity of 2° may occur if all the errors add in phase and are 90° out of phase with the dominant wave. The experimental results show that in practice errors of less than 1° can be obtained using commercially available magic-tees.

Appendix

Since $[S]$ is unitary, it follows that

$$U_{11}^2+|S_{12}|^2+|S_{13}|^2+|S_{14}|^2=1 \tag{16}$$

$$2|S_{13}|^2+U_{33}^2=1 \tag{17}$$

$$2|S_{14}|^2+U_{44}^2=1 \tag{18}$$

$$U_{11}(S_{12}^*+S_{12})-|S_{13}|^2+|S_{14}|^2=0 \tag{19}$$

$$S_{13}^*(U_{11}-S_{12})+S_{13}U_{33}=0 \tag{20}$$

$$S_{14}^*(U_{11}+S_{12})+S_{14}U_{44}=0. \tag{21}$$

These six independent equations have nine unknown variables. It is then in general necessary to know the values of at least three of them to solve for all the others. Because the diagonal elements are the reflection coefficients measured in the four reference planes, they seem an appropriate choice of values to use.

From (17)

$$|S_{13}|^2=\frac{1-U_{33}^2}{2}. \tag{22}$$

From (18)

$$|S_{14}|^2=\frac{1-U_{44}^2}{2}. \tag{23}$$

From (19)

$$S_{12}+S_{12}^*=\frac{U_{44}^2-U_{33}^2}{2U_{11}}.$$

Now

$$S_{12}=U_{12}+jV_{12},$$

$$S_{12}+S_{12}^*=2U_{12},$$

and hence

$$U_{12}=\frac{U_{44}^2-U_{33}^2}{4U_{11}}. \tag{24}$$

Substitution of (22) and (23) in (16) gives

$$|S_{12}|^2=\frac{U_{33}^2+U_{44}^2}{2}-U_{11}^2. \tag{25}$$

But

$$|S_{12}|^2=U_{12}^2+V_{12}^2 \tag{28}$$

whence

$$V_{12}^2=\frac{U_{33}^2+U_{44}^2}{2}-U_{11}^2-U_{12}^2. \tag{27}$$

Acknowledgment

The writer is very pleased to thank Dr. R. E. Collin for his fruitful discussions and R. Lépine for his help in the experimental work.

Excess Noise in Microwave Crystal Diodes Used as Rectifiers and Harmonic Generators*

J. M. RICHARDSON† AND J. J. FARIS†

Summary—**Excess noise produced by microwave excitation of silicon crystal diodes was studied for operation of the crystal as a detector and as a microwave harmonic generator. The noise appears at the detector terminals and also as noise sidebands of the microwave harmonic, thus degrading the spectral purity of the harmonic relative to that of the fundamental. Possible models of the processes involved are presented. Difficulties and technique of measurement are discussed. Observations for 1N26 crystals, used as detectors, doublers, and triplers, and excited by *X*-band power in the range 8 to 100 mw are presented, showing limitations on spectral purity set by the process of noise production during harmonic generation.**

Introduction: Motivation and Problem

In precision work in microwave measurements, for example, microwave spectroscopy and interferometry, it is important to know the spectral purity of the sources used because the problem is usually not that of the minimum detectable signal but that of the minimum detectable change in a strong signal. If the transmission and detection portions of an experiment have been made sufficiently noise free, the source noise temperature may set the limit of precision in the measurements.

The most important present source of monochromatic waves in the millimeter region is the crystal diode harmonic generator. This device is, for convenience, also frequently used in producing low-level centimetric waves from uhf inputs. Since there were indications that the output harmonics were rather noisy, a study of the multiplication process and the associated noise was undertaken. The existence of excess noise in a crystal detector having the familiar $1/f$ spectral density is already known, and it was asked whether these phenomena were related. For example, the excess noise currents flowing as a result of the fundamental microwave excitation and its rectification may become modulated onto the harmonic by virtue of the nonlinear nature of the crystal and appear as noise sidebands with spectral density and magnitude characteristic of the low-frequency excess noise.

The problem may then be stated as: Given a crystal diode n-harmonic generator excited by power P_1, at angular frequency ω, investigate the noise sideband power associated with the nth harmonic, S_n, if any. S_n may be investigated as a function of P_1 and frequency; and its relationship to S_0, the excess noise power of the crystal used as a detector, may also be investigated. The nature of S_n may be studied in any convenient way, but perhaps the simplest is by demodulation of the spectrum in the neighborhood of $n\omega$.

Models

The problem can be considered as a generalized mixer problem in which the exciting microwave may be thought of as the local oscillator.[1] Fig. 1 illustrates the model and Fig. 2 illustrates the spectral relations involved. The harmonic generator is fed at the terminals ω with high level microwave power P_1 in the range 10 to 100 milliwatts. Rectified power or harmonics will appear at the terminals dc, 2ω, $\cdots$ $n\omega$. For any particular harmonic generator, say a tripler, the terminals at the desired harmonic are connected to a matched load and an attempt to reactively terminate the other microwave terminals is made. The dc termination is a resistor providing self bias for the crystal.

In the absence of input power other than at the frequency ω, no other outputs except those just mentioned will occur. If, on the other hand, power is fed to the terminals β, perhaps by the internal production of a component of excess noise in the crystal, converted power will appear at all signal and image terminals, $n\omega \pm \beta$. In Fig. 2, the power at β and $n\omega \pm \beta$ is shown distributed over a small band to emphasize its possible noisy character. The band represents the limiting band of the apparatus. Interest is focused on near-carrier noise components (β small) for two reasons: 1) The severity of the effect is greater for small β due to the $1/f$ excess noise spectrum, and 2) it is desired to analyze experiments which may involve slow signal modulation of the carrier $n\omega$, as for example, by 30 cps Stark or Zeeman modulation of a microwave spectral line. Sidebands due to this signal modulation would then be superimposed on the noise-sideband power, to give some signal-sideband/noise-sideband power ratio.

Although the above description, in terms of generalized mixer theory, is undoubtedly a correct and potentially fruitful model, analysis of the problem was not attempted in these terms. This decision was taken because of the formidable problem of specifying the admittance matrix of the mixer at a particular P_1, and also as a function of P_1, and of specifying the terminating impedances of all the terminals.

* Manuscript received by the PGMTT, December 19, 1956. Part of this work was carried out under a program of research and development in basic instrumentation cooperatively supported by ONR, AFOSR, AEC, and NBS.

† Natl. Bur. of Standards, Boulder, Colo.

[1] H. C. Torrey and C. A. Whitmer, "Crystal Rectifiers," Rad. Lab. Ser., vol. 15, McGraw-Hill Book Co., Inc., New York, N. Y.; 1948.

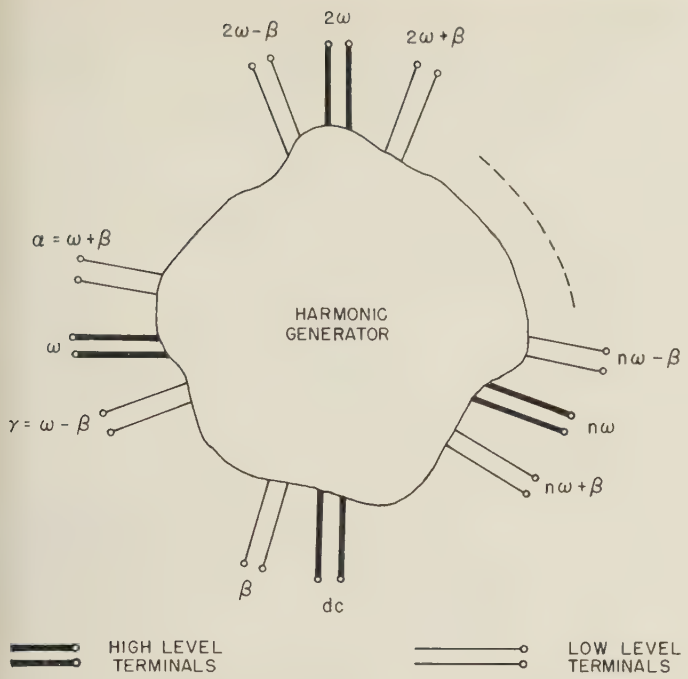

Fig. 1—Generalized mixer showing high- and low-level terminals at various frequencies of interest.

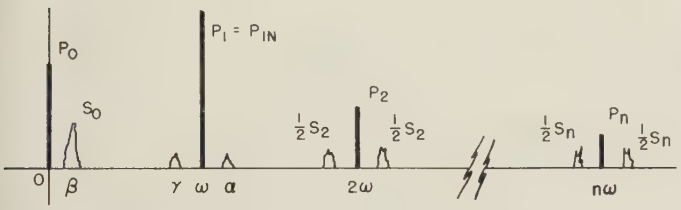

Fig. 2—Spectrum of interest in the detector-harmonic generator problem. The lines at 0, ω, 2ω, $\cdots$, $n\omega$ are spectral lines whose heights have been depicted proportional to the power they represent. The small bands represent spectral densities of noise power whose integrated values over a specified band are denoted by S_0, S_2, etc.

An alternative model was, therefore, used for guidance. Some current-voltage characteristic, $i(e)$, valid at all frequencies of interest,[2] is assumed, and is expanded about the origin in the power series

$$i = \sum a_m e^m. \tag{1}$$

In this series the applied voltage, e, has the form

$$e = E_0 + E_1 \cos \omega t + B(t) \tag{2}$$

where E_0 is the self bias developed across the diode terminals, $E_1 \cos \omega t$ is the applied microwave voltage at angular frequency ω of amplitude E_1 corresponding to P_1, and $B(t)$ is a time dependent virtual applied voltage descriptive of the excess noise generated by the crystal upon excitation. $B(t)$ may be thought of as narrow-band noise near the frequency β, whose magnitude is described by B. E_0 and β are functions of E_1 (or P_1).

Substituting (2) into (1) and retaining several terms in the power series because of the highly nonlinear characteristic and large excursion of e, it is possible to write expressions for P_n and S_n in terms of P_1, E_0, and B, and the coefficients a_m. The dependence of E_0 on P_1 is observable from the experiment. The result is that

$$S_n = G_n B^2$$

and

$$S_n/P_n = H_n B^2 \tag{3}$$

where G_n and H_n are functions of P_1, E_0, and the a_m. Eq. (3) have such form as to permit various dependences of the various S_n with P_1.

Problem of Measurement

Although the source is made as noise free as possible, it is unavoidably noisy to some degree, and care must be taken that the observed noise is not demodulated source noise, S_1, (that is, noise associated with P_1) in the case of the detector experiments, and does not arise from source noise modulated onto the harmonics in the case of the multiplier experiments. Source noise would appear at the detected output of the crystal with relative amplitude determined by S_1/P_1 and the shape of the P_1–P_0 curve. Analysis using the above described models suggests that noise arising from S_1 would appear on all harmonic outputs in relative strength determined by S_1/P_1, and the shape of the P_1–P_n curve.

Thus it was found necessary to carry out the measurements using techniques that balance out the effects of the noise modulation of the source. The rejection ratio required to insure that the measurements obtained were not influenced by the source noise modulation could be estimated by making measurements with the system both balanced and unbalanced.

As a further precaution, demodulation of the harmonics was always carried out using a bolometer, an excess-noise free device, so that it was certain that the bolometer output, if well above its own thermal noise level, consisted essentially of noise demodulated from the harmonic and its noise sidebands.

Technique of Measurement

Although interest was focused on the generation of millimeter waves from centimetric waves, measurements were conducted at X band to enjoy the convenience of complete instrumentation at the fundamental and the first few harmonics. Type 1N26 crystals, a useful type in millimeter wave generation, were used.

The source of X-band power used was a klystron, type SMX-32, operating as the final stage of a frequency multiplying chain. The first stage of this chain was a temperature-controlled quartz crystal oscillator.

Measurements of S_0, the excess noise in detectors, were made with the apparatus of Fig. 3. The detector mount terminating the branch produced by the shunt tee was used for two purposes. First, a bolometer could be placed in this mount to monitor the noise modulation on the output of the source. Second, a crystal

[2] This assumption is of course not strictly valid, as seen from the usual equivalent circuit of the crystal diode.

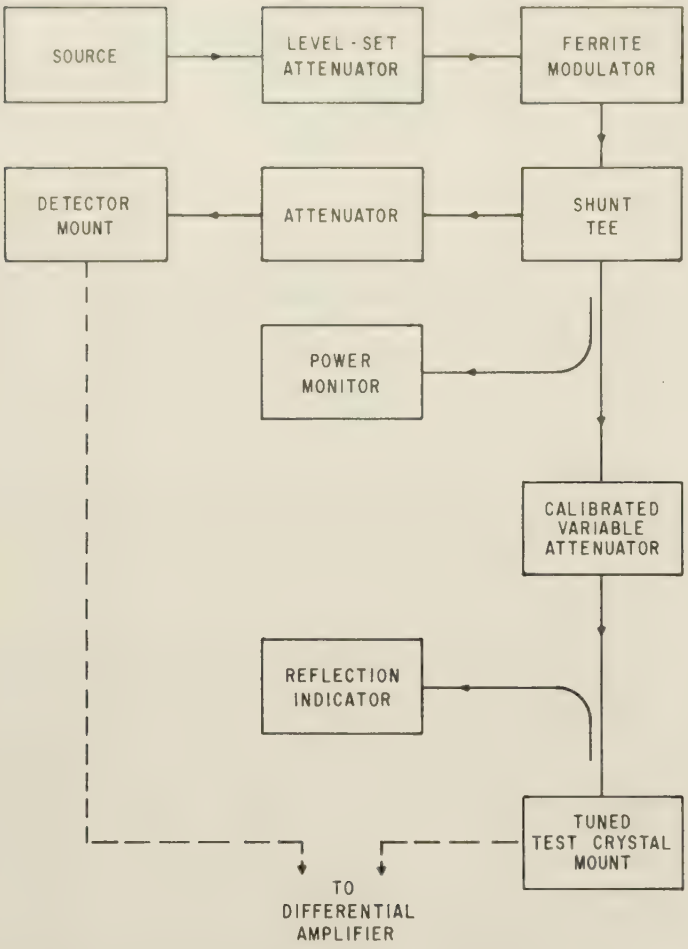

Fig. 3—Microwave circuit used for investigation of excess noise in detector diodes.

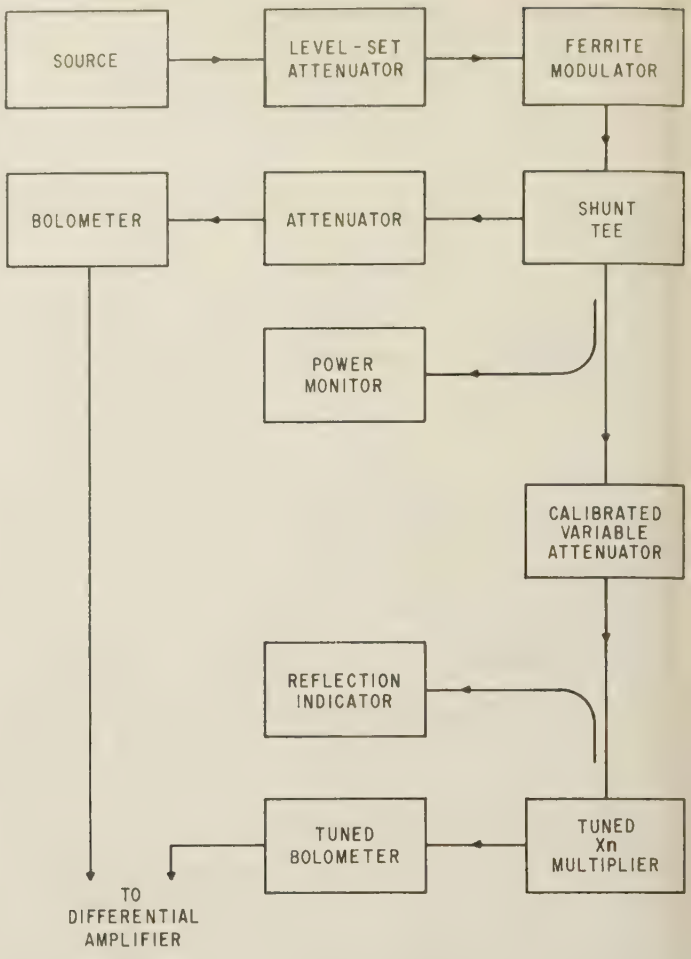

Fig. 4—Microwave circuit used for investigation of noise modulation introduced by crystal diode harmonic generators.

placed in this mount was used to obtain a signal to be introduced into a differential amplifier with the signal from the crystal under test. Thus the input to the differential amplifier consisted of in-phase detected source noise from each crystal and incoherent excess noise from each crystal. The former noise did not appear in the amplifier output because of the differential action, while the latter combined according to an rms rule.

The ferrite modulator was used for two purposes. First, it was used to produce modulation at the center frequency of the narrow-band amplifier to tune the test crystal to eliminate reflections. Second, it was used to produce modulation to enable adjusting the attenuator preceding the balancing detector for maximum discrimination against source modulation. Rejection ratios of over 100 times were easily obtained for the detected voltage due to source modulation. For all data taken, this rejection ratio was adequate.

Because of the balancing technique employed, in order to obtain a single measurement of S_0, the excess noise in the crystal under test, three measurements were needed. First, the noise present in the balanced system described above was measured, then the noise present in the test crystal and in the balancing crystal were each measured separately. From these three measurements, enough information was obtained to find the excess noise generated by the test crystal alone. The crystal under test was always operated with a load resistance of 10,000 ohms.

Measurements of S_2 and S_3 and P_2 and P_3 for doublers and triplers were made with the apparatus of Fig. 4. Again, it was found necessary to eliminate the effects of the source modulation by using a differential method. The bolometer terminating the branch formed by the shunt tee and the bolometer demodulating the multiplied power both produced signals due to the noise on the source output, whereas the bolometer detecting the multiplier output also detected the noise introduced by the process of multiplication. Thus the differential action of the circuit rejected the in-phase noise produced by modulation of the source and recorded only the noise produced by the multiplication. As in the measurements of S_0, it was necessary to adjust the power demodulated at the balancing bolometer to obtain maximum rejection of the in-phase signal. The ferrite modulator was used to produce a modulation for the purpose of making this

adjustment. It was found that a rejection of over 50 times could easily be obtained. For all of the data taken, this ratio was determined to be adequate.

Finally the multiplied power could be measured with a power bridge at the bolometer following the multiplier.

The multiplying crystals were always operated with the bias resistance that produced the maximum multiplied power output. When doubling, this resistance was usually in the range from 50 to 200 ohms. For tripling, a broad plateau of maximum power occurred for bias resistance of about 5000 ohms and above, therefore in this case the bias used was always 10,000 ohms.

The measuring apparatus is shown in Fig. 5. The audio-frequency harmonic analyzer was used as a narrow-band af voltmeter, centered at either 270 or 540 cps. Its output was averaged in a circuit with time constant of approximately 25 seconds and recorded with a recording milliammeter. Each measurement was taken by operating the recorder at least three minutes and the resulting trace was averaged visually.

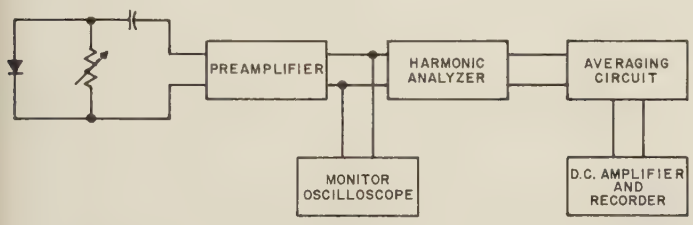

Fig. 5—Block diagram of noise recording apparatus.

Results

Results are presented as the square of a modulation coefficient because this is a measure of the spectral purity of the wave involved, namely the ratio of noise sideband power in a given band, S, to the carrier power, P. As described above, S is the remaining noise after elimination of the effect of source noise. We have

$$m_n^2 = 2S_n/P_n \qquad (4)$$

where $n=2$, 3 for the doubler and tripler, and $n=0$ for the detector. The definition of modulation coefficient used agrees with Goldman[3] for a complex waveform, and is on the basis of unit bandwidth. Values of S_n given by (4) may be used to obtain noise temperatures of the multipliers as sources if desired.

Table I shows the variations of spectral purity with crystal, input power, type of operation, and frequency. In general, a crystal which is noisy as a detector (large m_0) is also noisy as a multiplier. This result is expected if the addition of noise in the multiplication process arises from excess noise. The value of m_n^2 usually increases with P_1, for $n=0$, 2, 3 although there are exceptions. This fact substantiates at these high power levels

TABLE I
Excess Noise Modulation Coefficients Together with Outputs for 1N26 Crystals Used as Detectors, Doublers, and Triplers

Crystal No.	P_1 db below 100mw	$10^{12}m_0^2$ at 270~	$10^{12}m_2^2$ at 270~	$10^{12}m_2^2$ at 540~	$10^{12}m_3^2$ at 270~	V_0 (volts)	P_2 (μw)	P_3 (μw)
2	1	3.2	0.6	0.3	1.2	4.8	850	510
	3	5.3	0.6	0.4	1.2	4.2	550	320
	5	4.8	0.6	0.4	1.0	3.5	330	220
	7	4.8	0.6			3.0		
60	1	25.0	0.8	0.6	18.0	2.4	830	280
	3	13.0	0.5	0.5	8.4	2.4	550	240
	5	14.0	0.8	0.4	5.8	2.3	340	170
	7	13.0			3.6	2.2		100
	9	14.0				2.1		
61	1	200.0	3.6	1.4	140.0	2.3	980	250
	3	94.0	5.8	4.0	23.0	2.4	610	200
	5	59.0	10.2	8.4	27.0	2.4	330	120
	7	40.0	13.0	13.0	30.0	2.2	170	59
	9	30.0	19.0	10.9		2.0	74	
	11	15.0	16.0			1.6	26	
62	1	72.0	2.6	1.7	32.0	2.4	770	280
	3	42.0	2.0	1.4	20.0	2.4	530	220
	5	49.0	1.4	1.0	15.0	2.4	330	150
	7	50.0	1.4	0.6	8.4	2.3	170	83
	9	49.0				2.1		
	11	35.0				1.9		
63	1	29.0	0.4	0.3	19.0	2.7	700	270
	3	26.0	0.3	0.2	19.0	2.6	460	200
	5	24.0	0.2	0.1	19.0	2.5	290	110
	7	29.0			18.0	2.4		46
	9	30.0				2.3		
	11	36.0				2.0		

the strong dependence of excess noise production on input power quoted by some authors[4] as P_1^2 at lower power levels. It also is seen that the tripler output is less pure than the doubler output for all crystals and input powers. This fact is understandable in terms of the reduced efficiency of their harmonic production, whereas excess noise production for a given input power is unaltered.

Table I also shows that the noise modulation at 540 cps on the doubler output is smaller than that at 270 cps. This result can also be explained by the assumption that excess noise is the primary cause of the multiplier noise. It is known that excess noise has a power spectrum that varies approximately as $1/f$, so that modulation sidebands arising from this noise should have the same power spectrum by (3).

Finally, m_3^2 seems to bear a closer relation to m_0^2 than to m_2^2 as to both magnitude and dependence on P_1. This behavior is possibly related to the fact that m_0 and m_3 were observed using the same bias resistance, whereas m_2 was observed with a lower bias resistance.

In the practical case of a fundamental source of modulation coefficient m_1, the total relative noise in the output would probably be given by adding a term of the

[3] S. Goldman, "Frequency Analysis, Modulation and Noise," McGraw-Hill Book Co., Inc., New York, N. Y.; 1948.

[4] M. W. P. Strandberg, H. R. Johnson, and J. R. Eshbach, "Apparatus for microwave spectroscopy," *Rev. Sci. Instr.*, vol. 25, p. 776; August, 1954.

order of m_1^2 (due to an excess noise-free multiplier) to m_n^2 (due to excess noise only). Thus the amount of degradation of signal purity depends on the characteristics of the particular fundamental source used. In this work, the source had $m_1 = 0.65 \times 10^{-6}$ ($m_1^2 = 0.42 \times 10^{-12}$) so that the degradation was high with all tripler crystals and "noisy" doubler crystals, but not severe with "quiet" doubler crystals.

The rather important question of whether the multiplier noise produces fm sidebands in addition to AM sidebands was not answered by this study, since only the AM sidebands were recovered. However, if as suggested, the mechanism is that of excess noise, the production of fm sidebands should not occur.

Conclusion

The results of an investigation into the degradation of spectral purity by the processes of detection and harmonic generation in crystal diodes have been presented. No completely satisfactory model of the process of harmonic generation has been developed, but two possible approaches were presented. The measurements are difficult because of the need to avoid the influence of residual source modulation on the results. An X-band source of equivalent noise modulation index of about 0.7×10^{-6} for unit bandwidth centered at 270 cps from the carrier was satisfactorily used. For 1N26 crystals as detectors, doublers, and triplers excited with X-band input power from 8 to 100 mw, noise dependent on the individual crystal, input power, and frequency is added to the output. The noise modulation introduced by the multiplication process has characteristics similar to the excess noise observed in crystal detectors.

Further investigation, involving the examination of many more crystals, more complete spectral density data of the various noise powers, and fm noise would be desirable as an aid to the designer of precision experiments in the microwave and millimeter wave region.

Exponential Transmission Lines as Resonators and Transformers*

RABINDRA N. GHOSE†

Summary—**An attempt has been made to analyze the theory of an exponential transmission line from its complex reflection coefficient's standpoint and to indicate how the characteristics of an exponential line can be completely represented for any frequency with the help of the Smith Chart. It is shown that the optimum design parameters of an exponential transmission line which may be used as a transformer, with a frequency-sensitive load at one end, can be determined with the help of the Smith Chart and some derived equations. This paper also includes a study of the coaxial type exponential line which can be used as a series or parallel resonator. Theoretical expressions for the attenuation constant, stored energy, and Q for such types of resonator have been derived. Also indicated in this paper is the possibility of replacing the uniform-line coaxial-type resonators in many microwave and uhf wave filters by the exponential-line resonators, particularly when a large power-handling cpacity is warranted.**

Introduction

IN RECENT YEARS the exponential transmission line has found wide application in microwave networks as a matching device suitable for matching two unequal impedances over a wide band of frequencies. A general analysis of the exponential transmission line has been made by Burrows[1] and Schelkunoff.[2] The purpose of this paper is to analyze the theory of the exponential line from its reflection coefficient's standpoint and to indicate how the characteristics of an exponential line can be represented with the help of a Smith Chart which is primarily designed for uniform transmission lines. The possibility of using the exponential transmission line in the form of a resonator is also discussed in this paper.

General Equations and Their Solution

For any transmission line system the differential equations for the voltage and current can be represented by

$$\left.\begin{aligned}\frac{dV}{dz} + Z(z)I &= 0\\ \frac{dI}{dz} + Y(z)V &= 0\end{aligned}\right\} \tag{1}$$

where

V = voltage across the transmission line at z,
I = current in the transmission line at z,
Z = equivalent series impedance per unit length of the line,
Y = equivalent shunt admittance per unit length of the line.

For a nonuniform transmission line, $Z(z)$ and $Y(z)$ are functions of z; *i.e.*, they are functions of the position along the line. Eq. (1) will usually give rise to a set of second-order differential equations

$$\left.\begin{aligned}\frac{d^2V}{dz^2} - \frac{d}{dz}[\ln Z]\frac{dV}{dz} - ZYV &= 0\\ \frac{d^2I}{dz^2} - \frac{d}{dz}[\ln Y]\frac{dI}{dz} - ZYI &= 0\end{aligned}\right\}. \tag{2}$$

Walker and Wax[3] have shown that these second-order differential equations can be converted into a single first-order nonlinear differential equation

$$\frac{d\rho}{dz} - 2\gamma\rho + \frac{1}{2}(1-\rho^2)\frac{d}{dz}\ln Z_0 = 0 \tag{3}$$

where

$$\rho = \frac{V/I - Z_0}{V/I + Z_0}, \qquad Z_0 = \sqrt{Z/Y}$$

and

$$\gamma = \sqrt{ZY}.$$

For an exponential transmission line,[4]

$$Z_0 = ke^{\alpha z} \tag{4}$$

where k is the characteristic impedance of the line at $z=0$, and α is the rate at which the characteristic impedance changes exponentially with the position z.

From (3) and (4) one obtains the differential equation for an exponential line

$$\frac{d\rho}{dz} - 2\gamma\rho + \frac{\alpha}{2}(1-\rho)^2 = 0. \tag{5}$$

* Manuscript received by the PGMTT, January 30, 1957. Presented at the IRE-WESCON Conf., Los Angeles, Calif.; August 21–24, 1956.

† The Ramo-Wooldridge Corp., Los Angeles, Calif. Formerly with Radio Corp. of America, Camden, N. J.

[1] C. R. Burrows, "The exponential transmission line," *Bell Sys. Tech. J.*, vol. 17, pp. 555–573; October, 1938.

[2] S. A. Schelkunoff, "Electromagnetic Waves," D. Van Nostrand Co., Inc., New York, N. Y., p. 222.

[3] L. R. Walker and N. Wax, "Non-uniform transmission lines and reflection coefficients," *J. Appl. Phys.*, vol. 17, pp. 1043–1045; December, 1946.

[4] For an exponential line whose Z_0 decreases from $z=0$, α in (4) can be replaced by $(-\alpha)$.

If one is interested in the coaxial form of exponential line through which TEM waves propagate without cutoff, γ can be regarded as a constant function of the position z, since both α and $\beta = 2\pi/\lambda$ are independent of z. This is also true for the parallel-wire transmission line and the strip transmission line carrying TEM waves.

Thus, making use of the following transformation

$$\bar{\rho} = \rho + \frac{2\gamma}{\alpha}; \qquad S^2 = \left(\frac{4\gamma^2}{\alpha^2} + 1\right) \tag{6}$$

one obtains from (5)

$$\int \frac{d\bar{\rho}}{\bar{\rho}^2 - S^2} = \frac{\alpha}{2}\int dz + C \tag{7}$$

and

$$\rho(z) = -\left[\frac{2\gamma}{\alpha} + S\,\frac{\left(\tanh\frac{\alpha S z}{2} + \tanh SC\right)}{\left(1 + \tanh\frac{\alpha S z}{2}\tanh SC\right)}\right] \tag{8}$$

where C is the constant of integration which has to be evaluated from the boundary condition.

Let the boundary condition be so assumed that $\rho(l) = \rho_0$, where ρ_0 is known. From (8), then,

$$\tanh SC = -\left[\frac{\left(\rho_0 + \frac{2\gamma}{\alpha}\right) + S\tanh\frac{\alpha S l}{2}}{S + \left(\rho_0 + \frac{2\gamma}{\alpha}\right)\tanh\frac{\alpha S l}{2}}\right] \tag{9}$$

and

$$\rho(z) = -\left(\frac{2\gamma}{\alpha} - \bar{\bar{Z}}_{in}\right), \tag{10}$$

where $\bar{\bar{Z}}_{in}$ is the input impedance of a uniform transmission line with normalized surge impedance of one and which is terminated at the load end, $z = l$, by an impedance

$$\bar{\bar{Z}}_l = \left(\frac{\rho_0}{S} + \frac{2\gamma}{\alpha S}\right). \tag{11}$$

As the equivalent $\bar{\bar{Z}}_{in}$ can readily be obtained from the Smith Chart when α, γ, and ρ_0 are known, the effect of the exponential-line transformer in terms of the reflection coefficient and vswr at the input end can be determined without too much laborious computation even when a frequency-sensitive load with arbitrarily varying reflection coefficient is connected at the load end. It may be remarked that while computing $\bar{\bar{Z}}_{in}$, the electrical length of the line should be considered as $\bar{\beta}l$, where

$$\bar{\beta} = \beta\sqrt{1 - \frac{\alpha^2}{2\beta^2}} \tag{12}$$

for a lossless exponential line transformer.

To enable the transformer to work well beyond the cutoff frequency, it will be desirable to choose α such that

$$\alpha \ll \frac{4\pi}{\lambda}, \tag{13}$$

λ being the wavelength corresponding to the lowest frequency in the passband which has to be transmitted through the transformer. The fictitious impedance $\bar{\bar{Z}}_l$ in (11) is, in general, complex. Assuming the transformer is lossless and is operating well beyond cutoff

$$\gamma = i\beta$$

and

$$\bar{\bar{Z}}_l = \frac{\beta}{\bar{\beta}} - i\,\frac{\rho_0\alpha}{2\bar{\beta}}. \tag{14}$$

In order to make use of the method described, it is essential that $\bar{\bar{Z}}_l$ should be in the right half-plane, as otherwise one cannot make entries on the Smith Chart to compute $\bar{\bar{Z}}_{in}$. To ensure this, one can set

$$\frac{\beta}{\bar{\beta}} - \mathrm{Re}\left\{\frac{|\rho_0|}{2}\,\frac{\alpha}{\bar{\beta}}\exp\left[i\left(\theta + \frac{\pi}{2}\right)\right]\right\} \geq 0 \tag{15}$$

where θ is the phase angle of the reflection coefficient ρ_0 at the load end of the transformer. That is,

$$\beta \geq \frac{|\rho_0|}{2}\,\alpha\cos\left(\theta + \frac{\pi}{2}\right).$$

But $|\rho_0| \leq 1$ and the value of $\cos(\theta + \pi/2) \leq 1$. Hence,

$$|\rho_0|\cos\left(\theta + \frac{\pi}{2}\right) \leq 1$$

and

$$\beta > \frac{\alpha}{2}.$$

But this condition has already been assumed in order to enable the transformer to operate well beyond the cutoff frequency. Hence no difficulty will be experienced in computing $\rho(0)$ according to the method described above. An equivalent circuit describing the method of computing $\rho(0)$ is shown in Fig. 1. It should be recognized that this method will be of considerable help in synthesizing the design parameters of a transformer for optimum $\rho(0)$ over a frequency band with any specific load connection.[5]

Exponential Line as a Resonator

From the preceding analysis, it appears that a standing wave can be maintained in a section of lossless exponential line when ρ_0 is chosen ± 1. This suggests the possibility of the use of the exponential line as a resonator.

[5] Schelkunoff, *op. cit.* The reflection chart shown in Fig. 7.11 can be used to determine the complex reflection coefficient when the normalized impedance of the arbitrary load is known. Similarly, the input impedance of the transformer for an arbitrary load can be determined readily from Fig. 1 above and the reflection chart.

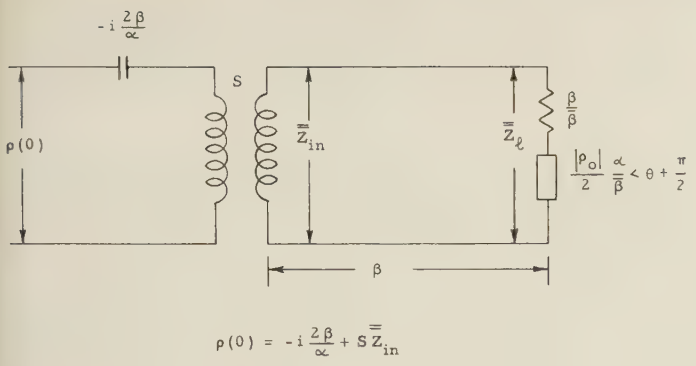

Fig. 1—Equivalent circuit of an exponential transformer.

Let it be assumed that one is interested in using a section of an exponential line as an infinite-impedance or parallel-resonance type resonator when one end of the line is short-circuited at $z=l$, as shown in Fig. 2. This is analogous to a $\lambda/4$ cavity for a uniform line

$$\rho_0\big|_{z=l} = -1, \qquad \rho(0) = 1. \tag{16}$$

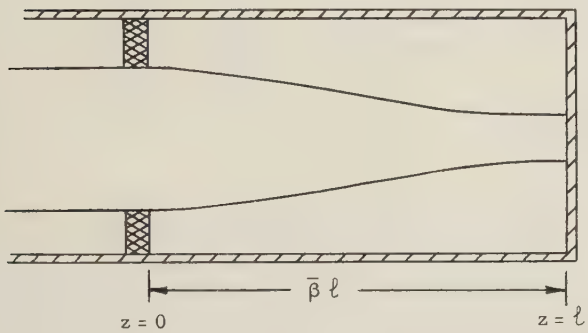

Fig. 2—Exponential resonator with Z_0 increasing with $z>0$.

From (10),

$$\frac{\alpha S l}{2} = (2k-1)\frac{\pi}{2}$$

where k is any integer. The required length for parallel resonance is

$$l_p = \frac{\pi(2k-1)}{\sqrt{4\beta^2-\alpha^2}}$$

and

$$l_{p,\min} = \frac{\lambda}{4\left(1-\dfrac{\alpha^2}{4\beta^2}\right)^{1/2}} \tag{17}$$

where a lossless line is assumed, such that $\gamma=i\beta$. Similarly, if one is interested in using the exponential line as a series resonator,

$$\rho_0\big|_{z=l} = -1, \qquad \rho(0) = -1, \qquad \frac{\alpha S l}{2} = n\pi \tag{18}$$

where n is any integer.

The length of the resonator is

$$l_s = \frac{\alpha\pi n}{(4\beta^2-\alpha^2)^{1/2}}$$

and

$$l_{s,\min} = \frac{\lambda}{2\left(1-\dfrac{\alpha^2}{4\beta^2}\right)^{1/2}}. \tag{19}$$

Fig. 3 shows the required length of the resonator for series- and parallel-type resonance.

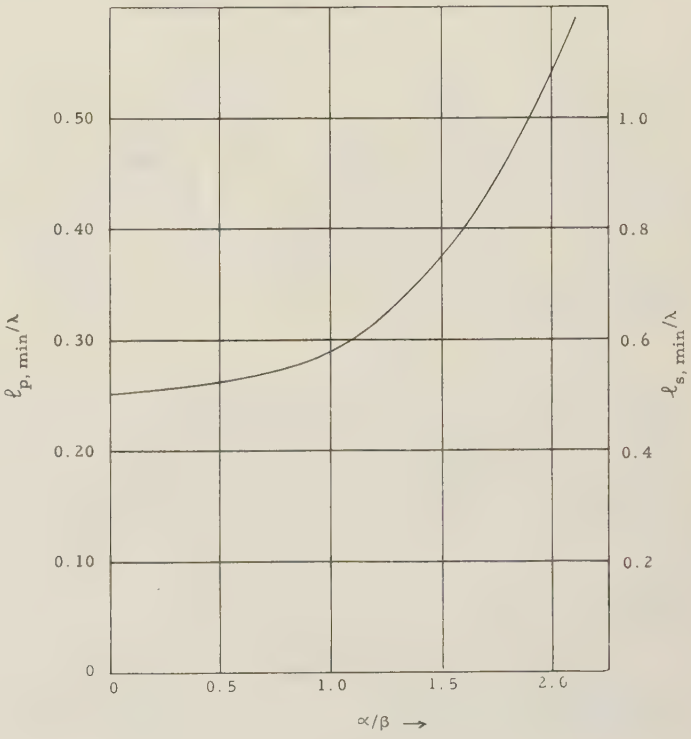

Fig. 3—Minimum resonant length of series and parallel-type exponential resonators.

Stored Energy, Wall Losses, and Q of an Exponential Resonator

From the differential equation of voltage in the exponential transmission line whose characteristic impedance increases with $z>0$, one obtains

$$V(z) = A\exp\left(\frac{\alpha z}{2} - i\bar{\beta}z\right) + B\exp\left(\frac{\alpha z}{2} + i\beta z\right) \tag{20}$$

where A and B are arbitrary constants. When a shorting plate is placed at $z=l$,

$$V(l) = 0,$$

$$\frac{A}{B} = -e^{i2\bar{\beta}l}, \qquad \bar{\beta} = \beta\sqrt{1-\frac{\alpha^2}{4\beta^2}}$$

and

$$V(z) = -2iBe^{i\beta l}e^{(\alpha z/2)}\sin(\bar{\beta}l - \bar{\beta}z). \tag{21}$$

Let the current at any z be represented as

$$I(\rho, z) = If(z).$$

For the TEM mode,

$$E_\rho(\rho, z) = \frac{\eta I f(z)}{2\pi\rho}$$

$$V = \int_{a(z)}^{b(z)} \frac{\eta I f(z)}{2\pi\rho}\, d\rho$$

and

$$E_\rho = -2iBe^{i\bar{\beta}l}e^{(\alpha z/2)}\frac{\sin(\bar{\beta}l - \bar{\beta}z)}{\left[\rho \ln \dfrac{b(z)}{a(z)}\right]}, \tag{22}$$

η being the intrinsic impedance of the free space. At resonance, the maximum stored electrical energy is the same as the maximum stored magnetic energy, and when the stored electrical energy is maximum, the stored magnetic energy is zero. Hence the stored energy in a section of an exponential line acting as a resonator can be obtained from its stored electrical energy alone.

Stored electrical energy

$$U = \frac{\epsilon}{2}\int_0^l \int_{a(z)}^{b(z)} \int_0^{2\pi} |E_\rho|^2 dz\rho d\rho d\phi$$

$$= M\epsilon\pi \int_0^l \int_{a(z)}^{b(z)} \frac{e^{\alpha z}\sin^2(\bar{\beta}l - \bar{\beta}z)}{\rho^2\left(\ln \dfrac{b(z)}{a(z)}\right)^2}\rho d\rho dz \tag{23}$$

where

$$M = 2|B|.$$

From the assumed variation of the characteristic impedance in an exponential line,

$$Z_0(z) = Z_0(0)e^{\alpha z}$$

$$= 60 \ln \frac{b(z)}{a(z)}. \tag{24}$$

Substituting the results of (24) in (23), one obtains

$$U = \frac{30\epsilon\pi M^2}{Z_0(0)}\left(l - \frac{\sin 2\bar{\beta}l}{2\bar{\beta}}\right). \tag{25}$$

For both series and parallel resonance, $\sin 2\bar{\beta}l = 0$,

$$U = \frac{30\epsilon\pi M^2 l}{Z_0(0)}$$

where ϵ is the dielectric constant of the medium inside the transformer. Fig. 4 shows a comparison of the stored energy in uniform and exponential type resonators.

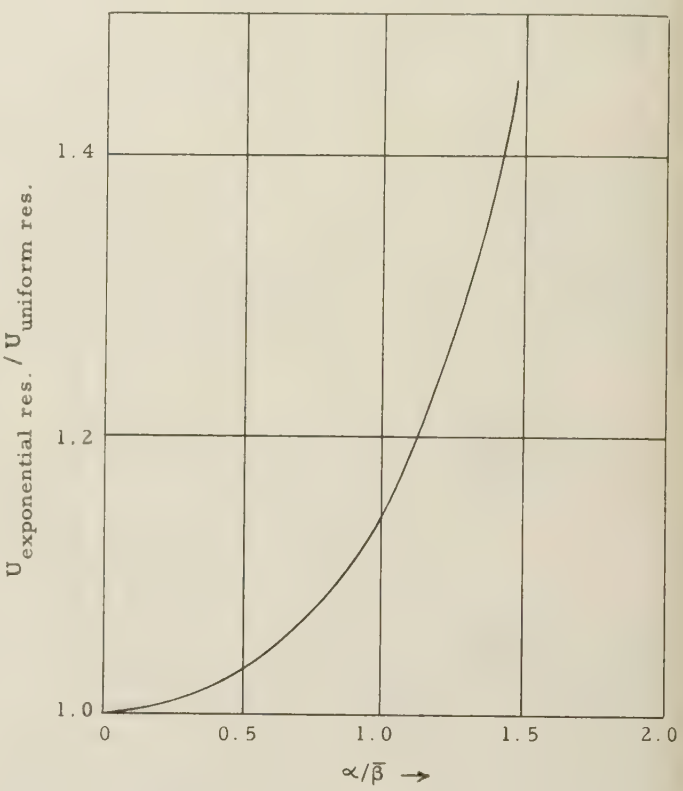

Fig. 4—Relative variation of stored energy in an exponential resonator.

The wall losses consist of the losses resulting from the tangential component of the magnetic field at the lateral surface and at the end plates of the resonator. These can be determined from the surface integral of the tangential H_ϕ over the entire surface.

For parallel resonance, analogous to the $\lambda/4$ type resonance in a uniform line resonator, the wall loss W becomes

$$W = \frac{R_s\pi M^2}{b\eta^2}\frac{3600}{Z_0^2(0)}\left\{\frac{Z_0(0)b}{60} + \frac{1}{2\alpha}\left\{\frac{\left(1 - e^{-\alpha l} + \dfrac{\alpha^2}{2\bar{\beta}^2}\right)}{1 + \dfrac{\alpha^2}{4\bar{\beta}^2}}\right.\right.$$

$$\left.\left. + \sum_{m=0}^{\infty}\left(\frac{Z_0(0)}{60}\right)^m \frac{1}{m!}\,\frac{1}{(m-1)}\left[\frac{e^{\alpha(m-1)l} - 1 - \dfrac{\alpha^2(m-1)^2}{2\bar{\beta}^2}}{1 + \dfrac{\alpha^2(m-1)^2}{4\bar{\beta}^2}}\right]\right\}\right\} \tag{26}$$

where R_s is the real part of the surface impedance of the metal forming the resonator.

If $Z_0(0)$ be chosen 60 ohms and

$$\alpha \to 0$$

then the Q of the resonator becomes

$$\frac{240\pi^2}{R_s}\left(8+\frac{\lambda}{a}+\frac{\lambda}{b}\right)^{-1}.$$

It is interesting to note that, when

$$\alpha \to 0$$

the exponential-line resonator becomes a uniform-line resonator and the Q of such resonator[6] is

$$\frac{240\pi^2}{R_s}\left(8+\frac{\lambda}{a}+\frac{\lambda}{b}\right)^{-1}.$$

The characteristic impedance of the lines is assumed to be the same in both cases.

The Q can be determined alternatively from the input reflection coefficient already derived. But the evaluation of Q from the field integrals reveals the characteristics of the resonator from the energy consideration.

Fig. 5 shows a comparison of Q for uniform-line and exponential-line resonators for different values of α/β, when $Z_0(0)=30$ ohms.

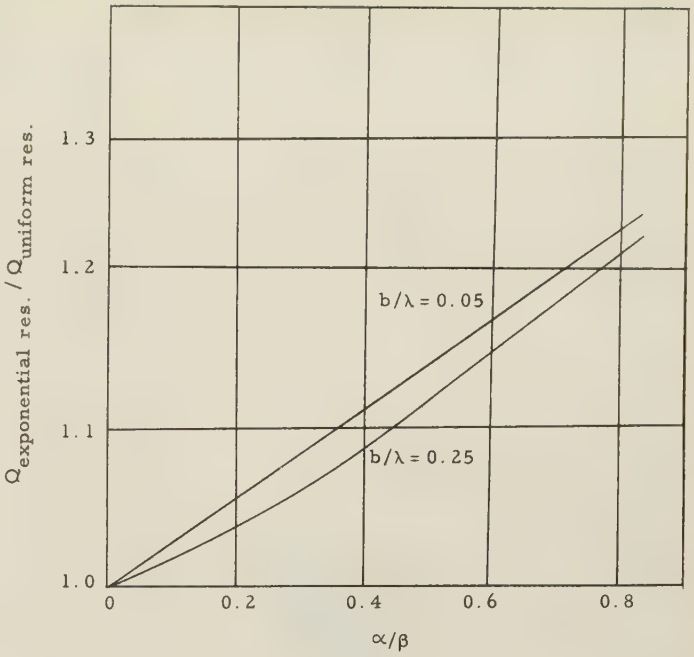

Fig. 5—Q gain in exponential resonator. Cavity length $= \dfrac{\lambda}{4\sqrt{1-\dfrac{\alpha^2}{4\beta^2}}}$.

Conclusion

An attempt has been made in this paper to describe a method by which the reflection coefficient of an exponential-line transformer can be determined readily, from the Smith Chart, particularly when a frequency-sensitive load or a transmission line whose input impedance changes with frequency is terminated at the load end. Analyses of this nature may be helpful in obtaining the optimum design parameters for the transformer for any specific load. Also discussed is the possibility of using the exponential-line resonator to indicate how, for some range of $Z_0(0)$, the Q of an exponential resonator can be increased greatly in excess of what would be expected in a uniform-line resonator for the same type of resonance. Similar analyses can be made for other nonuniform line resonators.[7]

[6] *Ibid.*, p. 280.

[7] R. N. Ghose, "Synthesis of Nonuniform Line," thesis submitted in partial fulfillment of requirements for degree of electrical engineer, Univ. of Ill.; 1956.

Correction

Tore N. Anderson, author of the paper "Rectangular and Ridge Waveguide," which appeared on pages 201–209 of the October, 1956 issue of these TRANSACTIONS, regrets the omission of the following reference. The illustration in Fig. 8 and the general equation for deflection of pressurized waveguide were obtained from James L. Briggs and Joseph B. Brauer, Technical Note RADC-TN-54-10, p. 3; August, 1954.

Correspondence

The Advantages of Expressing Standing-Wave Ratio in Decibels*

It has been the practice at Wheeler Laboratories for the past ten years to express standing-wave ratio in decibels as opposed to a numerical ratio. So far as we are aware, this practice first evolved in the Bell Telephone Laboratories. The relationship is defined as follows:

$$\text{db SWR} = 20 \log_{10} \text{VSWR}.$$

Expressing standing-wave ratio in db offers many advantages, as listed below.

1) SWR may be read by simple subtraction on a meter having a db scale. This avoids the necessity for precisely setting the level to unity on the ratio scale for the maximum-voltage location on the standing wave.

2) There is no need for designating SWR as a ratio of voltage (VSWR) or current or power, since decibels are so defined as to give the same number in any case. Similarly, expressing standing-wave ratio in db avoids the confusion between VSWR greater than unity, as is the custom in the U.S.A. and VSWR less than unity, as is the custom in Great Britain.

3) When expressed in db, SWR goes to to zero for zero reflection. This feature is an aid in plotting and in thinking; it is especially valuable in expressing tolerances.

4) When expressed in db, SWR is proportional to magnitude of reflection coefficient within 4 per cent out to 6 db SWR (VSWR of 2:1). By comparison, a plot of VSWR vs reflection coefficient shows a departure from proportionality that is ten times greater at the same value. The closer proportionality of the db scale results in easier interpretation of data.

5) The resultant of small reactive reflections in a lossless line adding in the worst phase may be determined by merely adding individual values of SWR expressed in db. For example, if a line contains ten bumps, each having a reflection of 0.5 db SWR, the maximum possible reflection is 5.0 db SWR.

6) Several computations involving reflection coefficients are simplified when SWR is expressed in db. One such computation is the determination of minimum insertion loss by the loss-circle method.[1]

These advantages, borne out in our own experience developing microwave components and antennas, lead us to recommend a wider adoption of the practice of expressing standing-wave ratio in db.

David Dettinger
Wheeler Labs., Inc.
Great Neck, N. Y.

* Received by the PGMTT, March 14, 1957.

[1] H. A. Wheeler and D. Dettinger, "Measuring the Efficiency of a Superheterodyne Converter by the Input Impedance Circle Diagram," Wheeler Monograph No. 9; 1949.

Contributors

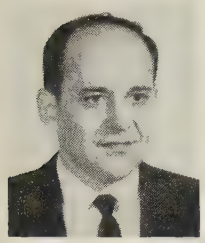

R. Bawer

Robert Bawer (S'47–A'50) was born on February 12, 1925, in Ellenville, N. Y. He first entered the University of Florida in 1942, returning after two years of military service to receive the bachelor of electrical engineering degree in 1947. From 1947 to 1949, he served as a research assistant at the Laboratory for Insulation Research, M.I.T. He received the M.S. degree in 1949 and in that year joined the staff of Melpar, Inc., where he was engaged in the design and development of multichannel communication equipment, railroad signaling and control devices, and microwave systems and components. In 1956 he left his position as project engineer at Melpar, Inc., to accept his present position as a principal engineer at the Emerson Research Laboratories in Washington, D. C.

❖

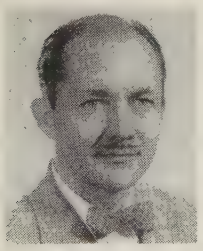

R. W. Beatty

Robert W. Beatty (S'43–A'45–M'50–SM'53) was born in York, Pa., on May 31, 1917. He received the degree of B.S. in electrical engineering in 1939 from the George Washington University, Washington, D. C., and the degree of S.M. in electrical communication in 1943 from the Massachusetts Institute of Technology, Cambridge, Mass. From 1940 to 1942, he was associated with the Naval Research Laboratory in work on underwater sound and radio direction finding. He was a staff aid at the M.I.T. Radar School in 1943 and served in the U. S. Naval Reserve from 1943 to 1946. He has had several years experience in the field of consulting radio engineering for the radio broadcast industry. Since 1948, he has been associated with the National Bureau of Standards, Boulder, Colo., working in the field of microwave standards, and is Chief of the Microwave Circuit Standards Section.

Mr. Beatty is a member of Sigma Tau, Theta Tau, RESA, and Commission I of the U.S.A. National Committee of the International Scientific Radio Union.

❖

Howard Boyet was born on August 2, 1924 in New York, N. Y. He received the B.S. degree in physics from the College of the City of New York in 1944 and the Ph.D. in physics from New York University in 1953. From 1944 to 1947, he did research in supersonic aerodynamics at the National Advisory Committee for Aeronautics. From 1947 to 1953 he was on the faculty of New York University as physics instructor and did research in aerodynamics and in the wave mechanical theory of atomic scattering. Since 1953, he has been engaged in research and development on solid state microwave devices with Bell Telephone Labs., Murray Hill, N. J.

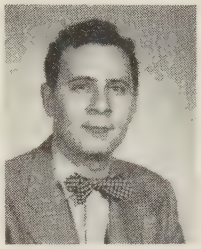

H. Boyet

Dr. Boyet is a member of the American Physical Society and the American Institute of Physics.

❖

Sinclair Chen was born in Shanghai, China, on June 8, 1930. In June, 1949 he came to the United States to attend Stanford University where he received the B.S. degree in electrical engineering in June, 1952. After graduation, he was employed by the Standard Coil Product Company in Los Angeles, Calif. From September, 1953 to September, 1954 he attended Syracuse University where he received the M.S. degree in electrical engineering in September, 1954. Since October, 1954, he has been a part-time research assistant and student in the Department of Electrical Engineering of The Ohio State University.

S. Chen

He is a member of Sigma Xi.

❖

Robert E. Collin (M'54) was born at Donalda, Alberta, Can., on October 24, 1928. He received the B.Sc. degree in engineering physics from the University of Saskatchewan in 1951. From 1951 to 1953, he studied at Imperial College, London, England, on an Athlone Fellowship. From 1953 to 1954, he was on a Canadian Defence Research Board grant. He received the Diploma of Imperial College and the Ph.D. degree from the University of London in 1954. Since then and up to the present time, Dr. Collin has been a scientific officer at the Canadian Armament Research and Development Establishment, Valcartier, P.Q., where he is engaged in microwave work related to guided missiles.

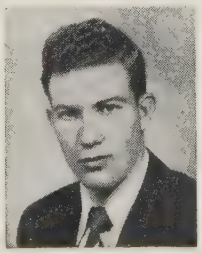

R. E. Collin

❖

John J. Faris was born in Grandview, Wash., on November 7, 1921. He graduated from Reed College, Portland, Ore., in 1943 and received the Ph.D. degree in physics from the University of Washington in 1951. Since that time he has been teaching physics, first at the Pacific University, Forest Grove, Wash., and since 1954 at Colorado Agriculture and Mining College. During the summer of 1955, he was employed by the National Bureau of Standards at Boulder, Colo.

J. J. Faris

His fields of major interest include secondary emission of electrons, solid state physics, and microwaves.

Dr. Faris is a member of The American Physical Society, The American Association of Physics Teachers, The American Association of University Professors, The Colorado-Wyoming Academy of Science, and Sigma Xi.

❖

For a photograph and biography of Rabindra N. Ghose, see page 76 of the January, 1957 issue of these Transactions.

❖

George P. Kefalas (S'50–A'52) was born in Granite City, Ill., on February 7, 1927. He received the B.S.E.E. degree in 1950 and the M.S.E.E. degree in 1951, both from the University of Illinois, Urbana, Ill.

G. P. Kefalas

From 1950 to 1951 he served as a research assistant at the University of Illinois, where he was engaged in experimental vhf-uhf receiver and antenna work for a signal reception study program. In 1951, he

joined the Sperry Gyroscope Co., where he worked in the design and development of microwave systems and components and missile guidance radars. He joined Melpar, Inc., in 1955 as a senior engineer where he was engaged in the design and development of microwave components. He is now directing the design and development of a proximity fuze as project engineer at Melpar.

❖

Herbert Kirschbaum (A'55) was born in Cleveland, Ohio, on February 6, 1920. He received the B.S. degree in 1942 from the Cooper Union, following which he entered the employ of the Westinghouse Electric Corporation. He received the M.S. degree from the University of Pittsburgh under the Pitt-Westinghouse cooperative plan in 1946. In 1946 he joined the staff of The Ohio State University to both teach and do research on pulse transformers. During 1952–1953, he took a leave of absence from Ohio State University to complete the requirements for the Ph.D. degree at Carnegie Institute of Technology. Upon returning to Ohio State University he has, in addition to teaching, been affiliated with the Antenna Laboratory of Ohio State University. He is an Associate Professor in the Department of Electrical Engineering at Ohio State.

H. KIRSCHBAUM

Dr. Kirschbaum is a member of Eta Kappa Nu and Sigma Xi.

❖

John M. Richardson (S'56) was born September 5, 1921, in Rock Island, Ill. He received the B.A. degree in physics from the University of Colorado in 1942, and served as Electronics Officer in the USNR from 1943 to 1946. He received the M.A. and Ph.D. degrees from Harvard University, the latter in 1951. He was subsequently employed by the Denver Research Institute and the National Bureau of Standards, the latter since 1952. His work in the Microwave Physics Section is concerned with the application of microwaves to problems of physical standards and constants, and he is currently working on a precision millimeter wave interferometer.

J. M. RICHARDSON

Dr. Richardson is a member of the American Physical Society, Sigma Xi, and the Research Society of America.

❖

Donald C. Stinson (S'50–M'57) was born in Malta, Idaho, December 7, 1925. He specialized in electrical engineering and received the B.S. degree from Iowa State College in 1947, the M.S. degree from California Institute of Technology in 1949, the E.E. degree from the University of California in 1953, and the Ph.D. degree from the University of California in 1956.

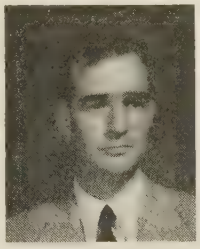

D. C. STINSON

He spent one year with General Electric Company as a test engineer, and for three summers was a member of the technical staff of the Research and Development Laboratories at Hughes Aircraft Company. Dr Stinson is now with the Missile Systems Division of Lockheed Aircraft Corp., Sunnyvale, Calif.

Dr. Stinson is a member of Sigma Xi, Eta Kappa Nu, and Pi Mu Epsilon.

Raymond M. Vaillancourt (A'54) was born in Levis, Quebec, Can., on September 14, 1926. He received the degree of B.A.S. in physics from Laval University, Quebec, in 1953. Since 1953, he has been a member of the scientific staff of the Canadian Armament Research and Development Establishment, Valcartier, Quebec, where he has been engaged in microwave studies related to guided missile applications.

R. M. VAILLANCOURT

Since 1954, he has been in charge of the microwave laboratory for undergraduates at Laval University.

Mr. Vaillancourt is an associate member of the Canadian Association of Physicists.

❖

Samuel Weisbaum was born on October 28, 1925 in New York, N. Y. He enlisted in the U. S. Army in 1943 and served with the 87th Infantry Division. In 1945 he entered New York University. He received the B.S. degree in physics in June, 1947, and the M.S. degree in 1948. In 1947, he was awarded the Morse Physics Medal. From 1950–1953 he was on the New York University faculty as a physics instructor doing research in microwave spectroscopy. He received the Ph.D. degree in physics in June, 1953. Since 1953 he has been engaged in solid state and microwave research and development with Bell Telephone Labs., Murray Hill, N. J.

S. WEISBAUM

Dr. Weisbaum is a member of the American Physical Society and Sigma Xi.

INSTITUTIONAL LISTINGS

The IRE Professional Group on Microwave Theory and Techniques is grateful for the assistance given by the firms listed below, and invites application for Institutional Listing from other firms interested in the Microwave field.

COLLINS RADIO CO., Cedar Rapids, Iowa
Complete Industrial Microwave, Communication, Navigation and Flight Control Systems

HUGHES AIRCRAFT COMPANY, Culver City, California
Radar Systems, Guided Missiles, Antennas, Radomes, Tubes, Solid State Physics, Computers

MARYLAND ELECTRONIC MANUFACTURING CORPORATION, College Park, Md.
Development and Production of Microwave Antennas and Waveguide Components

NATIONAL INSTRUMENT CO., INC., 23 E. 26 St., New York, N. Y.
Wide-Band Microwave Equipment, Simulated Flight Instruments, Lobe Switches, Custom Built Precision Apparatus

WEINSCHEL ENGINEERING CO., INC., Kensington, Md.
Attenuation Standards, Coaxial Attenuators and Insertion Loss Test Sets

WHEELER LABORATORIES, INC., 122 Cutter Mill Road, Great Neck, N. Y.
Consulting Services, Research & Development, Microwave Antennas & Waveguide Components

The charge for an Institutional Listing is $50.00 per issue or $140.00 for four consecutive issues. Applications for Institutional Listings and checks (made out to the Institute of Radio Engineers) should be sent to Mr. L. G. Cumming, Technical Secretary, Institute of Radio Engineers, 1 East 79th Street, New York 21, N. Y.

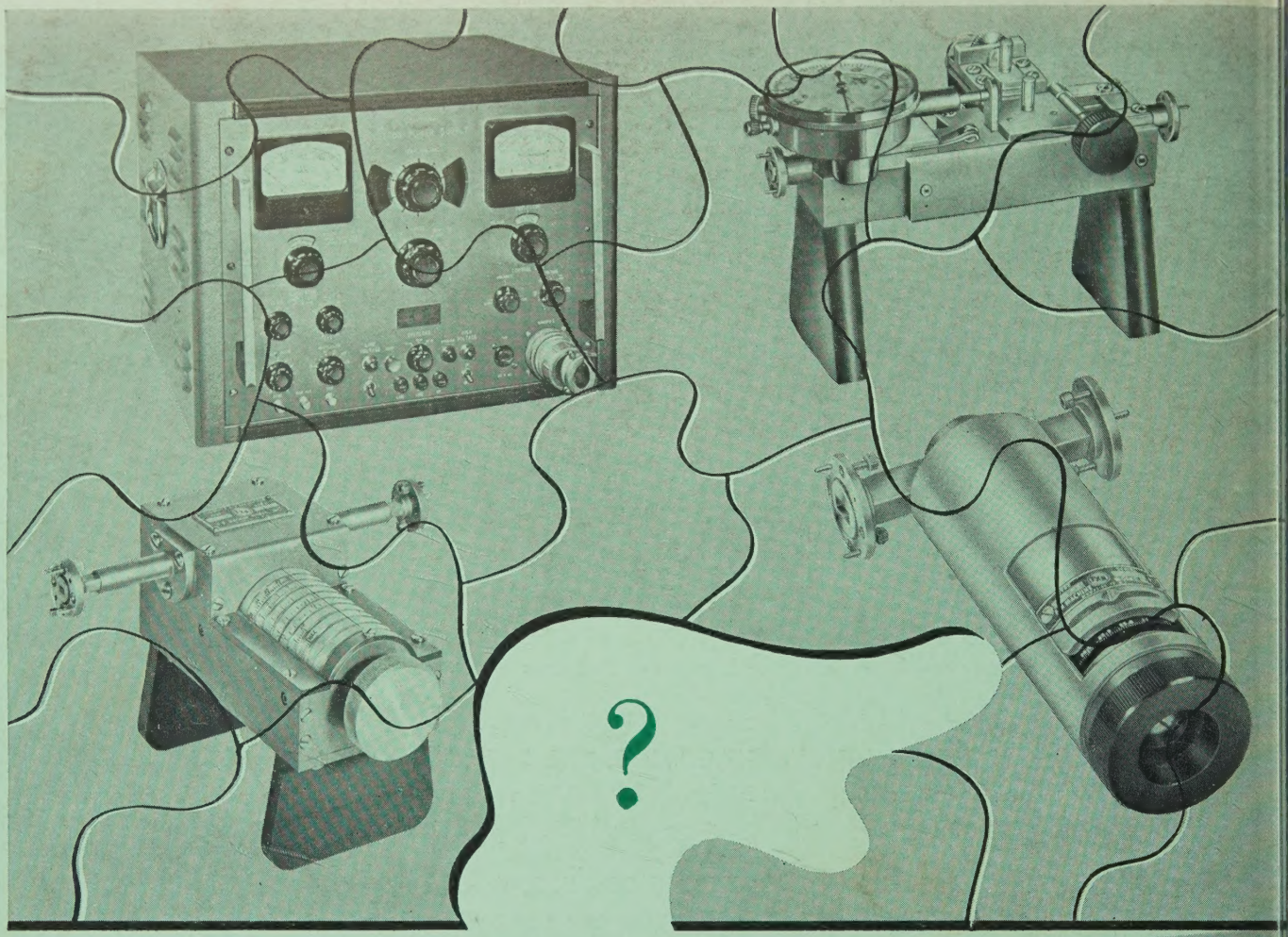

WHO MAKES THE MOST COMPLETE LINE OF MICROWAVE TEST EQUIPMENT?

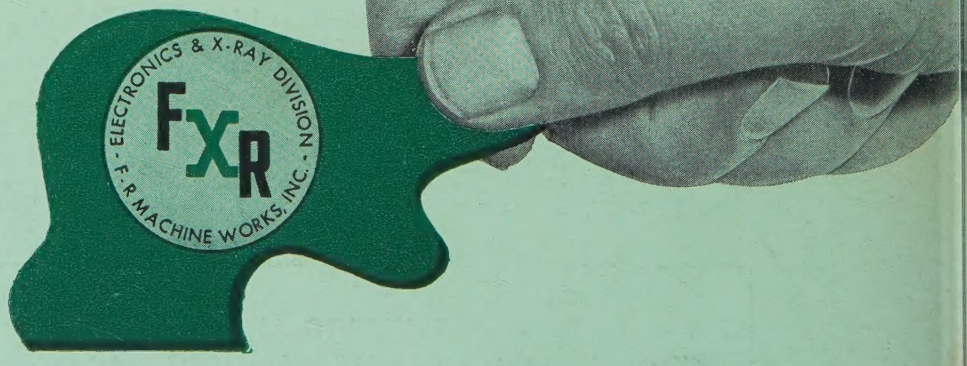

We don't make every type and size but we make more types and sizes than anyone else.

Electronics & X-Ray Division
F-R MACHINE WORKS, Inc.
Woodside 77, N. Y